Silica modified Co_3O_4 nanocubes as a model system for metal-support interaction in Co/SiO_2 catalyst for Fischer-Tropsch synthesis

Lebohang Macheli

BSc(Chemical Technology), NUL

University of Cape Town

Thesis submitted to the University of Cape Town in partial fulfilment of the academic requirements for the degree of **Master of Science** in Chemical Engineering

Centre for Catalysis Research

Department of Chemical Engineering

25 August 2014

The copyright of this thesis vests in the author. No quotation from it or information derived from it is to be published without full acknowledgement of the source. The thesis is to be used for private study or non-commercial research purposes only.

Published by the University of Cape Town (UCT) in terms of the non-exclusive license granted to UCT by the author.

University of Cape Town

Acknowledgements

Gratitude goes to Prof. Eric van Steen for his supervision through all the study endeavours. You have helped me develop my research skill, critical thinking and critical data analysis skill to solve scientific problems. You deserve to be crowned the best supervisor.

I would also like to thank my family for the support, through my entire study. Mr. Desmond Macheli, and my sisters Ponts'o Macheli and Althea Macheli always kept giving the words of encouragement through all the hardships of the study. Those phone calls you made always put a smile on my face.

Ka haoua meokho ka e koenyetsa ka hare ha ke lokela ho isa liteboho ho poho ea kanyesetsa e holang ka borofo oa ka Kholokoe, Tsepiso Edwin Macheli. Ho no se monate hoba hole le uena nako e telele, ho lula ke araba potso ea hao e reng na ke khutlela neng hae. Ho no se monate empa ke ne ke leka tsa bophelo ke betlela uena tsela. Empa u no mpha mochofane ha u no mpinela mohaleng u re ntoa e thata e thata bo-ntate le besitse poone, u re ke e loane joaloka "*mawiwi".* Ke e loanne ke hlotse. Ts'ebetso ena ke e abela uena.

Ke fetisetse liteboho ho metsoalle eaka e oeleng ea tsoha le nna ho khatheng tema, Gerard Leteba, Kubefu Maduna Molefi Matsutsu, Mopeli Khama, Ts'epang Khonthu, le eme le nna bonolong le boimeng, bobeng le monateng. Khaebana e ea le lokela mehaeso. Malefetsane Khesuoe le Tsoarelo Qhobela ke leboha ka ts'ehetso ea lona ho ka atlehisa phetheho ea mosebetsi ona. Le bile lere le seikokotlelo saka.

Special appreciation also goes to Miss Anna Petersen and Miss Rukaya Stracey for helping at the preliminary stage of this research. Your effort is highly acknowledged.

University of Cape Town

Declaration

I, **Lebohang Macheli** certify that this submission is my own, unaided work, except for the information obtained from literature sources and my prescribed supervisors. All sources of information have been adequately acknowledged and referenced. I have not received assistance from any other source in completing this submission.

Signature:…… Date:……..

Abstract

The aim of this study was to study the interaction between the silica and cobalt crystallites using a model of Co_3O_4-nanocubes whose surface was modified with tetraethyl orthosilicate. The model systems were prepared in two steps, viz. synthesis of the cobalt(III,II) oxide nanocubes via the sodium dodecylsulphate assisted oxidative precipitation and a surface modification of the nanocubes with tetraethyl orthosilicate. The obtained morphology and in particular the average crystallite size of Co_3O_4 nanocubes is affected by the temperature at which the reagents are mixed, the rate at which they are mixed as well as the time of reaction. The modification of the surface of the Co_3O_4-nanocubes with tetraethyl orthosilicate resulted in the formation of Co-O-Si ligands on the surface of Co_3O_4. This was confirmed in addition to (amorphous) SiO_2 using Fourier transformer infrared (FTIR) spectrometry. The surface treatment did not yield the formation of crystalline silica or a crystalline cobalt silicate phase as indicated by the absence of characteristic diffraction bands using XRD. Furthermore, there was no hard-to reduce material (e.g. cobalt silicate) as the TPR profiles showed only two peaks corresponding to the reduction of Co_3O_4 to metallic cobalt. The reduction behaviour of Co_3O_4 nano-cubes was, however, affected by the surface treatment with tetraethyl orthosilicate. A shift in the reduction profile towards higher temperatures was observed with increasing SiO_2 loading. This occurs as a result of increased activation energy for the reduction of the model catalysts upon modifying with tetraethyl orthosilicate, which might be ascribed to a strong interaction between cobalt and silica.

Surface modification of Co_3O_4 with SiO_2 prohibits sintering and the silica species may act as spacers between the cobalt particles. The Co-O-Si species are still present after the reduction of these model materials and during the Fischer-Tropsch synthesis. The Fischer-Tropsch activity is improved with a maximum activity improvement of about 15 times. The activity enhancement is larger than what is expected based on the increased metal surface area indicating that Co-O-Si surface species may also act as a promoter for the Fischer-Tropsch synthesis.

Table of Contents

List of figures

List of tables

Nomenclature

Abbreviation	Description
AAS	Atomic Absorption Spectroscopy
CNT	Carbon Nanotubes
DRIFTS	Diffuse Reflectance Infra-Red Fourier Transform Spectroscopy
FIC	Flow Controller
FID-GC	Gas Chromatograph Equipped With Flame Ionization Detector
FTIR	Fourier Transform Infrared
MSI	Metal Support Interactions
NTP	Normal Temperature And Pressure (298.15 K, 1 Bar)
PI	Pressure Indicator
PIC	Pressure Controller
PZC	Point of Zero Charge
RT	Room Temperature
STP	Standard Temperature And Pressure (273.15 K, 1 Bar)
TCD- GC	Gas Chromatograph Equipped With A Thermal Conductivity Detector
TEM	Transmission Electron Microscopy
TEOS	Tetraethyl Orthosilicate
TIC	Temperature Controller
TOPAS	Total Pattern Analysis Solution
TPR	Temperature Programmed Reduction
V	Flow Control Valve
WGS	Water Gas Shift

XRD	X-Ray Diffraction

1

1. Introduction

1.1 Brief background on Fischer-Tropsch synthesis

The production of high quality transportation fuels from syngas has attracted much interest (Kuboa *et al*., 2004; Mirzaei *et al.,* 2009). The Fischer-Tropsch synthesis is seen as a promising option for the production of fuels from syngas as it produces a great variety of products such as paraffin and olefins. It is defined as the heterogeneously catalyzed hydrogenation of carbon monoxide yielding long chain organic compounds (Schulz, 1985) and the reaction can be formally represented by:

$$nCO + 2nH_2 \rightarrow C_nH_{2n} + nH_2O \qquad \Delta H_{R,\,513K}\text{=-154 kJ/mol} \qquad (1.1)$$

The Fischer-Tropsch synthesis was first developed by Franz Fischer and Hans Tropsch in 1923 when they discovered the hydrogenation of CO over various catalysts yielding long chain hydrocarbons. The method was later commercialized in Germany for the conversion of coal to liquid fuels using a cobalt catalyst (Dry, 2002). The Fischer-Tropsch process has been applied on a large scale by e.g. Sasol and PetroSA in South Africa, Shell in Malaysia, and Sasol and Shell in Qatar. Nowadays, Sasol in South Africa converts coal to liquid fuel using an iron-based catalyst. All the other industrial processes convert natural gas into liquid fuels using either an iron based catalyst (PetroSA in South Africa) or cobalt based catalyst. The main drawbacks for the application of the Fischer-Tropsch process are basically related to the capital cost, cost of raw materials, volatile price of crude oil and environmental concerns, which brings a cognitive thought to the researchers to develop the Fischer-Tropsch catalysts with high specific activity and that are economically more viable.

1.1.1 Environmental performance of the Fischer-Tropsch fuels

The Fischer-Tropsch process is known to produce fuels with improved environmental performance compared to the petroleum fuels (US Environmental Protection Agency, 2002). The emissions from the Fischer-Tropsch fuels are characterized by reduced nitrogen oxide (NO_x) content. They are also characterized by little or no particulate matter due to their low content in sulfur and aromatics (US Environmental Protection Agency, 2002). A performance test on heavy duty trucks showed a decrease of the amount of hydrocarbons, carbon monoxide and nitrogen oxides in vehicle emissions when using a Fischer-Tropsch derived fuel (Lutz, 2001).

Greenhouse gas emission and energy consumption studies have been taken into account in the life cycle assessment performed on both petroleum fuels and fuels derived from natural gas using the Fischer-Tropsch process (Khan, 2009). In the assessment, emissions and energy consumption were examined from resource extraction to end use. In their life cycle assessment, using the market in Europe and Fischer-Tropsch plants in Qatar, Khan (2009) reported that the greenhouse gas emissions from a refinery of petroleum fuels is 7% higher than the emissions from fuels derived from natural gas using the Fischer-Tropsch process. However, according to Shag (2009), fuels derived from the Fischer-Tropsch process produced twice as much CO_2 per barrel of fuel compared with average fuel when using coal as a source.

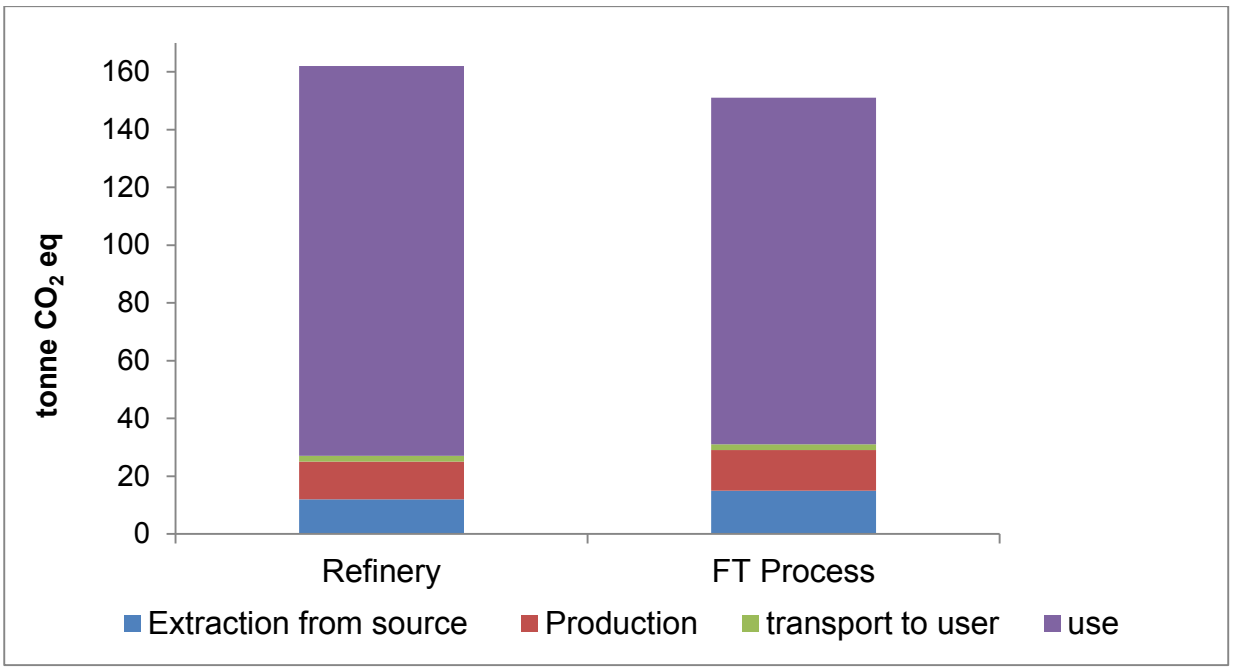

Figure 1.1: A comparison of CO_2 emissions for fuel produced via the Fischer-Tropsch process using syngas derived from natural gas and that produced from crude oil (Khan, 2009).

1.1.2 Economic viability of the Fischer-Tropsch process

The economic viability of the Fischer-Tropsch process is dependent on the price of crude oil since all the Fischer-Tropsch fuels have to compete with crude oil-derived fuels (Dry, 2001). According to White and Gray (2011), diesel fuel produced from coal can be economically viable when crude oil prices reach $94 per barrel. This equates to diesel production cost prices in the range of $2.70 per gallon of petroleum diesel. The viability of the Fischer-Tropsch process could be affected negatively, if the raw material used in this process (e.g. natural gas) rises.

1.1.3 Fischer-Tropsch Process performance

The overall efficiency of the Fischer-Tropsch process has recently been published with estimated yield and efficiency of the individual process units (Unruh *et al*., 2010; Tijmensen *et al*., 2002). These studies indicate that efficiencies in terms of chemical energy and carbon recovered in the hydrocarbon product may be expected in the range of 30 -50 and 25 - 45%, respectively using natural gas as the feed (Unruh *et al*., 2010).

2

2. Literature Review

2.1 Catalysts for the Fischer-Tropsch synthesis

A classical Fischer-Tropsch catalyst consists of the active metal, a support or binder and promoters. The active metal should interact strongly with CO and should have the ability to dissociate chemisorbed CO. Metals, which are catalytically active for the Fischer-Tropsch synthesis, include nickel, iron, cobalt and ruthenium (Shah and Perotta, 1976). *Table 2.1* summarizes the comparison of the four catalytically active metals for the Fischer-Tropsch synthesis. Only iron and cobalt are economically viable on an industrial scale. Nickel has a very high selectivity for low molecular weight products as it has a strong hydrogenation activity and hence it is not a feasible catalyst for the industrial Fischer-Tropsch process (Dry and Steynberg, 2004). Furthermore, at elevated pressure and low temperature, nickel tends to form volatile nickel carbonyl resulting in loss of nickel from the catalyst (Schulz, 1999). Ruthenium requires an activity over the life time of the catalyst 100000 times larger than that of iron (Dry, 2004). Although the Fischer-Tropsch activity of ruthenium is relatively very high compared to the activity of other metals, the high cost of ruthenium (due to its limited supply) makes it prohibitive to use this metal in an industrial Fischer-Trospch process (Dry, 1996). Cobalt and iron have therefore been employed as the catalytically active components in the Fischer-Tropsch process.

Table 2.1: Comparison of four catalytically active metals for the Fischer-Tropsch synthesis (adapted from Morales and Weckhuysen, 2006)

Active metal	X_{CO}	WGS activity	Hydrogenation activity
Ni	+	±	+++++
Fe	+	+++	+
Co	+++	±	+++
Ru	+++++	±	+++

2.1.1 Iron as a Fischer-Tropsch catalyst

Iron is a relatively abundant metal which is catalytically active for the Fischer-Tropsch synthesis. Iron is cheaper than the other catalytically active metals for the Fischer-Tropsch synthesis, such as nickel, cobalt and ruthenium, due to its abundance,. Iron oxides are known to be inactive for the Fischer-Tropsch synthesis. The iron phases catalytically active for the Fischer-Tropsch reaction are the metallic iron (Gracia *et al*., 2009) and iron carbides as the both have the ability to dissociate CO (Petersen *et al*., 2010). There are two types of carbide phases formed; the octahedral (O) carbides (ε-Fe_2C, ε-$Fe_{2.2}C$) and trigonal prismatic (TP) carbides (□-Fe_5C_2, θ-Fe_3C, Fe_7C_3). The high CO partial pressure in the gas phase favors the formation χ-Fe_5C_2 (O'Brein *et al*., 2006). The transformation of the O-carbides to χ-Fe_5C_2 phase at higher temperatures, or higher CO partial pressure, is thought to be due to the combination of lower strain, carbon diffusion limitations, and lower vibrational entropy, ultimately resulting in a higher relative thermodynamic stability and kinetic preference for χ-Fe_5C_2 (de Smit *et al*., 2010; Mogorosi, 2012). Magnetite has also been found in the spent tron based Fischer-Tropsch catalysts. It is formed via the oxidation of Fe_2C at high temperatures under hydrothermal conditions (Muhler *et al*., 1990). The formation of magnetite that thus affects the activity of the catalyst can be formally represented by:

$$3Fe_2\mathrm{C} + 11H_2O \rightarrow 2Fe_3O_4 + 3CO + 11H_2 \qquad (2.1)$$

Furthermore, over iron based catalysts, carbon dioxide is formed. The formation of carbon dioxide can formally be represented by the water gas shift reaction in *Equation 2.2*:

$$\mathrm{CO} + H_2O \rightarrow H_2 + CO_2 \qquad (2.2)$$

The water-gas-shift reaction is undesired in the context of the Fischer-Tropsch synthesis if the feed is derived from natural gas as it represents a loss in carbon. Moreover, it changes the feed gas composition in favor of a hydrogen richer mixture which in turn decreases the chain growth probability due to the higher availability of hydrogen on the catalyst surface (Dry, 2004). However, the water gas shift is desired for synthesis gas derived from feed stock with high content of carbon (e.g coal), as it produces the required hydrogen and maintains the H_2:CO ratio duiring the Fischer-Tropsch synthesis .

2.1.2 Cobalt as a Fischer-Tropsch catalyst

Cobalt as a Fischer-Tropsch catalyst has some advantages over iron. These include the ability to achieve a high conversion per pass (Prins *et al*., 2004), low rate of attrition and selectivity to paraffins (Khodakov *et al*., 2007). The high selectivity to long chain paraffins is a further advantage if diesel is desired as the product. Furthermore, cobalt based catalysts are more resistant to deactivation and chemical attrition as compared to iron based catalysts (Khodakov *et al*., 2007). The extent to which the Fischer-Tropsch reaction is inhibited by water at high conversion over cobalt catalysts is much less than over iron catalysts (van Berge and Everson, 1997). Consequently, cobalt is favoured over iron in application where high per pass conversion is required (van Berge and Everson, 1997).

The catalytically active phase for the Fischer-Tropsch synthesis is the metallic cobalt (Iglesia, 1997). Smaller metallic crystals are expected to show higher activity per unit mass of the catalytically active metal, because of higher surface area to volume ratio. However, cobalt crystallites less than 6-8 nm may re-oxidize under realistic Fischer-Tropsch conditions especially at high water-to-hydrogen ratios, thereby resulting in loss of active metal (van Steen *et al*., 2005, Fischer *et al*.). The cobalt oxide phases are known to be inactive for the Fischer-Tropsch synthesis. The maximum usage of the relatively expensive cobalt could be could therefore be attained by using cobalt particles close to 8 nm (van Steen and Claeys, 2008). In order maintain the required activity and to prevent attrition and sintering, there crystallites are dispersed over a support.

2.2 Supported catalysts

The typical supports used for the cobalt based catalyst for Fischer-Tropsch synthesis are porous transition metal oxides (silica, alumina, titania), carbon or even silicon carbides (Jacobs *et al*. 2002). The conventional way of preparing these catalysts is by impregnating the active metal precursor salt on to the support followed by calcination. Recently, the catalyst has been prepared by first preparing active metal crystallites followed by dispersion over the support in various solvents (Park *et al*., 2012; Fischer *et al*., 2012).

2.2.1 Role of a support

Cobalt-based Fischer-Tropsch catalysts are usually supported to improve mechanical stability while at the same time maintaining the required cobalt activity in the system (Storsæter *et al*., 2005). The rate of chemical attrition and sintering are reduced when the active metal is supported as each particle of the active metal is held at one position by the support (Storsæter *et al*., 2005). The interaction between the support and the catalytically active metal may be strong enough to prohibit sintering of the active metal which occurs through metal-metal interactions and hence to maintain the dispersion of the catalytically active metal (Storsæter *et al*., 2005; Jacobs *et al*., 2002).

2.2.2 Dispersing active metal on to the support

The dispersion of catalytically active carrier on support materials may occur via physisorption and chemisorption. The physisorption occurs through the electrostatic attraction of the catalytically active metal and the support. The impregnation of the active metal over the support depends on the surface zeta potential difference of the support in different solvent. The dispersion becomes possible if the charge of the surface zeta potential difference of the catalytically active carrier in a particular solvent is opposite to that of the support in that particular solvent.

Chemisorption occurs through the formation a chemical bond during the impregnation of the catalytically active substrate over the support. Such chemical bonds could be formed through strong electrostatic adsorption of the catalytically active material on to the negatively charge support-O^- species present on the support material surface at pH greater than PZC. The Metal-O-Support bond may also be formed during the solid-state interactions of the support oxides. Park and coworkers (2012) observed the formation of the Co-O-Al in the catalysis prepared by impregnation Co_3O_4 nanocubes on alumina in hexane after calcinations at 350°C. The interaction between the cobalt and alumina for the catalysts prepared via this route showed a higher CO conversion per pass in the Fischer-Tropsch synthesis (Park *et al*., 2012). Cobalt catalysts with higher dispersion on silica have also been reported by Herranz *et al*. (2009) using the impregnation of Co_3O_4 on silica.

2.2.3 Effect of support on the performance of the catalyst

The interaction between the metal and the support is an important factor that affects the dispersion of the metal catalyst (Coville and Liu, 2002). The synthesis of highly dispersed cobalt metal catalysts requires the initial formation of small CoO and Co_3O_4 crystallite (Suriye *et al*., 2005). Different supports interact differently with cobalt. The difference in the interaction could be affected by surface properties of the support, e.g. the presence of surface hydroxyl (M-OH) groups and porosity of the support.

Alumina

Alumina supported cobalt readily forms poorly reducible aluminate-type species (Jongsomjit *et al*., 2001) or a cobalt oxide phase that interacts strongly with the support (Jacobs *et al*., 2002). The interaction between alumina and cobalt may thus lower the reducibility of ionic cobalt. The aluminate-type species readily forms as divalent cobalt ions may diffuse into the alumina matrix. The surface of alumina contains surface hydroxyl (Al-OH) groups which interact strongly with the cobalt oxides.

Titania

The activity of Co/TiO_2 catalysts depends on the titania crystal phase. Co/anatase catalysts are active at 480 K - 550 K while Co/rutile remains inactive for the Fischer-Tropsch synthesis even at 670 K (Cheshechnikova *et al*., 1989). However, a mixture of rutile and anatase affects the hydrogen uptake of the catalysis to a certain extent and thus affects the methane selectivity (Cheshechnikova *et al*., 1989). Anatase is often used as a support, since it is reported to form defect structures with Ti^{3+} on the surface (Gao *et al*., 1996). These defect structures form a strong metal support bond resulting in a hard-to-reduce cobalt species. It is now well accepted that partial reduction of TiO_2 gives rise to TiO_x suboxide species ($x < 2$) which may migrate on to the surface of metal particles covering the metal particles (encapsulation or decoration) without changing in the metal particle size (de la Pena O'Shea *et al*., 2011). Although it has initially been thought that the encapsulation is detrimental, Yu *et al*. (2013) showed that surface decoration of cobalt with TiO_2 results in a relatively higher CO conversion. Even though Yu and colleagues (2013) attribute the increase in conversion to the suppression of CO hydrogenation due to strong metal support interaction the other

reason for increased conversion could be due to reduced degree of sintering as the cobalt particles are encapsulated by TiO_2.

Silica

The interaction between cobalt and silica support is generally regarded as relatively weaker (Gao *et al*., 1996; Jacobs *et al*., 2002; Soled *et al*., 2003) than the interaction between cobalt and alumina or titania. The interaction between cobalt and silica is strongly dependent on the preparation variables such as starting materials, preparation technique as well as cobalt source. A weak interaction yields larger particles and higher reducibility and conversely a stronger interaction yields smaller particles and a lower reducibility (Jacobs *et al*., 2002). The interaction should be strong enough to give a well-dispersed, thermally stable catalyst but weak enough to allow high reducibility.

Silicon Carbide

Due to few hydroxyl groups on the surface of the β-SiC, the metal-support interactions are less pronounced when SiC is used as a support for cobalt based catalyst (de la Osa *et al*., 2012). Unlike the oxidic supports, silicon carbide does not form hard-to-reduce compounds such as Co_2SiO_4, $CoTiO_3$, and $CoAl_2O_4$ during catalyst preparation and Fischer-Tropsch synthesis. As such, the degree of reduction is higher for cobalt catalyst supported on β-SiC than other oxidic supports. The disadvantage of the weaker interaction of SiC with cobalt is that it results in a high degree of sintering. Recently silicon carbide has been modified with oxides to reduce the degree of sintering (Koo *et al*., 2014). Due to its good thermal conductivity properties, silicon carbide has the ability to efficiently remove heat generated during the Fischer-Tropsch synthesis thus improving the selectivity of C_{5+} hydrocarbons to 80% as compared to Co/Al_2O_3 catalyst that achieved 54% C_{5+} selectivity while operated at similar reaction conditions (de la Osa *et al*., 2012).

Carbon

Carbon has an inert surface and therefore hardly forms irreducible materials. The distinctive properties of carbon that make it considerable for Fischer-Tropsch synthesis uniform pore size distribution, pore structure, inert surface properties, and resistance to acid and base environment (Tavasoli *et al*., 2008). While comparing metal-support

interactions of Co/CNT to Co/Al_2O_3 Tavasoli *et al*. (2008) found that the metal-support interactions of Co/CNTs are weaker and such improve the reducibility. Higher reducibility, however, implies lower dispersion. Contrarily, Yang *et al*., (2012) prepared Co/ordered-mesoporous carbon (Co/OMC) catalysts by simply tuning the carbon precursor furfuryl alcohol content, and solved contradiction between dispersion and reducibility to some extent.

2.2.4 Surface properties of the SiO_2 supports

The surface functional groups of SiO_2 are silanol groups Si-OH, which exist in various forms such as isolated, vicinal, and germinal and the siloxane groups Si-O-Si (Brinker and Scherer, 1990; Parks, 1962). These silanol groups play a major role in the metal-support interactions as bond formation between active metal and the silica support usually occurs through silanol groups. Surface silanol formation could be affected by parameters such as temperature and surface energy of the support. At temperatures above 1073 K silanol groups form siloxane (Iler, 1979). The surface properties of the silica may be modified by the introduction of a ligand on the surface such as tetraethyl orthosilicate.

Effect of temperature

According to Gardezi *et al.* (2012) under ambient conditions the silica gel surface exhibits hydrophilic character and is entirely covered with water molecules. The hydrophilic behavior of silica at ambient conditions was further noted by Iler (1979) when he found that a dehydroxylated silica surface resulted in steady rehydration when the pellets were exposed to ambient air. However, the silanol groups upon heating to 1073 K may condense and form siloxane groups that remain on the SiO_2 (Ling *et al*., 2011a). Any loss of surface silanol groups may result into a weaker metal-support interaction.

The effects of surface energy of surface silanol formation

The surface energy of the support relative to that of the active metal is another important factor to consider during the choice of the catalyst support. A surface is the termination of a crystal structure. This termination results in the atoms on the surface having less neighbouring atoms than those in the bulk causing the properties of the

atoms on the surface to differ from those in the bulk (Romanowski, 1969). The reduction in the number of neighboring atoms leads to a higher energy of the surface than that of the atoms in the bulk of the structure thereby changing the surface energy (ɣ) of the material (Swart *et al.*, 2007). To enhance their stability, as surface may reconstruct, form new surfaces (and as a consequence novel crystal shapes) or sinter (Titmuss *et al.*, 1996). Surface reconstruction may result in the change in the position of the atoms near the surface. This may consequently result in the the loss or formation of silanol groups on the surface and as such may indirectly affect metal-support interaction.

Surface modification of silica support

Surface modification refers to a process of transforming the chemical arrangement of the catalyst surface. The conventional way in the Co/SiO_2 systems is to modify the surface of the silica support. The silica surface can be modified either by physical treatment (thermal or hydrothermal) that leads to change in ratio of silanol and siloxane species on the silica surface or by chemical treatment that leads to change in chemical characteristics of silica surface (Jal *et al*., 2004). Surface modification result in a change in the hydrophobic nature of the catalyst (Jal *et al*., 2001). This may as a consequence result in a change in metal dispersion which may in turn result in a change in activity and selectivity.

Catalyst surfaces can be modified by either organo-functionalization, where the modifying agent is an organic group, or inorgano-functionalization, in which the group anchored on the surface, can be an organometallic composite or a metallic oxide. Ojeda *et al*. (2006) reported the silylation of the Co/SiO_2 catalyst. In the silylation processes, silicon containing organo-compound is introduced on the catalyst surface. The organo-silicon compound is introduced onto the catalyst surface by reacting with the surface silanols (Ojeda *et al*., 2006). Gun'ko *et al*. (2000) studied the surface modification of the Co/SiO_2 with hexamethyldisilazane (HMDS) to form trimethylsilyl groups according to the following scheme:

$$2Si\text{-}OH + (CH_3)_3\text{-}Si\text{-}NH\text{-}Si\text{-}(CH_3)_3 \longrightarrow 2Si\text{-}O\text{-}Si\text{-}(CH_3)_3 + NH_3 \qquad (2.3)$$

The trimethyl silyl groups on the surface of the Co/SiO_2 catalyst are reported to improve the hydrophobic nature of the catalyst (Ojeda *et al*., 2006). It is proposed that

the highly hydrophobic nature of the silica surface impedes the water molecules produced in the reaction from re-adsorbing onto the active sites. Therefore, the number of active sites available for CO adsorption and dissociation would increase leading to higher catalytic activity of the silylated sample for Fischer−Tropsch synthesis (Ojeda *et al*., 2006). Kim *et al*. (2005) reported that silylation of the support surface decreased the interaction between cobalt and support and enhanced the reducibility of cobalt oxide in the supported cobalt catalysts, and consequently increased its catalytic activity for Fischer-Tropsch synthesis. A reduction in methane selectivity on the silylated Co/SiO_2 catalyst has also been reported (Kim *et al*., 2005).

When performing an organo-functionalization of $Co/Ru/SiO_2$ with CH_3 groups using tetramethyl chlorosilane as a CH_3 precursor, Shi and co-workers (2008) found that modified catalysts had good thermal stability. They further reported an improved selectivity to C_{5-11} in the Fischer-Tropsch synthesis due to the hydrophobic surface of CH_3-modified $Co/Ru/SiO_2$ catalysts.

2.3 Metal-Support Interactions (MSI)

The primary role of supports has been reported by many researchers as to increase the dispersion of the catalytically active phase. However, the interaction between the catalytically active metal and the irreducible supporting oxide may result in the introduction of a strong chemical bond between the catalytically active phase or its precursor and the support. The introduction of the bonding is usually regarded as detrimental since it reduces the amount of catalytically active material. However, a study by Schwab and Koller (1968) showed that the electron transfer between the oxide and the metal could modify the properties of the metal. Tauster and co-workers (1978) showed that the chemisorption properties of the metal were drastically altered by the interaction with an oxide. The ability of the catalyst to adsorb H_2 and CO was reduced. This was ascribed to metal-support compound formation. Chemisorption studies demonstrated that there are strong interactions between the titania surface and the supported metals, provided the systems are activated in hydrogen at sufficiently high temperature. Such treatment reduces the surface of TiO_2, removing oxygen through H_2O formation and creating Ti^{3+} ions (Tauster *et al*., 1978). This may also result in a decrease in the chemisorption uptake of H_2 and CO on TiO_2-supported Pt

(Vannice *et al*., 1985). The results provided direct evidence that adsorption capacity for CO and H_2 can be decreased by a change in the chemical nature of surface Pt atoms as well as by physical blocking of the Pt surface by migrating TiO_x species. Vannice and coworkers (1985) also recognized that metal-support interactions may affect the heat of adsorption of reactants and as such influence the rate of reaction. Furthermore, the bonding interactions between the oxide and the metal may modify the interfacial energy between the oxide and the metal (Cargnello *et al*., 2012).

2.3.1 Contact effect/formation support overlayers

The contact effect refers to the effect caused by partially reduced support oxides that are in contact with the active metal without necessarily forming a chemical bond with the active metal. During reduction, the support gets partially reduced creating the oxygen vacancies and thus increasing the surface energy. In order to minimize the surface energy, the support creeps on to the surface of the active metal (Tauster *et al*., 1978; Bell, 2003). Fu *et al*. (2005) suggested that this creeping reaction consists of two steps: (i) the first process involves the Ti mass transport of interstitial Ti cations (Ti^{n+} n=3 or 4) in the near surface region, supported by the high diffusivity of titanium in TiO_2 at high temperature (500–800 K). (ii) in the second process the mass transfer of TiO_x over metal nanoparticles is produced. Thus, high metal surface energies and low oxide surface energy can lead to the decoration process (Fu *et al*., 2005).

The creeping of the TiO_2 onto the surface of catalytic active material is regarded as unfavorable as it blocks the catalytically active surface and hence affects the accessibility of the metal. In the presence of partially reduced TiO_2, the Co^{3+} metal site is reduced to Co^{2+} metal sites forming the non-reducible $CoTiO_3$ (Rayner, 2011). However, the vacancies on the other hand, are reported to facilitate the CO dissociation and thus enhance the activity of the catalyst (Vannice and Sudhakar, 1984). The contact sites are also conducive for hydrogen adsorption and as such enhance methane formation (Vannice and Sudhakar, 1984). In the case of alumina and silica supports formation of irreducible cobalt aluminate and cobalt silicate species is reported by Park *et al*., (2012) and Rayner, (2011).

2.3.2 Ligand effect of metal support interaction

The interaction between the catalytically active metal and the irreducible supporting oxide may result in the introduction of a strong chemical bond between the catalytically active phase or its precursor and the support. The formation of these bonds is referred to as the ligand effect and may occur during catalyst pretreatment when the catalyst is exposed to high temperatures i.e. during calcination or during catalyst synthesis. The hydroxyl groups on the surface of both the active metal oxide and the support are believed to play a major role in the formation of these ligands which are thought to be formed through a hydrolysis reaction (Mogorosi, 2012; Qing *et al*., 2011). For instance, the Co-O-Si bridges may be formed via the adsorption of cobalt onto the silica surface. This may occur via strong electrostatic absorption, which is dependent on the point of zero charge (PZC; PZC of SiO_2 is at pH 2-3) (Ling *et al*., 2011a). PZC is a pH at which the surface silanol groups remain neutral. At pH below the PZC the silanol groups are protonated and attract the anions from solutions. At pH above PZC the silanol groups are deprotonated into $Si\text{-}O^-$ surface species. The $Si\text{-}O^-$ species then attracts the positively charged cobalt ions (Ling *et al*., 2011b). However, at pH greater than 5, silica partially dissolves due to high concentrations of OH^- that weakens the surface bonding of silica (Ling *et al*., 2011a).

2.3.3 Generation of metal-support interaction via different methods of catalyst synthesis

Different approaches have been employed in the synthesis of Co/SiO_2 catalyst depending on the desired characteristic of the catalyst. Different synthesis procedures yield catalysts with different metal-support interaction effects, dispersion, and mechanical strength. The different methods include incipient wetness method, solid state impregnation method, sol gel method, reverse microemulsion (Khodakov *et al*., 2007; Niemela, 1997).

In aqueous solutions, cobalt ions are solvated by the water molecules and exist as $[Co(H_2O)_6]^{2+}$ complex (Ortega-Zarzosa *et al*., 2002). The water molecules that surround the cobalt ion first shell may be further deprotonated forming a hydroxo ligand OH^- or O^{2-}. The complexes can further undergo successive deprotonation forming $[Co(H_2O)_{6-x-y}(OH)_xO]$ complexes (Kogelbauer *et al*., 1995). These complexes according Brinker and Scherer (1990) may undergo acid-base equilibria forming cobalt oxo-hydroxo

complexes that in the presence of another cluster containing hydroxo functionalities such as $Si(OR)_m(OH)_n$ could give rise condensation reactions forming Co-O-Si bridges.

The Co-O-Si bond could also be formed through strong electrostatic adsorption of the cobalt ion onto the negatively charged $Si\text{-}O^-$ species present on the silica surface at pH greater than PZC. The Co-O-Support bond may also be formed during the solid-state interactions of the oxides. Park and coworkers (2012) observed the formation of the Co-O-Al in the catalysis prepared by impregnation Co_3O_4 nanocubes on alumina in hexane after calcinations at 350°C. The interaction between the cobalt and alumina for the catalysts prepared via this route showed a higher activity (Park *et al*., 2012). Cobalt catalysts with higher dispersion on silica have also been reported by Herranz *et al*. (2009) using the impregnation of Co_3O_4 on silica.

Incipient wetness impregnation

The incipient wetness impregnation involves dissolving the required amount of precursor salt (e.g $Co(NO_3)_2{\cdot}6H_2O$) into deionized water with addition to the support (e.g SiO_2) by drying and calcinations (Saib *et al*., 2006). This method has the ability to produces small particles; however, it is difficult to obtain a narrow particle size distribution (Khodakov *et al*., 2007). Variables that can affect the resultant catalyst are the rate of addition of precursor solution, rate of drying, temperature and duration of heating as well as pretreatment of the support (Niemela, 1997).

Solid state impregnation

The solid state impregnation method involves synthesizing the cobalt oxide nanoparticle followed by impregnation into the silica support in hexane. The catalyst is then dried and calcined in air. This method improves the cobalt support interaction (Park *et al*., 2012; Herranz *et al*., 2009). The interaction between the cobalt and alumina for the catalysts prepared via this route revealed that alumina reduced methane selectivity as compared to the conventionally prepared catalyst (Park *et al*., 2012).

Reverse microemulsion precipitation

The reverse micelle method by Hayashi *et al*. (2002) involves the mixing of water, a hydrocarbon and a surfactant to form a microemulsion. Two sets of microemulsion containing the metal salt [$Co(NO_3)_2{\cdot}6H_2O$] and a precipitating agent are mixed followed by the addition of the support. Alternatively, a precipitating agent may be added directly to the microemulsion containing the metal precursor. Microemulsion technique offers numerous advantages for producing nanoparticles as it allows control of size, which are smaller in size than those produced via impregnation. This thus results in 30% higher conversion in the Fischer-Tropsch synthesis (Hayashi *et al*., 2002).

Strong electrostatic adsorption

The strong electrostatic adsorption method uses the concept of electrostatic attraction of oppositely charged particles as used by Ling *et al*. (2011a). The pH of the precursor solution is adjusted such that is above the PZC of silica. The support is then added and shaken while monitoring pH change as well as cobalt uptake. The samples are then filtered, dried and calcined. This method offers high dispersion of cobalt on the support with a particle size down to 3 nm (Hench and West, 1990).

Sol Gel

The sol gel method is a method that comprises of the gelation of a solution of colloidal powders, hydrolysis of nitrate precursors followed by hypercritical drying of gels and hydrolysis and polycondensation of alkoxide precursors followed by aging and drying under ambient atmospheres (Bianchi *et al*., 2001). In sol gel method, a cobalt salt [$Co(NO_3)_2{\cdot}6H_2O$] is dissolved in water and added to a mixture of a support alkoxide (such as Tetramethyl orthosilicate) with alcohol. The alkoxide is hydrolysed with water and may further condense and form Co-O-Support bonds at room temperature and controlled pH.

2.3.4 Consequences of metal-support interactions

Metal-support interactions may result in the formation of a strong chemical bond. This chemical bond has been regarded as detrimental because it results in the loss of active sites. A study by Bell (2003) has, however, shown that metal support interactions may

result in the formation of new active site for the adsorption of syngas. Different effects of metal support interactions are observed from different types of metal support interactions, viz. overlayer formation and ligand effect.

Consequences of the formation of overlayers

The surface energy ratio of the support to that of active material ($\gamma_{support}$ / γ_{Co}) should be approximately one for better catalyst stability. However, for TiO_2, SiO_2 and Al_2O_3 this ratio is always less than one and this may result in the Co/support system minimizing its energy resulting in the formation of a support-overlayer on the active material as reported by Bell (2003) for Ru/TiO_2 systems. TiO_2 is highly likely to form overlayers as it has the smallest surface energy Bell (2003). The resulting metallic core decorated by a thin layer of a metal oxide allows us to develop core-shell nanomaterials which display unusual optical, magnetic and electronic properties.

The formation of this overlayer is regarded as unfavorable as it may result in coverage of catalytically active material and hence affects the activity of the catalytically active metal precursor. Conversely, the formation of overlayers controls the selectivity towards the different products by the formation of electron-deficient sites from the metal–support interface, in close proximity to metallic sites (Gandia and Montes, 1994).

Consequences of the ligand effect

During Co-O-Si bond formation surface silicates maybe formed and they are regarded to be detrimental as they are very hard to reduce at relative low temperatures (Okamoto and Polansky, 1991; Kogelbauer *et al*., 1995). Hydrothermal treatment at 493 K leads to a catalyst with lower reducibility due to the formation of non-reducible cobalt silicates. It has been reported that hydrothermal treatment of the partially reduced catalyst or hydrothermal treatment of the calcined catalyst in the presence of hydrogen produces cobalt silicates (*see Equation 2.3)*, while hydrothermal treatment of the calcined catalyst in air does not result in their formation (*see Equation 2.4)* implying the importance of CoO formation in the formation of these compounds for calcination in absence of air and in presence of air respectively (Iglesia *et al*., 1993). Formation of silicate in catalysts which had been used for Fischer–Tropsch synthesis was also reported. The dynamic behavior of silica thus offers an inimitable prospect to tailor interactions on the Co-SiO_2 catalyst based on a unique catalytic prerequisite.

$$2\,CoO + SiO_2 \xrightarrow{in\ a\ non\ oxidising\ atmosphere} Co_2\,SiO_4 \qquad (2.3)$$

$$6\,CoO + O_2 \xrightarrow{in\ air} 2Co_3\,O_4 \qquad (2.4)$$

The ligand effect has been reported to increase CO conversion to hydrocarbons as a result of the suppression of CO hydrogenation due to the ligand effect type of metal support interaction (Stracey, 2013). In that study, TiO_2 was incorporated onto the surface of cobalt and it is believed that this type of metal support interaction affects the adsorption strength of CO and enhancing the rate of CO dissociation. In a study by Mogorosi (2012) where the active metal was iron, this type of interaction resulted in the increased selectivity to methane implying the hydrogen availability was increased. The ligand effect in the Co/SiO_2 systems has not been studied using the inverse method and as such, the aim of this study is to understand the effect of the ligand-like SiO_2 on the surface of Co_3O_4.

2.4 Models for tailoring metal-support interactions

Different models have been developed in order to try to understand the effects of metal-support interactions in the Co/SiO_2 system in the Fischer-Tropsch synthesis. These different approaches result in different catalyst properties such as dispersion, availability of active sites to reactants. The effects of support porosity may vary with the different approaches. The different approaches include: the convention approach (the core shell approach as well as the inverse approach (Ortega-Zarzosa *et al*., 2002; Rodriguez and Hrbek,, 2010; Yin *et al*., 2009).

2.4.1 Conventional approach

A conventional approach *(see Figure 2.1)* is whereby the metal is dispersed on the support. In this model system, the reported interaction of cobalt and silica is that of the formation of cobalt silicates through the migration of the cobalt atoms into the silica matrix (Ortega-Zarzosa *et al*., 2002). It is worth noting that cobalt silicate formation is undesired as it results in loss of active metallic cobalt due to their highly irreducible nature. Kogelbauer *et al*. (1995) also reported the formation of cobalt silicate which is

hard to reduce. The effects of support porosity (e.g reduced number of active sites) have been reported by Xiong *et al*. (2005) while using the conventional approach.

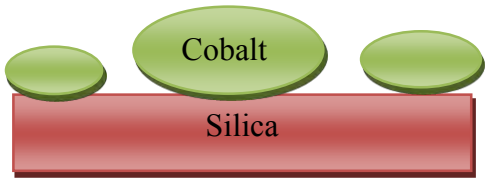

Figure 2.1: Conventional catalyst model for tailoring metal-support interactions

2.4.2 Core-shell approach

The second model that could be used in the tailoring of metal-support interactions could be the core-shell model (see *Figure 2.2*). In this model system, the active metal forms the core while the porous oxide material forms a shell around the active species. The shell should be porous enough to let the reactants reach the active core metal. Yin *et al*. (2009) realised the formation Si-O-Co bridges when a core shell catalyst was formed with cobalt forming the core while the silica formed the shell and this interaction of the silica and the cobalt enhances the thermal stability of the cobalt and improves resistance to sintering.

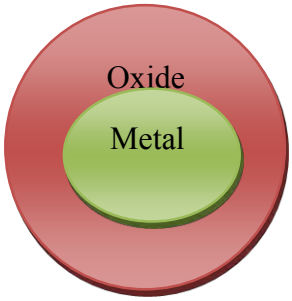

Figure 2.2: Core/shell catalyst model for tailoring metal-support interactions

2.4.3 Inverse approach

In the inverse catalyst (see *Figure 2.3*), a support is rather incorporated on the metal and the oxide nanoparticles become exposed to the reactants. The reactants can therefore have a direct interaction with the oxide, metal sites and the metal-oxide interface (Rodriguez and Hrbek, 2010). This approach eliminates the contributions of support porosity to the activity of the catalyst and helps in the understanding of the ligand effect.

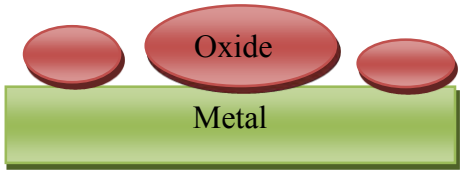

Figure 2.3: Inverse catalyst model for tailoring metal-support interactions.

2.5 Promoted catalyst

A promoter is added to catalyst to improve the performance of a catalytically active material in a chemical reaction. By itself the promoter has little or no catalytic effect to the overall reaction. Some promoters interact with active components of catalysts and thereby alter their activity. The interaction may cause changes in the electronic or crystal structures of the catalytically active material. Commonly used promoters are metallic ions incorporated into metals and metal oxide catalysts. Some promoters are added to the catalyst material in order to enhance the dispersion, to improve the Fischer-Tropsch selectivity, e.g. decreasing the methane production (Morales and Weckhuysen, 2006). The promoters can also preserve catalytic activity of cobalt by preventing the carbon deposition (Huffmann *et al.*, 1995).

Cobalt Fischer-Tropsch catalysts are reported to be less sensitive to promoter effect as compared to iron-based Fischer-Tropsch catalyst (Iglesia *et al*., 1993). Huffmann *et al.* (1995) observed some oxidation of the unpromoted Co/SiO_2 during $CO/H_2/H_2O$ exposure. They also found that K-promoted Co/Al_2O_3 was oxidized during reaction while the unpromoted catalyst did not change during reaction.

2.5.1 Structural promoters

Structural promoters affect the formation and stability of the active phase of a catalyst material. Their main purpose is to stabilize the Co active phase by either preventing the formation of metal-support compounds or preventing the agglomeration and sintering of the Co particles under Fischer-Tropsch operation conditions (Morales and Weckhuysen, 2006). Takeuchi *et al*. (1985) reported that with the addition of rhenium to Co/SiO_2, ethanol was produced with hydrocarbons, and the catalytic activity enhanced with an increase in the amount of rhenium. Further results on improved

selectivity of cobalt by the addition of ruthenium as a structural promoter were reported by Diehl and Khodakov (2009). Addition of ruthenium as a promoter also enhanced the cobalt activity by increasing the cobalt dispersion (Reinikainen *et al*., 1998). Structural promoters may also increase the reducibility of cobalt.

2.5.2 Reduction promoters

In the case of reducible oxide, the promoter could alter the reducibility of the metal by partially transferring oxygen to and from the metal (Cargnello, 2012). Improved cobalt reducibility was reported by Huber and co-workers (2001) when they promoted Co/SiO_2 with Gd. During reduction of the catalyst, the neighbouring Gd_2O_3 crystallites are reduced to GdO_x clusters which migrate to the cobalt metal surface where they assist the reduction process by extracting oxygen atoms from the cobalt oxide surface (Huber *et al*., 2001). Addition of ruthenium to the Co/Al_2O_3 resulted in an enhanced degree of cobalt reduction and hence increasing the number of surface cobalt metal atoms (Storsæter *et al*., 2005). Ruthenium has a greater impact on the cobalt reducibility than the dispersion, resulting in an almost two-fold improvement in the number of active sites available for reaction after reduction at 623 K, while maintaining essentially the same average particle size (Jacobs *et al*., 2002).

2.5.3 Electronic promoters

An electronic promotion effect by an oxide on the metal through electron transfer has been proposed by Jiang *et al*. (1983). Electronic promotion occurs when the oxide interact directly with the catalytically active phase (Morales and Weckhuysen, 2006). Electronic promotion affects the local electronic structure of an active metal mostly by adding or withdrawing electron density near the Fermi level in the valence band of the cobalt (Morales and Weckhuysen, 2006). According to Morales and Weckhuysen (2006), the electronic donation or withdrawal may lead to an increased intrinsic turnover frequency or change in product selectivity. However, supporting metal particles on reducible oxide species, such as TiO_{2-x}, may lead to the blockage of surface cobalt atoms during pre-reduction or even at the reducing conditions present within many Fischer–Tropsch reactors (Resasco and Haller, 1983).

2.6 Problem statement

The modern Fischer-Tropsch catalysts for the conversion of synthesis gas (H_2/CO) into liquid fuels are typically cobalt-based catalysts. The active metal is typically supported on an inorganic oxide, e.g. silica. Silica has been regarded as an inert support that only supplies a platform for the dispersion of cobalt in the Fischer-Tropsch synthesis. As such, little attention has been paid to the contribution of silica support to the system. This has led to different studies taking direction towards effects different support on dispersion, neglecting studying on the actual contribution of the metal-support interaction on the activity on the active metal. However, there is always a physical or chemical interaction between the support and the catalytically active components thus making the support rarely inert. During the preparation, metal-support compounds, such as cobalt silicates, can be formed. These compounds are difficult to reduce and the formation of these compounds is typically regarded as detrimental, since it results in a loss of cobalt which can be transformed into the active cobalt metal.

Recent results obtained in the Centre for Catalysis Research at the University of Cape Town have shown that metal-support compounds may result in promotion of the catalytically active material (Stracey, 2013). An enhanced activity was obtained, when modifying a model catalyst with tetrabutyl-orthotitanate mimicking the formation of metal-titanates (Stracey, 2013). The question remains whether silica-cobalt compounds show a similar behavior.

In this study, a model cobalt catalyst will be prepared (e.g. using the hydrothermal oxidative precipitation). The surface of the model catalyst will be modified with tetraethyl-orthosilicate with the aim to form Co-O-Si surface species (see *Figure 2.4*). The amount of these species will be varied. The model catalysts will be characterized using FTIR (to determine the extent of Co-O-Si and Si-O-Si formation), TPR (to determine the degree of reduction), and classical techniques, such as XRD and electron microspcopy, to determine the average crystallite size and shape of the active metal. The model catalysts will be tested for their activity in the Fischer-Tropsch synthesis at standard conditions.

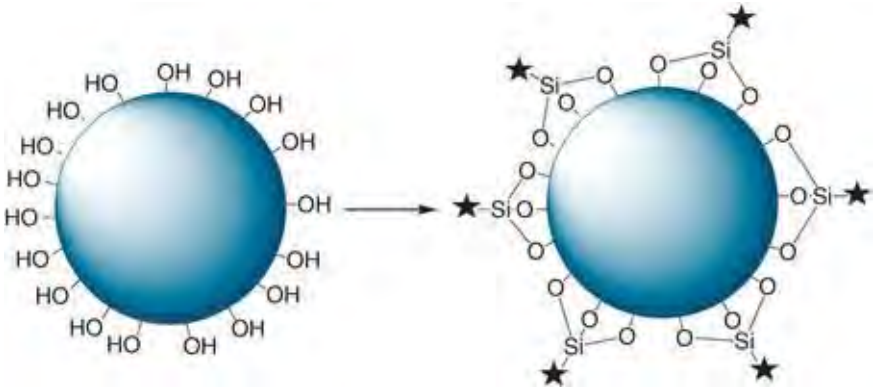

Figure 2.4: Surface silylation of cobalt oxide surface.

It is desired to synthesize silica modified Co_3O_4 nanocubes with the ability to adjust the strong interaction between the supported cobalt and the silica supports. The designed modification should result in the favoured reduction degree, dispersion, and metallic surface area of supported cobalt simultaneously aiming at improved Fischer-Tropsch synthesis activity.

3

3. Experimental

In this study, Co_3O_4 nanocubes were synthesized, which were subsequently modified with tetraethyl-orthosilicate to act as model system to investigate the role of Co-O-Si ligands in Fischer-Tropsch catalysts. Following the modification the model catalysts were characterized using AAS, electron microscopy, X-ray diffraction, FTIR and TPR to determine the elemental composition, the morphology of the model catalysts, the extent of formation of Co-O-Si bonds, and the effect of modification on the reducibility of the model catalyst. Catalyst testing was performed in a fixed bed reactor followed by characterization of the spent catalyst using H_2-chemisorption. AAS was used to determine the elemental composition of the spent catalyst.

3.1 Synthesis of Co_3O_4 nanocubes by hydrothermal oxidative precipitation

The hydrothermal oxidative precipitation method (Feng and Zeng, 2003; Liu *et al*., 2005) was used to synthesize Co_3O_4 nanocubes. This involved dissolving 1.8 g of NaOH (45 mmol) in 180 mL deionized water in a three-necked round-bottom flask. Subsequently, 5.4 g sodium dodecylsulphate (20 mmol) was added to the solution. The three-necked flask, with a reflux condenser mounted on top, was immersed into an oil bath. A solution containing 5.3 g $Co(NO_3)_2{\cdot}6H_2O$ (20 mmol, Merck, >99.0 %) in 20.0 mL water was subsequently added either at room temperature or at 368 K. In the case of mixing reagents at 368 K, the rate of addition of the 1.0 M cobalt nitrate solutions was varied between 10 mL/s and 10 mL/min (a total of 20 mmol of cobalt was added). Different crystallite sizes of Co_3O_4 were synthesized at 368 K by varying the reaction time from 3 hours to 8 hours.

3.1.1 The effect of initial temperature of reactants

In order to determine the effect of initial temperature of mixing of reagents, 20.0 mL of a 1.0 M cobalt nitrate solution was added to180 mL of an aqueous solution containing 1.8 g NaOH and 5.4 g sodium dodecylsulphate at room temperature. The temperature was subsequently increased to 368 K at a heating ramp of 5 K/min. In the second experiment, 20.0 mL of a 1.0 M cobalt nitrate was added to 180 mL of an aqueous solution containing 1.8 g NaOH and 5.4 g sodium dodecylsulphate at 368 K. The flasks were kept in the oil bath at 368 K for 5 hours. The whole process was carried out under constant stirring by a magnetic stirrer at 500 rpm. The black slurry formed was naturally cooled to room temperature. The slurry was subsequently centrifuged at 5000 rpm for 5 min. After removal of the supernatant, the solid was re-suspended in a 1.0 M HCl solution to dissolve unreacted precursor compounds (α-$Co(OH)_2$, $Co(II)(OH)_{2-x}(NO_3)_x{\cdot}nH_2O$, and $Co(II)_{1-x}Co(III)_x(OH)_2(NO_3)_x{\cdot}nH_2O$). The mixture was then centrifuged 8 times with 50 mL aliquots of an aqueous 1.0 M HCl-solution. This was done repeatedly to obtain phase-pure Co_3O_4. The black paste (purified Co_3O_4) left in the centrifuge tubes was re-suspended in deionized water and re-centrifuged. This latter washing step was also repeated 5 times. The nanoparticles were then calcined in a static oven at 473 K for 2 hours.

3.1.2 The effect of rate of addition of $Co(NO_3)_2{\cdot}6H_2O$

In order to determine the effect of the rate of addition of the $Co(NO_3)_2{\cdot}6H_2O$ (Merck, >99.0%) solution , 20.0 mL of a 1.0 M cobalt nitrate solutionwas added to 180 mL of an aqueous solution containing 1.8 g NaOH and 5.4 g sodium dodecylsulphate at 368 K using different addition rates (10 mL/s, 2 mL/min and 10 mL/min). The flasks were kept in the oil bath for further reaction at 368 K for 8 hours. The whole process was carried out under constant stirring by a magnetic stirrer at 500 rpm. The black slurry formed was naturally cooled to room temperature. The slurry was subsequently centrifuged at 5000 rpm for 5 min. After removal of the supernatant, the recovered solid was washed with an aqueous 1.0 M HCl-solution and subsequently with distilled water as described in *section 3.1.1.*

3.1.3 The effects of reaction time

The reaction time was investigated at 368 K. The cobalt nitrate solution (20 mL, 1.0 M; $Co(NO_3)_2{\cdot}6H_2O$ purchased from Merck, >99.0%) was added to 180 mL of an aqueous solution containing 1.8 g NaOH and 5.4 g sodium dodecylsulphate. The reaction time (measured from the time of addition of cobalt nitrate solution) was varied from 3 hours to 8 hours; the flasks were kept in the oil bath at 368 K. The whole process was carried out under constant stirring by a magnetic stirrer at 500 rpm. After the reaction, the Co_3O_4 crystals were purified subsequently with a 1.0 M aqueous HCl-solution and distilled water as described in *section 3.1.1.*

3.2 Surface silylation of Co_3O_4 nanocubes

The silylation of the Co_3O_4-nanocubes was performed in a method analogous to the method described by Mogorosi (2012) for the silylation of hematite. The synthesized Co_3O_4 (0.5 g) was re-suspended in 300 mL n-hexane by stirring for 1 hour with a magnetic stirrer bar (2.5 cm) at a stirring speed of 500 rpm. 50 mL of a solution of tetraethyl-orthosilicate (97%, Fluka) of different concentrations (0.1-1% Vol/Vol) in n-hexane was added to the suspension. The TEOS soultions in n-hexane were prepared by mixing a measured volume of TEOS using a pipette into a known volume of n-hexane. Typically, the modified sample was contacted for 5 hrs with the tetraethyl-orthosilicate containing solution. After 5 hours, the modified sample was recovered by settling and decantation. The solid sample was washed 5 times with 50 mL with n-hexane. The samples were subsequently dried and calcined in a static oven at 393 K[a] for 2 hours and at 473 K for 2 hours respectively. During the drying and calcination step, the sample was prepared by thinly spreading over the bottom of a porcelain crucible. To determine the rate of uptake of tetraethyl-orthosilicate on the surface of Co_3O_4, a 50 mL aliquot was withdrawn from the samples at time intervals of 0.5 hours and analysed for its silicon and cobalt content. A schematic diagram for the surface silylation of the nanocubes is shown in *Figure 3.1*

[a] The set temperature in drying oven for drying wet sample

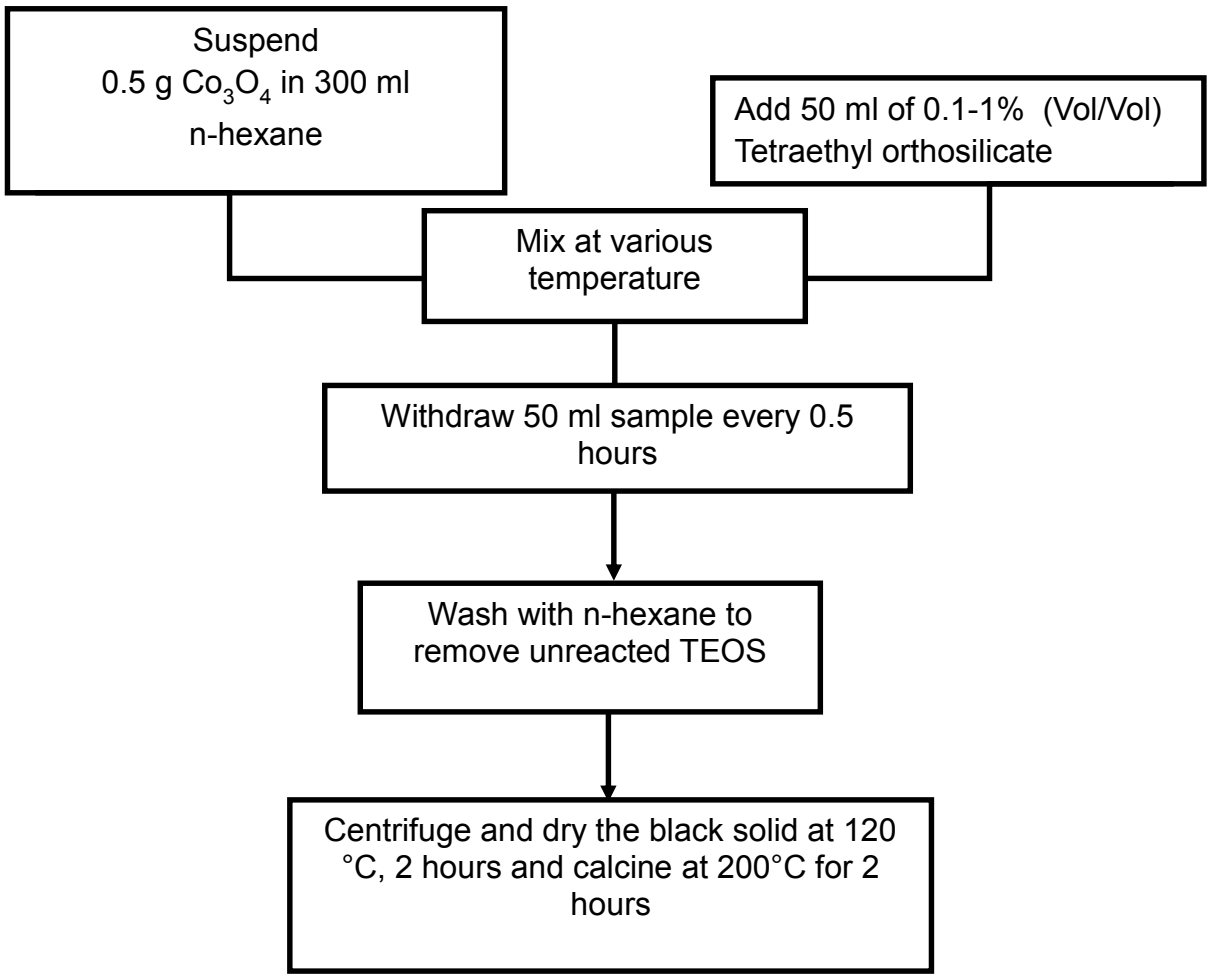

Figure 3. 1: The schematic diagram for the silylation of Co_3O_4 nanocubes

3.3 Supporting the model catalysts onto silicon carbide

The model catalyst were dispersed on to β-SiC microspheres (SiCAT, $d_{particle}$= 100 μm) prior to their test for activity in the Fischer-Tropsch synthesis to minimize effects of sintering during the Fischer-Tropsch synthesis and the catalyst activation. The target cobalt loading was 7 % w/w. Co_3O_4 nanocubes was re-suspended in different solvents, viz. water at pH 6.5, diluted nitric acid at pH 5.9, ethanol or 10 % vol/vol oleic acid in n-hexane. The diluted nitric acid solution (pH 5.9) was prepared by dilution of concentrated nitric acid with distilled water; the pH was measured using an electronic pH meter. The pH meter was calibrated by placing the electrode in the solution of pH 7 buffer and allowing the display to stabilize. The display was set to read 7 by adjusting calibration knobs on the pH meter. The electrode was removed from the buffer and rinsed with deionized water and dried using a tissue. The electrode was subsequently

placed in a solution of pH 4 buffer and allowing the display to stabilize. The display was set to read 4 by adjusting calibration knob on the pH meter. The electrode was subsequently rinsed and dried. 0.1 g of Co_3O_4 was added to each solvent and 0.9 g of β-SiC was subsequently added . The mixtures were re-sonicated for further 1 hour followed by subsequent drying in a static oven at 393 K for 2 hours and calcination 473 K for 3 hours respectively.

3.4 Characterization of the model catalyst

The model catalysts were characterised with FTIR to confirm the presence of Co-O-Si surface species, XRD for phase determination, electron microscopy to determine their morphology as well as elemental composition, temperature programmed reduction (TPR) to determine their reduction behaviour.

3.4.1 Scanning Electron Microscopy (SEM), and Energy Dispersive X-ray analysis (EDX)

The composition of both purified Co_3O_4 and the silica modified Co_3O_4 was determined using a scanning electron microscope (LEO S444 SEM, L_α: K_α, UK) equipped with a Four Quadrant Back Scatter Detector and an energy dispersive Fissons Kevex X-ray spectrometer (EDX). The composition of the purified synthesized Co_3O_4 nanocubes was determined both prior to and after calcination at 473 K. The composition of the modified samples was determined after calcination at 473 K. Sigma software was used to determine the actual Si loading on the catalyst. Si loading was determined as a ratio of Si atoms to Co atoms. The standard deviation associated with measurement was determined by taking the average of 4 line scans of each sample. Sample preparation involved sprinkling dry Co_3O_4 powder on an aluminium stub covered with a carbon tape.

3.4.2 Transmission Electron Microscopy (TEM)

The samples were analysed for their morphology using a JEM200CX (JEOL, JAPAN) which was operated at 120 kV. The powdered samples were ultrasonically suspended in methanol for 10 minutes. A drop of each suspension was transferred onto a carbon coated copper grid. The samples were then allowed to dry at room temperature. After drying, the samples were placed into the microscope for viewing. The TEM images were then analyzed with image analysis tool (ImageJ)[b] to determine the crystallite size and size distribution. The error associated with the measurement of the particle size was determined by measuring 70 particles on the images.

3.4.3 Phase composition determination with X-ray power diffraction

The phase composition of the model catalysts was determined using a Bruker AXS D8 Advance X-ray laboratory diffractometer operated at 40 kV and 40 mA utilizing a Co source (λ_{Co}-K_{α} = 0.178897 nm) and a VÅNTEC position-sensitive detector. A sample was placed in a sample holder and inserted into the XRD machine for scanning. Diffraction scans were taken in the range $20^{o} < 2\theta < 80^{o}$ and compared to the standard compounds reported in the JCPDS data file. All diffraction patterns were recorded in the step-scan mode with a step size of 0.05 degrees and a scan rate of 0.5 deg/min. Crystalline phases were determined by comparing measured peaks with known patterns from the International Centre for Diffraction Data PDF 2 database using the search match tool in EVA and particle sizes were calculated using Rietveld refinement in Topas software.

3.4.4 Confirmation of Co-O-Si bonds with FTIR

The catalysts were tested for the presence of the Co-O-Si and Si-O-Si surface species using a FTIR spectrometer (Nicolet 5700). The analysis was done *exsitu* to confirm the presence of these species prior to reduction and *insitu* to confirm these species after reduction. FTIR spectrometer (Nicolet 5700) was used to determine the extent of metal support interactions (Co-O-Si) in the modified catalysts and the extent of auto condensation of the tetraethyl-orthosilicate as indicated by the formation of Si-O-Si bridges. The characteristic wavenumbers of the Si-O-Si bonds are at 800 cm^{-1} and

[b] A public domain Java image processing program inspired by National Institute of Mental Health

1080-1100 cm^{-1} while those of the Co-O-Si bridges are at 1020-1035 cm^{-1} and 661 cm^{-1} (Puskas et at., 1992).

Exsitu studies

The sample was prepared by diluting 0.5 mg of the model catalyst with 0.2 g of KBr and then pressed into pellets. A total of 1200 scans were taken in the range between 400 and 4000 cm^{-1} for each sample after a background scan of KBr was taken in the transmission mode at the resolution of 8 cm^{-1}.

Insitu studies

FTIR was also performed to determine the behaviour of the catalyst upon reduction as to confirm the presence of Co-O-Si after reduction. The KBr diluted model Co_3O_4 catalyst (0.5 mg Co_3O_4 in 0.2 g KBr) was placed in the sample holder of the Praying Mantis high temperature chamber after a background scan of pure KBr was taken. An infrared spectrogram was immediately taken at room temperature with 500 scans at a resolution of 8 cm^{-1}. The temperature of the cell was then raised to 623 K at a ramp rate of 5 K/min in the presence of hydrogen (flow rate 40 mL/min (NTP)) to reduce the catalyst.

3.4.5 Temperature Programmed Reduction (TPR)

Temperature programmed reduction was used to investigate the reduction behaviour of the model catalyst. The analysis was carried out in a quartz reactor in a Micromeritics AutoChem2950 (Micromeritics Instrument Corp., USA). The TPR was regularly calibrated using AgO.

Calibration of the TPR

30 mg of silver oxide (AgO) was used as a standard for the analysis. AgO is used as a standard because it's easy to reduce. The standard sample was reduced using 5% hydrogen in argon at a flow rate of 50 mL(NTP)/min. The sample was heated from room temperature to 773 K using a heating rate of 5 K/min. Relative errors are typically ± 1.2 % for TPR as determined from the repeated calibration data. The relative amount of hydrogen consumed for the model catalysts was determined from the respective

peaks. The area of a peak is related to the amount of a compound in the gas mixture by a calibration factor.

$$\dot{n}_{H_2,consumed} = f_{TPR,i} \cdot A \quad (3.1)$$

where

$$f_{TPR,i} = \frac{n_{H_2\ for\ reduction\ AgO}}{Area_{Ag2O}} = \frac{n_{Ag2O}}{Area_{Ag2O}} = \frac{m_{Ag2O}}{124 \cdot \frac{g}{mol} \cdot Area_{Ag2O}} \quad (3.2)$$

The calibration factor was determined to 0.65 ± 0.03.

Determination of reduction behavior of model catalysts

About 0.03 g of each sample was loaded into the quartz reactor and was degassed at 393 K under 50 mL/min (NTP) argon for 1 hour. This was done to ensure a complete removal of excess moisture and other contaminants from the model catalyst samples. The temperature was then decreased to 340 K followed by the change in gas composition to 5 % H_2/Ar (vol/vol) keeping the flow rate at 50 mL/min (NTP). The temperature was increased from 340 K to 1173 K using constant heating rates of 5, 10 and 15 K/min.

3.4.6 Metal surface area in spent catalyst

Dispersion of cobalt in the spent catalyst was determined using H_2 chemisorption. This was performed in a Micromeritics ASAP 2020 analyzer which conducts chemisorption using the static volume method. The set-up includes a vacuum line, gas dosing system and a line connected to the sample holder. The sample holder which is a U-tube made of quartz was loaded with 0.5 g of sample sandwiched between two layers of glass wool. The sample holder was then placed in a 383 K oven overnight in order to remove any adsorbed moisture. The sample holder was mounted on to the Micromeritics ASAP 2020 analyzer. The catalyst was reduced *insitu* for 12 hours at 493 K with hydrogen. Following the reduction, hydrogen was removed from the system using helium as a purge gas prior to evacuation. The H_2-chemisorption was conducted at 398 K.

Elemental analysis of cobalt in spent catalyst.

In order to determine the actual amount of cobalt in the spent catalyst, all the samples from the H_2-chemisorption analysis was added to 50 mL of 3 M hydrofluoric acid to form a colored solution of cobalt fluoride. The concentration of cobalt in solution was determined using atomic absorption spectrometry (AAS).The instrument was calibrated by preparing standard cobalt solutions. A calibration graph of absorbance against concentration was plotted. The calibration graph of the AAS is plotted in *Appendix 9.1.*

3.5 Fischer-Tropsch Synthesis

The Fischer-Tropsch synthesis was carried as a test reaction to monitor the effect of surface modification on the activity of the model catalyst. This was carried out in a fixed bed reactor. The SiC supported catalyst (1.0 g of catalyst containing 0.1 g of cobalt oxide) was loaded into the reactor and reduced with hydrogen. After the reduction process, syngas was passed over the catalyst for the synthesis to occur. The reaction stabilised after 44 hours. The products were analyzed on-line with a TCD-micro GC and off-line with FID-GC to determine the conversion and selectivity.

3.5.1 Reactor system

The Fischer-Tropsch synthesis was performed in a fixed bed reactor system shown in *Figure 3.2*. The flow rates of all gases were regulated by different mass flow controllers (FIC-1, FIC-2 and FIC-3). A reference gas is used as an internal standard for analysis. The gas is N_2/cyclohexane mixture containing 0.05 vol-% cyclohexane. The mixture is fed directly into the product stream via a flow controller before the product ampoule sampler (AS-1). The reactor system is pressurized using argon and controlled using a needle valve (V-9) and allowing argon to flow through the system. The gases are either directed to the reactor or to the bypass using a four way valve. Synthesis gas goes to the reactor while argon flows via the bypass stream to control the pressure in the reactor or vice versa. The reactor temperature is controlled through feedback system with a thermocouple (TI) placed inside the reactor. The temperature along the exit lines was maintained at 453 K. The exit line is connected to the micro-GC with a TCD for online sampling whereas offline sampling is conducted using glass ampoules.

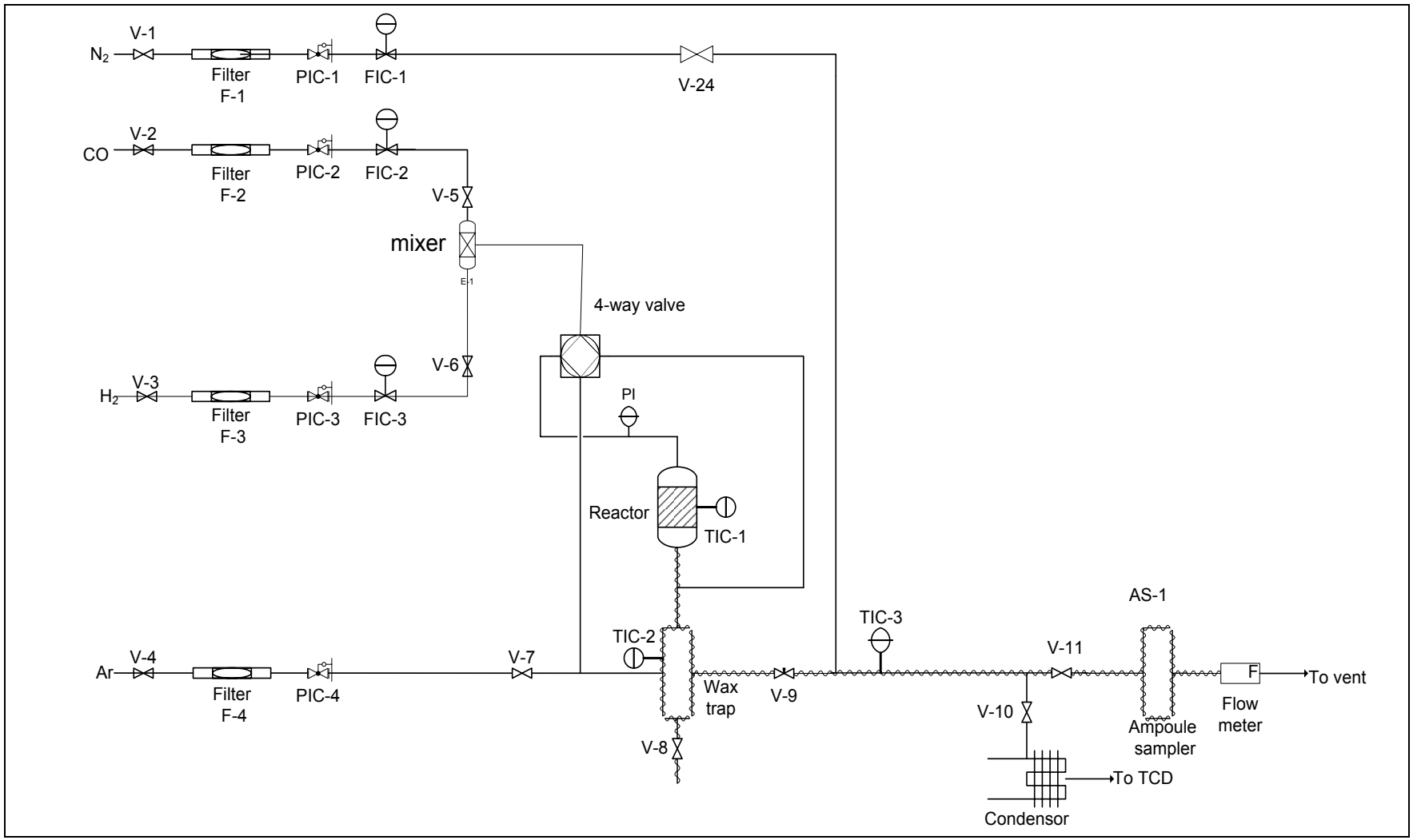

Figure 3.2: The Fischer-Tropsch reactor setup.

3.5.2 Synthesis

The inertness of the system was tested using 1.0 g β-SiC (SiCAT, $d_{particle}$= 100 µm), which was loaded into the reactor (10 g of SiC (200-250 µm) was then added to fill the reactor) and tested for its Fischer-Tropsch activity. β-SiC was first treated with hydrogen at 573 K for 16 hours. The temperature was subsequently reduced to 493 K and syngas at the H_2:CO ratio of 2 was flown over the catalyst bed. Online TCD-GC was used to determine the conversion

Loading the reactor

0.1 g of the catalyst supported on 0.9 g of β-SiC (SiCAT, $d_{particle}$ = 100 µm) nano-spheres was diluted with 2.0 g silicon carbide ($d_{particle}$ = 200-250 µm) using ethanol to make a homogeneous slurry. The slurry was dried at 343 K for 1 hour and subsequently loaded into the reactor. 10 g of SiC (200-250 µm) was then added to fill the reactor. The catalyst dilution with silicon carbide which has a high thermal conductivity served to facilitate heat removal. *Figure 3.3* depicts the fixed bed reactor used in the Fischer-Tropsch synthesis.

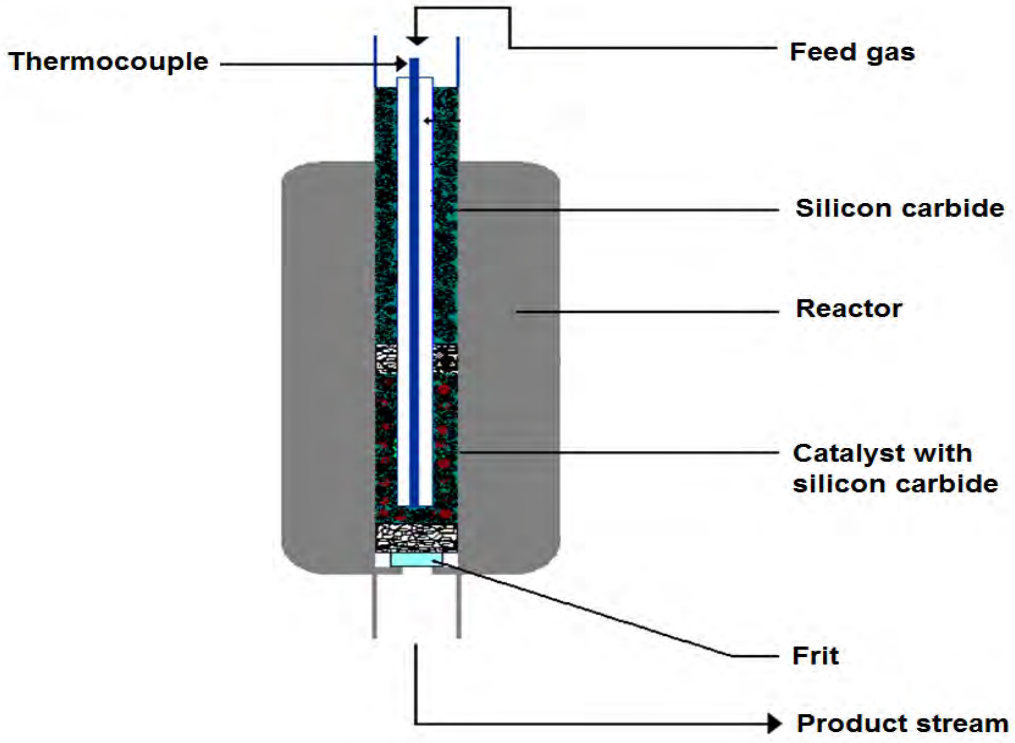

Figure 3.3: Reactor configuration and packing (adapted from Mogorosi, 2012)

Leak test

The setup was pressure tested to ensure that there are no leaks by tightening all connection points. All exit control valves in the system were closed and the argon control valve is opened and the system is pressurized to 20 bar. The system was then left at that pressure over night. The system is then isolated and pressure change is monitored for a period of 24 hours. The acceptable leak rate corresponds to a pressure drop of maximum of 1 bar over a period of 24 hours. A sample calculation for the acceptable leak rate is shown in *Appendix 9.2.*

Fischer-Tropsch synthesis

Having passed the pressure test, the gas flow was changed to 40 mL/min (NTP) H_2 at 1 bar to initiate the reduction of Co_3O_4 to metallic Co. The reduction program was started and the temperature in the reactor was increased to 623 K using a heating rate of 5 K/min. After the reduction process is complete Ar was passed over the reactor to keep the catalyst under an inert environment, while the synthesis gas flowed over the bypass. The temperature was reduced to 493 K. The flow rates of the H_2 and CO were set at 20 mL/min (NTP) and 10 mL/min (NTP) respectively (using the flow controllers FICs). The reference gas was then set at 10 mL/min (NTP). The system was then pressurized to 20 bar using Ar. A total of 8 samples of the synthesis gas flowing over the bypass were taken to confirm the flow rates and feed ratio. Once the flow rates are confirmed, the four way valve was switched back to reactor flow and reaction was started.

Unloading the reactor

The spent catalyst was passivated by flowing CO_2 over the catalyst bed at the flow rate of 20 mL/min (NTP) for 2 hours at room temperature. The catalyst was removed by first removing the 10.0 g of the SiC that was on top of the catalyst bed initially added for the even heat distribution in the SiC was obtained. The catalyst was then recovered by separating from the silicon carbide using a 150 µm sieve. The morphology of the spent catalyst was analysed with TEM. H_2-chemisorption was used to determine the effect of surface modification on the dispersion of the catalyst. Dispersion is determined as the number of active sites available per total amount of cobalt present. As such, the total amount of cobalt present in the recovered catalyst has to be determined Using AAS.

3.5.3 Sampling

Sampling was divided into two parts. The inorganic gases and methane were analyzed using an on-line method whilst the organic compounds were analyzed using an off-line method.

On-line sampling

On-line sampling was carried on a GC-TCD (Varian 4900) equipped with three columns that are connected three different channels with different detectors. Nitrogen was used as an internal standard for the on-line analysis where H_2, N_2, CO, CH_4 and CO_2 were analyzed using a GC (Varian 4900) equipped with thermal conductivity detector (TCD). The operating conditions and the gases detected in each column are given in *Table 3.1.*

Table 3.1: Sampling condition of the micro GC equipped with a TCD

	Channel 1	Channel 2	Channel 3
Gases analysed	CO, N_2, CH_4, Ar	CH_4, CO_2	H_2
Column temperature (K)	353	353	353
Carrier gas	H_2	He	Ar
Inlet gas pressure (kPa)	150	100	150
Injection time (ms)	120	120	120
Injector temperature (K)	313	313	313
Back flush time (s)	160		160
Sampling time (s)	180	180	180
Columns	20m, Molecular Sieve 5A	10m, Porapak Q	10 m, Molecular Sieve 5A

The TCD was calibrated using calibration gas mixtures with known composition. The peak areas obtained from the TCD analysis were then used to calculate the relative calibration factors normalized for nitrogen, f_{TCD}, for each species. The calibration factors used in this study are shown in *Table 3.2.*

Table 3.2: Calibration factor for the TCD-reading of the various gases relative to nitrogen gas

Gas	Calibration factor
Hydrogen	13.49 ± 0.10
Nitrogen	1.00 ± 0.05
Carbon monoxide	0.76 ± 0.02
Methane	0.67 ± 0.03
Argon	0.87 ± 0.05

Relative errors (repeatability of this analysis technique) are typically ±3.0 % for TCD as determined from the repeated calibration data obtained at different calibration times (Appendix 9.3). The relative amount of each gaseous compound can then be determined from the respective peaks of the GC-TCD in a chromatogram. The area of a peak is related to the amount of a compound in the gas mixture by a calibration factor. The GC-TCD was calibrated using gas mixtures of known composition and the internal standard chosen was nitrogen. The molar flows were therefore determined relative to the molar flow rate of N_2 using:

$$\dot{n}_i = f_{TCD,i} \cdot \left(\frac{A_i}{A_{N_2}}\right) \cdot \dot{n}_{N_2} \qquad (3.1)$$

where

$$\dot{n}_{N_2} = \frac{\dot{V}_{N_2}}{V_m} \qquad (3.2)$$

Where $\dot{V}_{N_2}$ is volumetric N_2 flow rate at NTP and V_m is the Avogadro volume at the temperature at which it was determined (NTP; $24.4\frac{l}{mol}$).

Off-line sampling

The exit stream containing the products, unreacted gases and reference gas (cyclohexane) was sampled by inserting the capillary end of an evacuated ampoule though the septum into the heated product stream at the sampling point. The capillary was then broken inside the sampling device by turning the breaking fork and some of the product vapor was sucked into the previously evacuated chamber of the ampoule. The ampoule was then sealed off using a butane flame and taken for gas chromatograph (Varian 3400) coupled with flame ionization detector (FID). Conditions of the gas chromatographic analyses are given in *Table 3.3.*

Table 3.3: GC-FID operating conditions

Detector	Flame ionisation detector (FID), T=523 K
Column	Column RTx-1 (Restek)
	Fused silica capillary column, 60 m x 0.25 mm
	Stationary phase: 0.5 µm dimethyl siloxane (crosslinked)
Carrier gas	Hydrogen
Introduction gas	Nitrogen
Column head pressure	2.9 bar (absolute)
Injector	Split injector, T = 523 K
	Split ratio 1:20
Temperature program	Initial T = 218 K 1.5 min, isothermal
	At 20K/min to 273 K, 0 min isothermal
	At 14K/min to 373 K, 0 min isothemal
	At 16K/min to 553 K, 23 min isothermal

The FID detector is a carbon specific detector. The carbon atoms show different response depending on to which other atoms they are attached. The carbon atoms attached to the oxygen atoms show a weaker response. The theoretical mass specific response factor proposed by Kaiser (1969) has been used to explicate the difference in carbon response factor depending on the species to which it is attached. Here the response of the carbon atoms not bonded to oxygen is 1 while that bonded to on oxygen atom with one bond is 0.55. The response factor for the carbon atom with a double bond to oxygen is zero. The resulting factor is thus calculated using:

$$f_i = \frac{N_C}{N_{C(no\ O)} + 0.55 \cdot N_{C(O)}} \qquad (3.3)$$

Where N_C is the total number of carbon atoms in a molecule, $N_{C(noO)}$ is the number of carbon atoms not connected to an oxygen atom and $0.55N_{C(O)}$is the number of carbon atoms connected to one oxygen atom via a single bond.

The molar flow rate of an organic compound, n_i, can be derived from results of FID analyses as follows:

$$\dot{n}_i = \frac{N_{CH_X,C}}{N_i} . \frac{f_i . A_i}{f_{CH_X} . A_{CH_X}} . \dot{n}_{CH_X,ref} \qquad (3.4)$$

Where $\dot{n}_i$ is the molar flow rate of compound *i*, $N_{CHX,}$ is the number of carbon atoms in CH_x, N_i is the number of carbon atoms in compound *i*, f_i is the compound *i* response factor, A_i is the peak area of compound *i* in the GC chromatogram, f_{CH4} is the response factor for methane, A_{CHx} is the peak area in the chromatogram and $\dot{n}_{CHx,ref}$ is the molar flow rate of the reference cyclohexane. The yields and selectivity of the product compounds are calculated using:

$$Y_i = \frac{\dot{n}_i}{\dot{n}_{CO,in}} \qquad (3.5)$$

$$S_i = \frac{Y_i}{X_{CO}} \qquad (3.6)$$

Or on a carbon basis

$$Y_{i,C} = \frac{\dot{n}_{i,C}}{\dot{n}_{CO,in}} \qquad (3.7)$$

$$S_{i,C} = \frac{Y_{i,C}}{X_{CO}} \qquad (3.8)$$

The integral Fischer-Tropsch synthesis rate (r_{FT}) can be expressed as follows:

$$r_{FT} = \frac{\dot{n}_{CO,in} - \dot{n}_{CO,out} - \dot{n}_{CO2}}{m_{cat}} \qquad (3.9)$$

Where m_{cat} is mass of the catalyst sample.

4

4. Results

4.1 Synthesis of Co_3O_4 nanocubes

The synthesis of highly dispersed supported cobalt metal catalysts requires the initial formation of small Co_3O_4 crystallites that are to be supported (Suriye *et al*., 2005). The dispersion of these particles before being supported also plays a major role in their porperties. It is desired to synthesize Co_3O_4 nanocubes. The nanocubes will then be modified with tetraethyl orthosilicate mimicking formation strong metal support interaction. The effect of the initial temperature, at which the cobalt precursor salt is added to the precipitation solution, on the morphology of Co_3O_4 nanocubes shall be determined. The effects of rate of mixing of reactants as well as the effect of reaction time on the morphology of Co_3O_4 shall also be determined.

The driving force for both the formation and the growth of crystals is super-saturation. This arises from the concentration of solute exceeding the equilibrium (saturation) solubility concentration. Crystal size and crystal size distribution are dependent on the rate of nucleation and rate of crystal growth. Nucleation is the initiation of a phase change in a small region, such as the formation of a solid crystal from a liquid solution. Nucleation is affected by time allowed for nucleation to occur, the rate of mixing of reactants, and temperature. It could be expected that different crystal size distributions could be obtained by varying the rate at which $Co(NO_3)_2{\cdot}6H_2O$ solution is added to the NaOH solution. It could also be reckoned that desired particle size could be varied by varying the reaction time.

4.1.1 The effect of initial temperature of mixing of reactants

The effect of the initial temperature of mixing of reactant was tested by mixing the reactants at room temperature and at 368 K (reaction temperature). In one experiment, the $Co(NO_3)_2{\cdot}6H_2O$ solution was added to the NaOH solution containing sodium dodecylsulphate at room temperature at the addition rate of 10 mL/min and heated to 368 K. The reaction mixture was then kept at 368 K for 5 hours. In the other experiment, the reagents were first heated to 368 K and then mixed; the $Co(NO_3)_2{\cdot}6H_2O$ solution was added to the NaOH solution containing sodium dodecylsulphate at 368 K at the addition rate of 10 mL/min. The reaction mixture was kept at 368 K for 5 hours. When mixed at room temperature at the addition rate of 10 mL/min, Co_3O_4 formed truncated cubes *(Figure 4.1)* and when reagents were mixed at 368 K, the Co_3O_4 took a cubic geometry (*Figure 4.2)*. The main mechanism for the formation of different geometries is not clear. The crystallite size distribution was modelled using a log-normal distribution (*see Figure 4.3)*. The material synthesized after mixing at room temperature had to be modelled using two distributions. The small sizes contributed to 35% of the crystallites and had an average size of 17.1 ± 4.3nm and the larger 25.6 ± 3.0 nm. Mixing at 368 K results in a distribution which is better described using a single log-normal distribution and the average size is now 23.8 nm ± 4.5 nm.

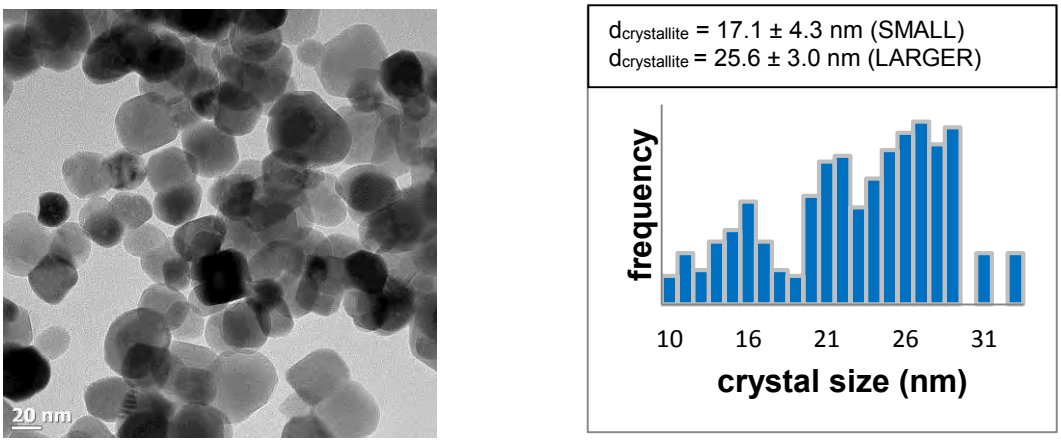

Figure 4.1: The TEM images of Truncated Co_3O_4 nanocubes synthesized by mixing reactants at room temperature, The crystallite size distribution size for the crystals is shown on the right.

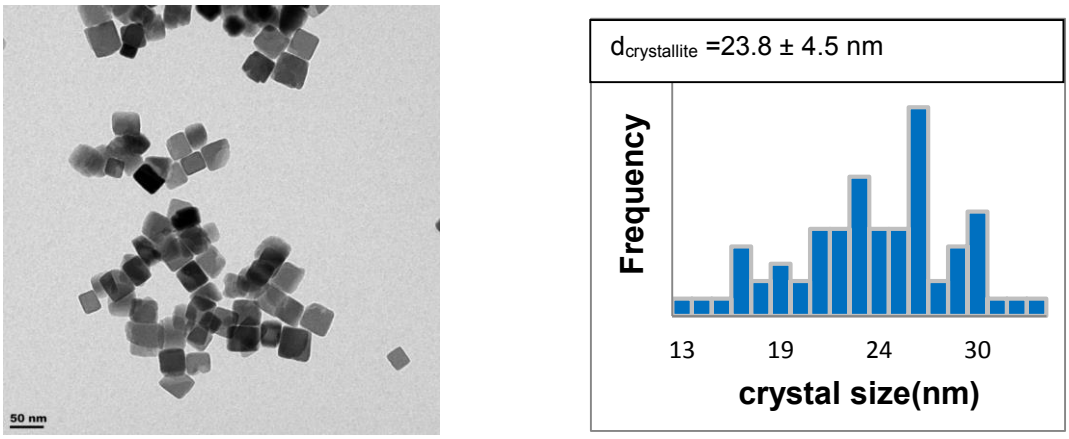

Figure 4.2: The TEM images of Co_3O_4 nanocubes synthesized by mixing reactants at 368 K. The crystallite size distribution for the crystals is shown on the right.

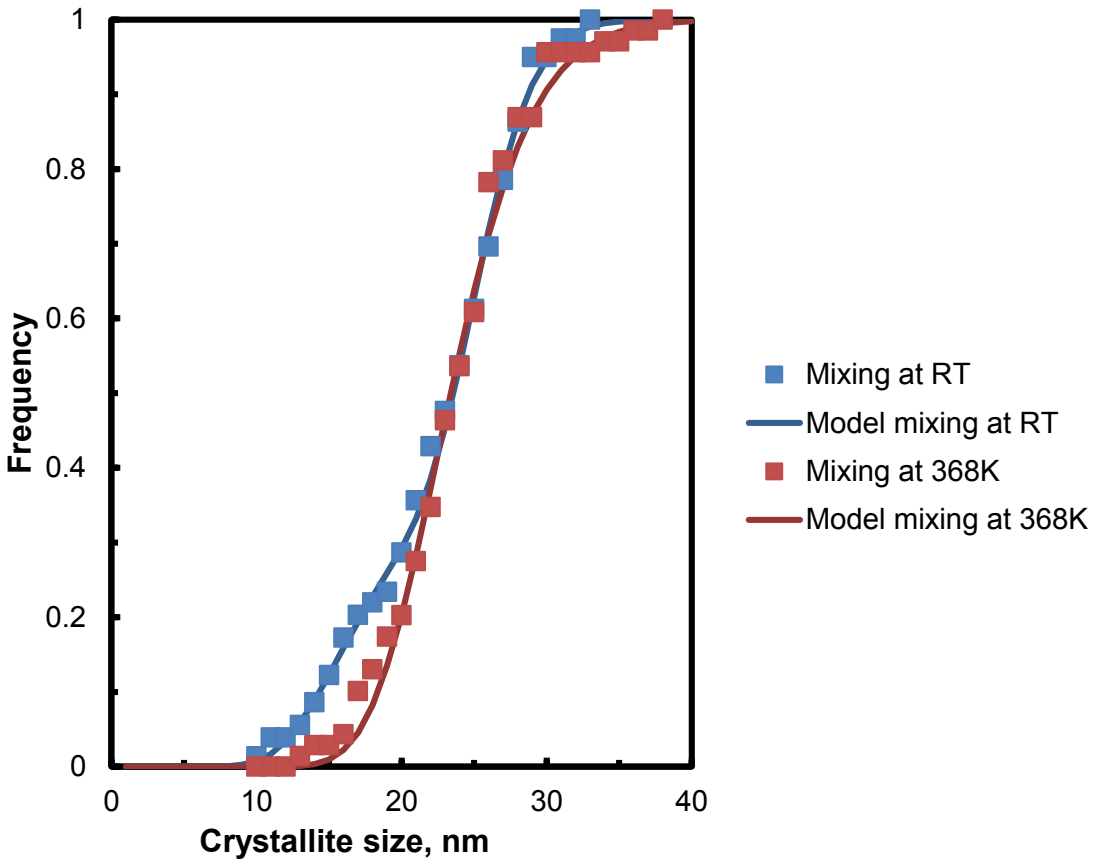

Figure 4.3: Cumulative frequency curves for the modelled log normal size distribution

The different morphology of the Co_3O_4 particles in this experiment could be attributed to different pathways/intermediates through which the Co_3O_4 is formed. When mixing the reagents at room temperature the reaction mixture instantly turned deep blue followed by deep brown and finally black, whereas when mixed 368 K, the reaction mixture remained pink, green, brown, then black. This difference in colour suggests that different routes that result in different intermediate were followed in the crystal growth of the Co_3O_4 nanocubes. However, both the average particle size and the particle size distribution do not seem to be affected by the temperature at which the reagents are mixed.

4.1.2 Effect of rate of addition of $Co(NO_3)_2 \cdot 6H_2O$ to NaOH solution on Co_3O_4 morphology

The effect of the rate of addition of the cobalt nitrate solution to an aqueous solution containing NaOH and sodium dodecylsulphate was investigated at a synthesis temperature of 368 K and a synthesis time of 8 hrs. From the TEM micrographs in *Figures 4.4-4.6* it can be seen that the addition rate of the nitrate solution to the hydroxide (i.e rate of mixing of reactants) can be used to control the morphology of the nano-crystallites. For the slowest addition rate of $Co(NO_3)_2$ solution at 368 K, the average particle size is larger e.g. for the addition rate of 2 mL/min, the average particles size is 30.9 ± 9.2 nm. This difference in average particle size could be attributed to the fact that nucleation starts at the time of contact of reactants. The fastest addition (10 mL/s) resulted in the geometry of the nanocubes becoming indefinite with the average particle size of 20.4 ± 4.5 nm (*see Figure 4.6*). For the addition rate of 10mL/min the average particle size obtained was 49.1 ± 5.3 nm. *Figure 4.7* shows cumulative frequency curves for the modelled log normal size distribution for the Co_3O_4 synthesized at different mixing rates.

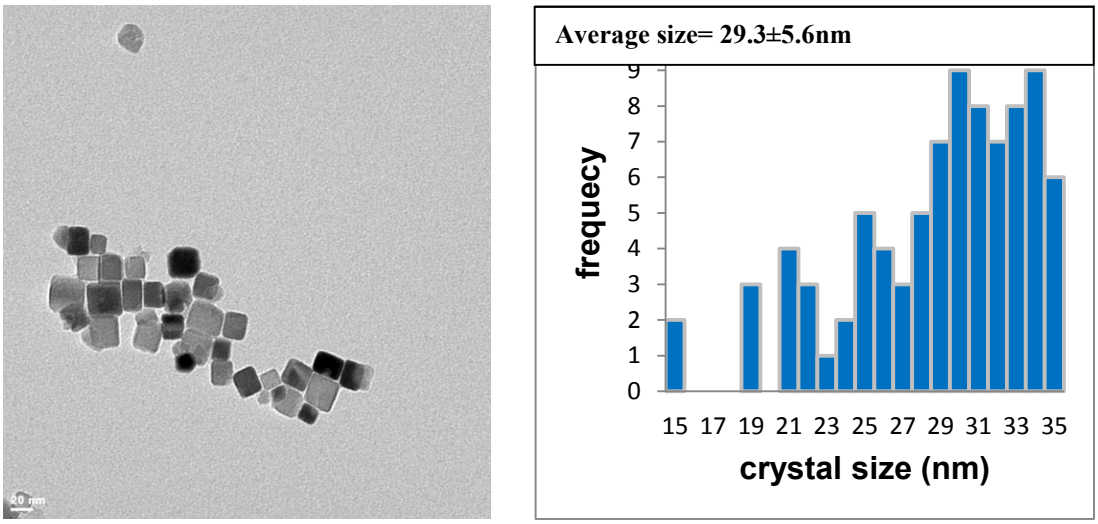

Figure 4.4: Morphological characteristics of Co_3O_4 synthesized at an addition rate of the cobalt nitrate solution 2 mL/min ($T_{synthesis}$ = 368 K; $t_{synthesis}$ = 8 hr).

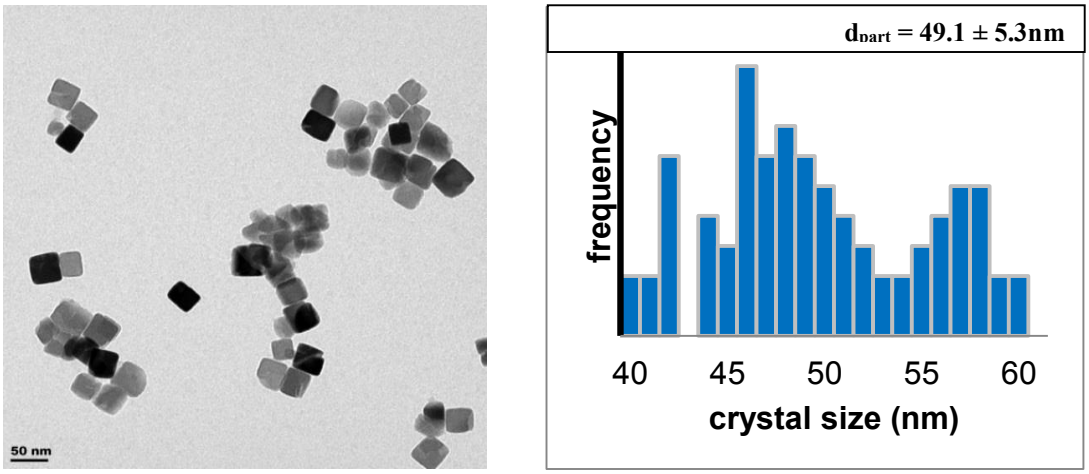

Figure 4.5: Morphological characteristics of Co_3O_4 synthesized at an addition rate of the cobalt nitrate solution 10 mL/min ($T_{synthesis}$ = 368 K; $t_{synthesis}$ = 8 hr).

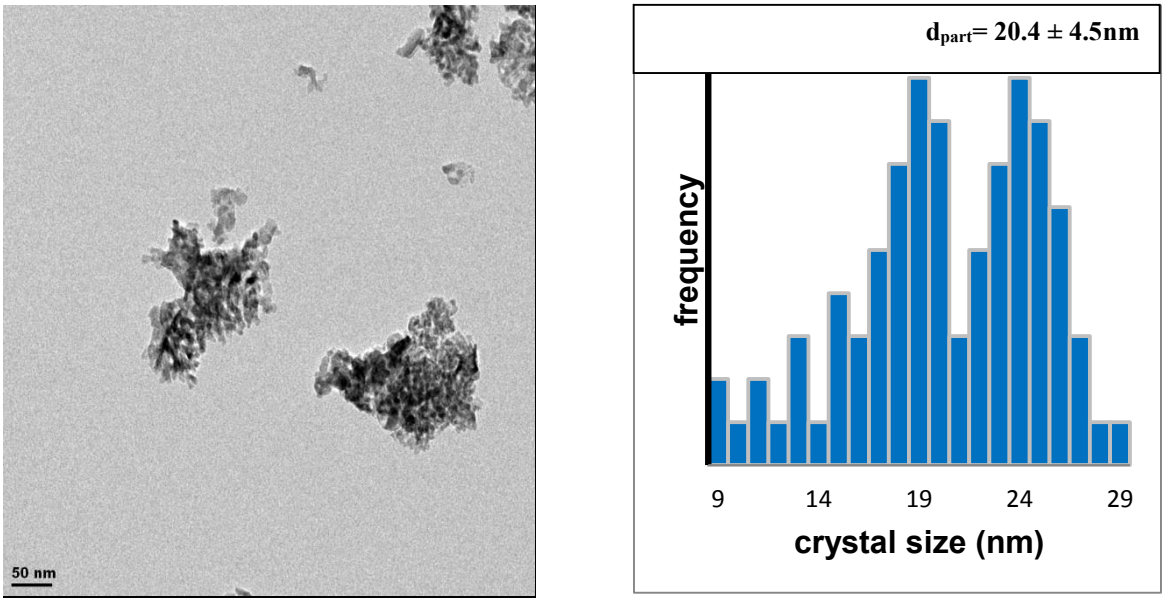

Figure 4.6: Morphological characteristics of Co_3O_4 synthesized at an addition rate of the cobalt nitrate solution 10 mL/s (Tsynthesis = 368 K; tsynthesis = 8hr).

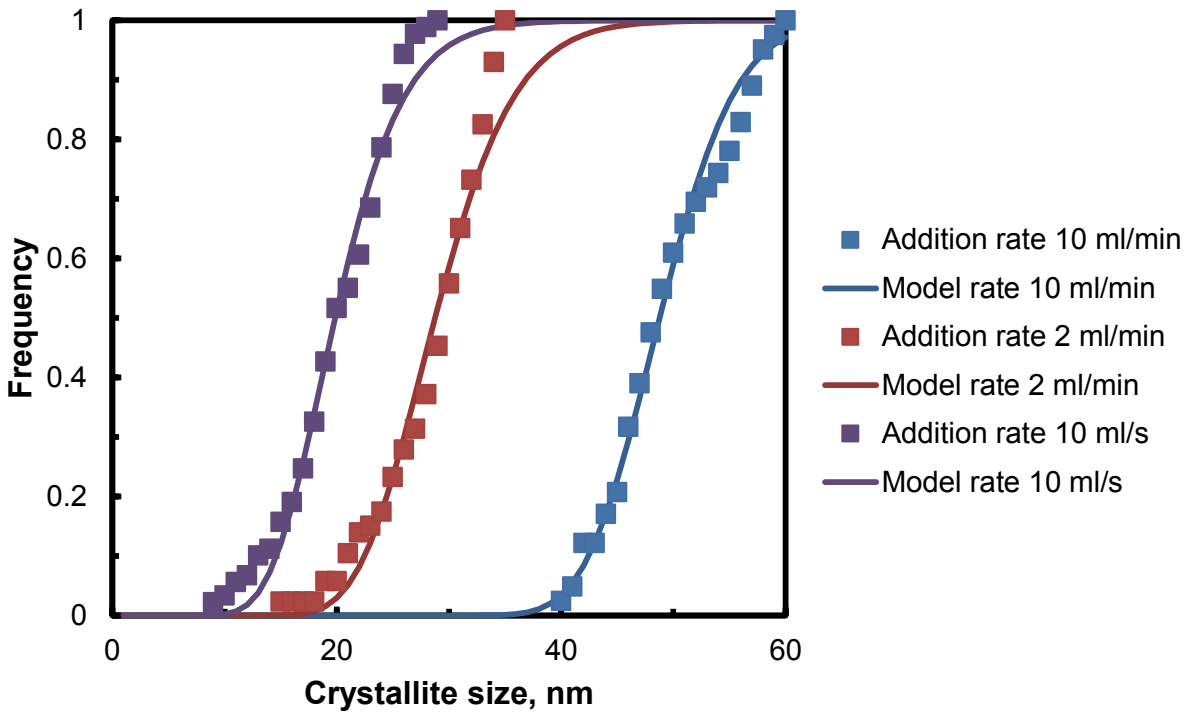

Figure 4.7: Cumulative frequency curves for the modelled log normal size distribution for the Co_3O_4 synthesized at different mixing rates.

4.1.3 Effects of aging time on particle size

Co_3O_4 was synthesised using hydrothermal method that involves the dissolving sodium hydroxide and sodium dodecylsulphate in distilled water and heating to 368 K. Subsequently, a 1.0 M aqueous solution of cobalt nitrate was added. The resulting mixture was kept at 368 K for various time periods (3 hours to 8 hours) in order to obtain different crystallite size. The average crystallite size increases with increasing aging time. Heating for 3 hours results in average particle size of 14.6 ± 1.2 nm, 5 hours result in an average particle size of 23.8 ± 4.5 nm while 8 hours result in 49.1 ± 5.3 nm (see *Figure 4.8, 4.9 and 4.10).* The Co_3O_4 synthesized take a cubic shape. This reduction in agglomeration is attributed to the encapsulation of each particle by sodium dodecylsulphate, thus reduces particle agglomeration. The lack of non-crystalline matter, from both TEM and XRD patterns indicates that the wash with HCl after the synthesis was successful. The XRD pattern observed is of pure crystalline Co_3O_4 (Hou *et al*., 2008).

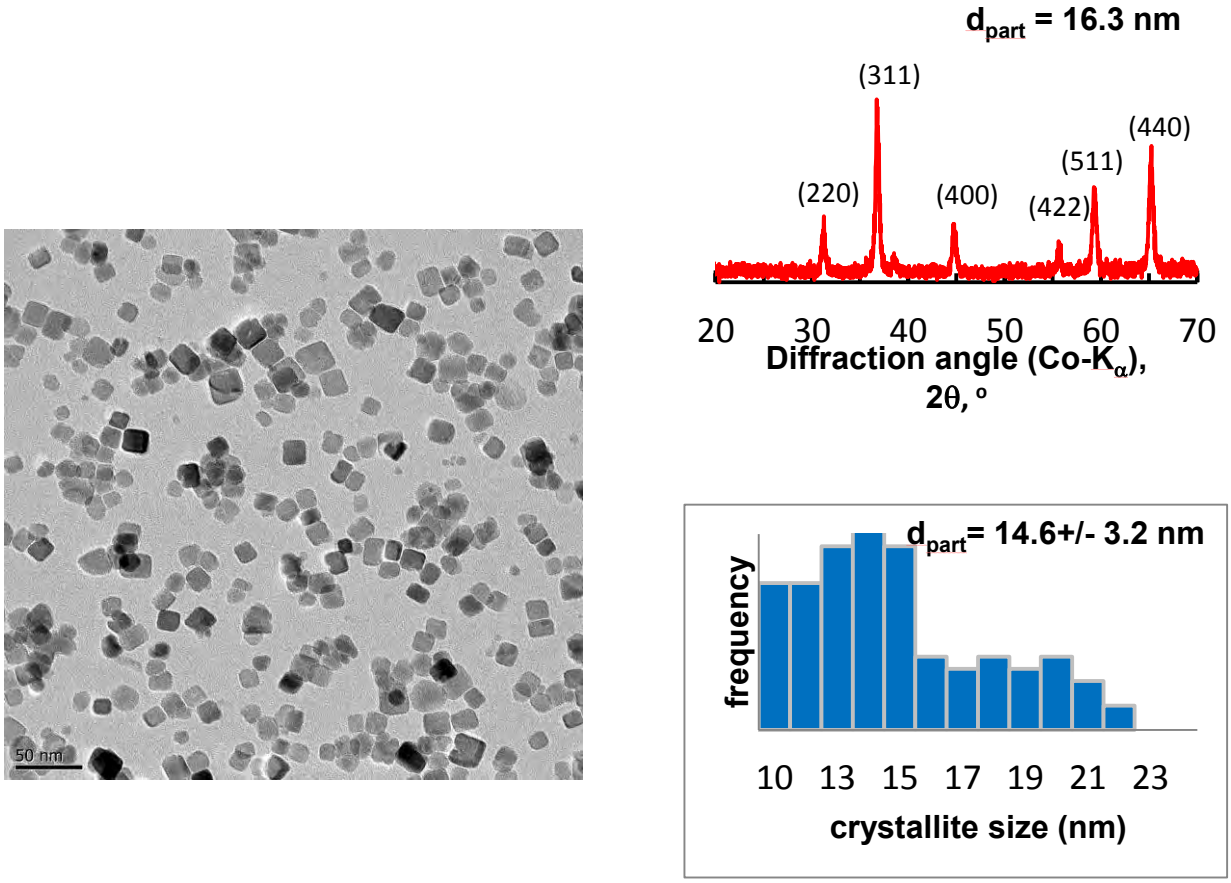

Figure 4.8: Morphology of Co_3O_4 nanocubes synthesized at 368 K for 3 hours (rate of addition of cobalt nitrate solution: 10 mL/min)

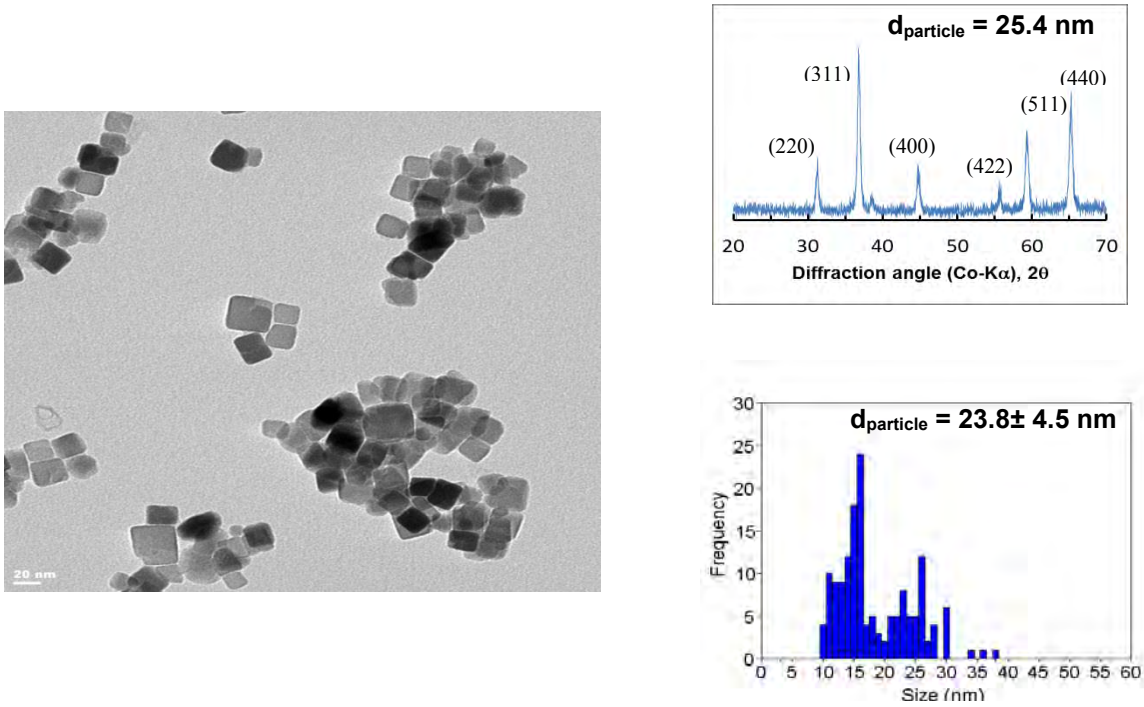

Figure 4.9: Morphology of Co_3O_4 nanocubes synthesized at 368 K for 5 hours (rate of addition of cobalt nitrate solution: 10 mL/min).

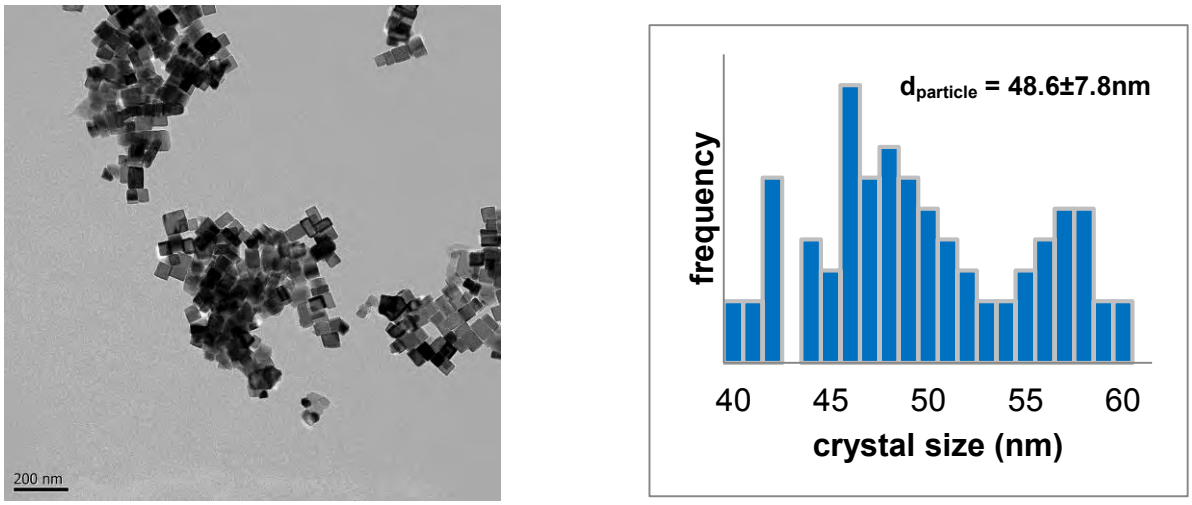

Figure 4.10: Morphology of Co_3O_4 nanocubes synthesized at 368 K for 8 hours (rate of addition of cobalt nitrate solution: 10 mL/min).

The yield of Co_3O_4 nanocubes vary from 20% to 67%. With increasing reaction time, both the yield and the average particle size increase. *Table 4.1* shows the yields obtained at different reaction times. The amount recovered is a function of time. The yield becomes less for samples prepared at short aging time. This is because most of the cobalt is not yet converted into Co_3O_4 but remain in the form of (□-$Co(OH)_2$,$Co(II)(OH)_{2-x}(NO_3)_x{\cdot}nH_2O$, and $Co(II)_{1-x}Co(III)_x(OH)_2(NO_3)_x{\cdot}nH_2O$) and dissolve during the HCl wash. This statement is supported by the fact the largest recovery of 67% was obtained for sample with a size of 50 nm with reaction time of 8 hours. The yield of Co_3O_4 nanocubes has a relationship with aging time as observed from *Figure 4.11.* The yield increases with increasing crystal size. While on the other hand amount recovered is dependent on the time of reaction, allowing more time for the reaction results in increased average particle size. This therefore makes it harder to obtain smaller particle at a higher yield.

Table 4.1: Yield of Co_3O_4 and the resulting average particle size as a function of the synthesis time.

$t_{synthesis}$, hrs	$Y_{Co_3O_4}$, %	$d_{Co_3O_4}$, nm
3	20	14.6±1.2
5	35	24.2±4.2
8	67	49.7±5.4

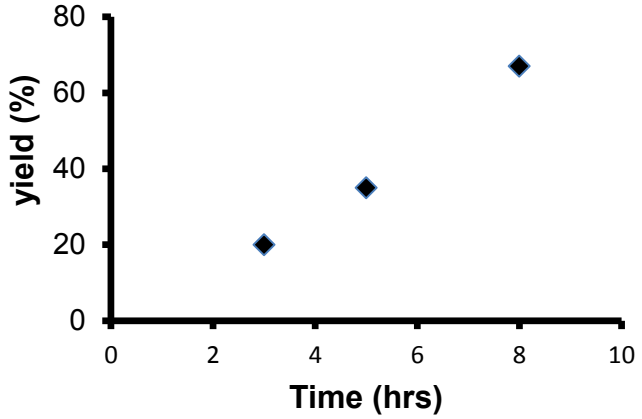

Figure 4.11: Effect of aging time on the yield of recovered Co_3O_4.

4.1.4 Elemental analysis of synthesized Co_3O_4

The composition of the synthesized Co_3O_4 nanocubes was determined using SEM/EDX. The error associated with measurement was computed from 5 line scans of the sample at different selected regions. The SEM/EDX shows the surface of the unmodified Co_3O_4 sample to be composed of cobalt, oxygen and chloride (*see Table 4.2)*. However upon 2 hour heating at 473 K in an oven, the chloride was completely desorbed (possibly as HCl). The molar ratio of cobalt to oxygen in Co_3O_4 is theoretically 3:4 or 42.8:57.2. However, the determined ratio was 40.9:59.1. This increase in the amount of oxygen could be attributed to other oxygen containing compounds such as water on the surface of the catalyst.

Table 4.2: Composition of the prepared Co_3O_4 nanocubes as determined by SEM/EDX

	% atomic composition	
Element	**before calcination**	**after calcination at 473 K**
Co	39.5 ± 6.0	40.9 ± 5.5
O	57.1 ± 5.1	59.1 ± 7.1
Cl	3.4 ± 0.9	0

4.1.5 Summary on the synthesis

The Co_3O_4 nanocubes were synthesized via the sodium dodecylsulphate assisted hydrothermal oxidative precipitation. The phase composition of the as synthesized Co_3O_4 nanocubes was determined using XRD. The morphology of the Co_3O_4 nanocubes is affected by the temperature at which the reagents are mixed, the rate at which they are mixed as well as the time of reaction. The average particle size of the Co_3O_4 can be manipulated by varying the reaction time. The average particle size of the Co_3O_4 is a function of the yield obtained. The minimum average particle size of the Co_3O_4 attained was about 14.6 nm (determined from TEM). However, Co_3O_4 with an average size 23.8 nm were used for further investigation of the metal support interaction. The rationale behind the choice of the 23.8 nm over the 14.6 nm Co_3O_4 nanocubes is that the 23.8 nm cubes were obtained at a relatively higher yield.

4.2 Surface Modification of Co_3O_4 with TEOS

The surface modification of Co_3O_4 nanocubes may occur through the reaction of the surface hydroxyl groups on the Co_3O_4 surface with the silanes via the inorgano-functionalization where silane anchors on the Co_3O_4 surface through the formation of Co-O-Si bond. In the modification process, Co_3O_4 (0.5 g) was re-suspended in n-hexane (300 mL). 50mL of 1% vol/vol (40mM) solution of TEOS in n-hexane was subsequently added to the suspension containing Co_3O_4 to make a total volume of 350 mL and mixed for 5 hours. The concentration of TEOS in the final suspension then became 6.0 mM. The concentration of TEOS was kept low to avoid self-condensation of the TEOS.

4.2.1 Modelling the rate of TEOS uptake

The composition of the TEOS treated samples was also determined using SEM/EDX after different contact times of the tetraethyl orthosilicate containing solution and the Co_3O_4 nano-cubes (*see Appendix 9.4 for sample EDX graph).* The Si/Co mol ratio was determined as function of the time for adsorption (see *Figure 4.12).* The TEOS loading on the Co_3O_4 increases with increasing time for adsorption reaction for the first 5 hours. Equilibrium was virtually attained after 5 hours of silylation using an initial concentration of 6.0 mM of TEOS in as an initial concentration. The equilibrium mol ratio is ca. 0.06 mol Si/mol Co. The rate of tetraethyl orthosilicate uptake as a function of time was modelled as a first order reaction, viz.

$$\boldsymbol{TEOS} + * \rightleftharpoons \boldsymbol{TEOS}*$$

Hence the rate of uptake can be modelled as:

$$\frac{d\theta_{TEOS}}{dt} = k_1 \cdot [TEOS] \cdot \theta_* - k_{-1} \cdot \theta_{TEOS}$$

And hence the Si/Co ratio as a function of time is given by:

$$\frac{Si}{Co} = \left(\frac{Si}{Co}\right)_{max} \cdot \frac{1 - e^{-(k_1 \cdot [TEOS] + k_{-1}) \cdot t}}{1 + \frac{k_{-1}}{k_1 \cdot [TEOS]}}$$

A best, physically realistic fit was obtained with k_{-1}=0 (including k_{-1} in the fit resulted in negative values for this rate constant). The obtained fit is shown in Figure 4.12 and the obtained fitting parameters are given in Table 4.3. It should be noted that the fit is not good. This can be mainly attributed to the increase in the rate of TEOS-uptake observed between 1 and 3 hours implying some autocatalytic process. An attempt to model the uptake as an autocatalytic reaction did not result in a significant improvement in the fit of the data

Table 4.3: Modelling the rate of uptake of tetraethyl orthosilicate on Co_3O_4 using

$$\frac{Si}{Co} = \left(\frac{Si}{Co}\right)_{max} \cdot \frac{1 - e^{-(k_1 \cdot [TEOS] + k_{-1}) \cdot t}}{1 + \frac{k_{-1}}{k_1 \cdot [TEOS]}}$$

	Langmuir-isotherm[1]
k_1·[TEOS], hr^{-1}	0.37 ± 0.17
$(Si/Co)_{max}$, mol/mol	0.66 ± 0.11
R^2	0.9318
Variance	42.5

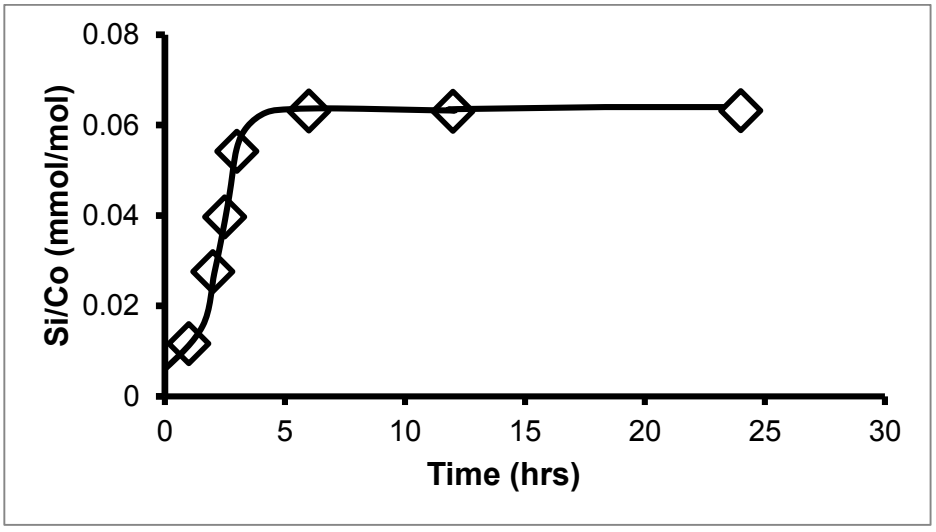

Figure 4.12: Effect of contact time on silylation of Co_3O_4

4.2.2 Uptake of TEOS as a function of concentration

Different initial concentrations of TEOS were used for the silylation process to determine the effect of the concentration of TEOS on the uptake of tetraethyl orthosilicate by Co_3O_4 nano-cubes. In all experiments the contact time between the Co_3O_4 nanocubes and the solution containing tetraethyl orthosilicate was kept constant at 5 hours as it is the time where maximum uptake was observed at highest initial TEOS concentration i.e 6.4 mM TEOS in n-hexane. The initial concentrations used were 6.40 mM, 1.60 mM, 0.64 mM, 0.26 mM, 0.13 mM. Lowering the initial concentrations resulted in lower surface coverage. The obtained silicon loading of the model catalyst varied from 0.003 mol Si/mol Co to 0.06 mol Si/mol Co (*Table 4.4)*.

Table 4.4: Effect of initial concentration of TEOS on the final uptake on the surface of Co_3O_4

$[TEOS]_{initial}$ (mM)	**$[TEOS]_{final}$[1] (mM)**	**Si loading (mol Si/mol Co)**
6.40	5.79	0.060
1.60	1.40	0.030
0.64	0.58	0.009
0.22	0.23	0.006
0.13	0.12	0.003

[1] The final concentration of TEOS in the suspension was calculated using the initial concentration of TEOS, the uptake of TEOS and the initial mass of Co_3O_4 added: $[TEOS]_{final} = \frac{V(350ml)\cdot[TEOS]_{initial} - 3\cdot\frac{m_{Co_3O_4}}{M_{Co_3O_4}\left(240.8\frac{g}{mol}\right)}\cdot\left(\frac{Si}{Co}\right)_{sample}}{V(350ml)}$

Figure 4.13 shows the graph of Si/Co mol ratio against equilibrium final concentration of TEOS. The final TEOS concentration was determined by calculating the difference between the amount of TEOS in the initial suspension and the amount adsorbed onto Co_3O_4 nanocubes as determined from SEM/EDX (see *Appendix 9.4.)* The uptake of the TEOS on the Co_3O_4 seems to follow a Langmuir-type of behaviour obtaining saturation at high coverage. The uptake curve can either be described using a Langmuir isotherm or more accurately an isotherm involving more than one tetraethyl orthosilicate molecule per 'site'. The variance indicates that from a statistical view point more than one tetraethyl orthosilicate molecule is adsorbed per 'active' site on Co_3O_4. However, the accuracy of fit depends highly on the accurate determination of the

Si/Co-ratio in these samples. A measurement at high concentration of TEOS is needed to confirm a maximum uptake of TEOS by Co_3O_4 of ca. 0.067 mol/mol.

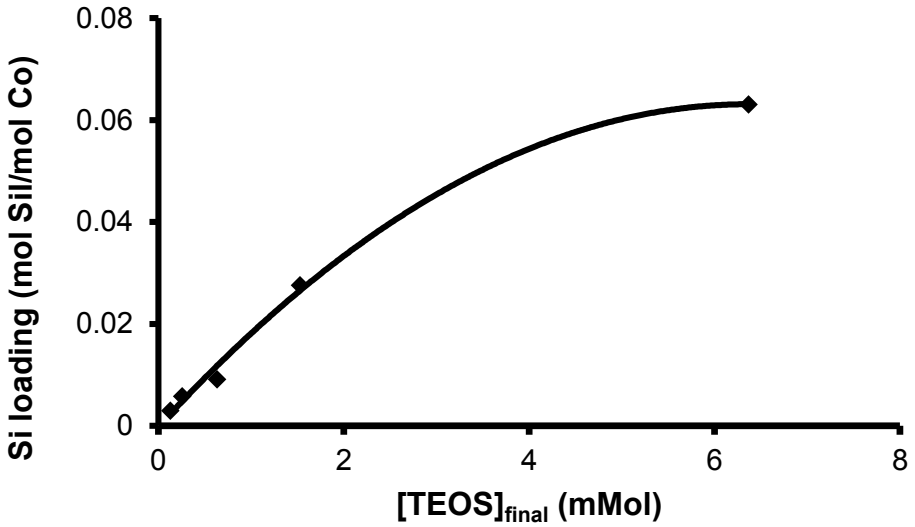

Figure 4.13: Uptake of tetraethyl orthosilicate on Co_3O_4-nanocubes as a function of the final concentration of tetraethyl orthosilicate in the solution (as determined from the difference between the initial concentration and the amount of silicon taken up by the nanocubes).

Table 4.5: Modelling the uptake of tetraethyl orthosilicate on Co_3O_4

	Langmuir-isotherm[1]	Multiple uptake of TEOS[2]
K, mM^{-n}	0.44 ± 0.21	0.89 ± 0.06
n	1	1.68 ± 0.08
$(Si/Co)_{max}$	0.092 ± 0.021	0.067 ± 0.001
R^2	0.9731	0.9997
Variance	$1.5 \cdot 10^{-5}$	$2.1 \cdot 10^{-7}$

1 $$\frac{Si}{Co} = \left(\frac{Si}{Co}\right)_{max} \cdot \frac{K \cdot [TEOS]_{final}}{1 + K \cdot [TEOS]_{final}}$$

2 $$\frac{Si}{Co} = \left(\frac{Si}{Co}\right)_{max} \cdot \frac{K \cdot [TEOS]^{n}_{final}}{1 + K \cdot [TEOS]^{n}_{final}}$$

4.2.4 Effects of surface silylation on phase composition

The phase composition of the model catalysts after silylation was determined using XRD. The most intense peaks in the spectra occur at 2θ angles of 21.98, 36.35, 43.05, 43.83, 52.39, 64.39, 70.04 and 77.40 which are characteristic diffraction lines of spinel Co_3O_4 using a Co-K_α source (Eva software, CCD). All peaks correspond to Co_3O_4 diffraction planes thus showing the only phase present is Co_3O_4. The diffraction patterns do not show any evidence for a change in the phase composition (see *Figure 4.14)* as only the peaks for crystalline Co_3O_4 are seen in all the samples. It should be noted that even the presence of amorphous silica, which is typically noted by a broad, diffuse band at ca. 2θ = 22º (de Souza *et al*., 2000) could not be observed. This might be due to the relative small amount of silica present in the samples.

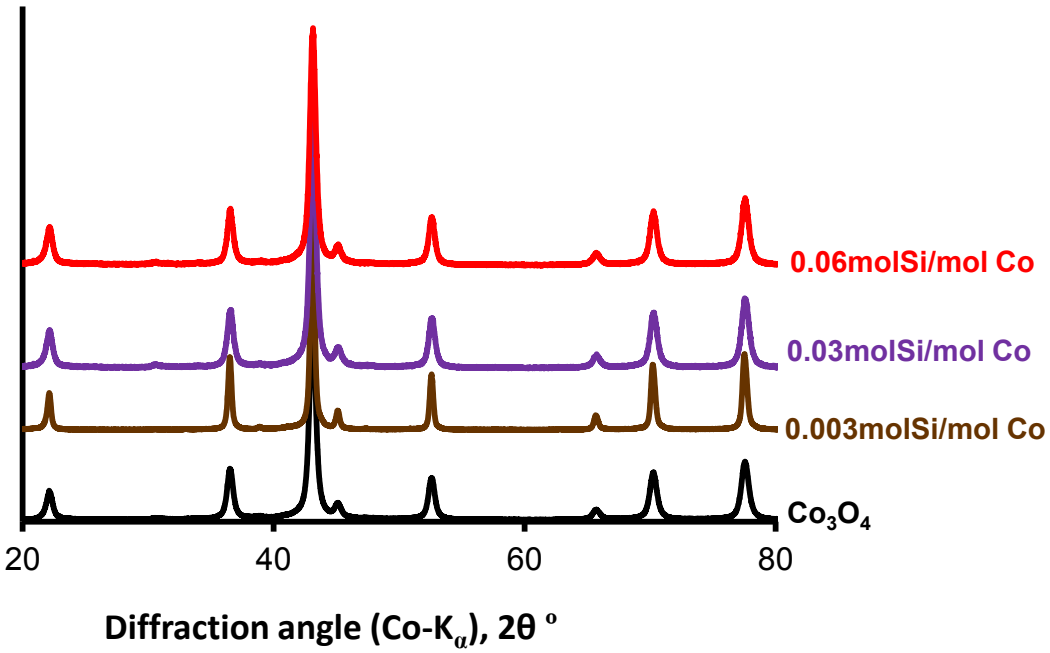

Figure 4.1: XRD pattern of the model catalyst with different silicon loading.

Topas was used to analyse average crystal size of the Co_3O_4 phase in the model catalysts (see *Table 4.6)* The error associated with measurement was determined by repeating the XRD analysis of the samples three times. The average crystal size of the samples is not affected by surface silylation.

Table 4.6: Crystallite size of the model catalyst determined from XRD-line broadening analysed using Topas.

Si loading (mol Si/mol Co)	$d_{Co_3O_4}$ (nm)
0	24.5±0.8
0.003	25.1±1.7
0.030	26.1±0.7
0.060	23.9±1.2

4.3 Supporting Co_3O_4 on β-SiC-microspheres

The samples were dispersed on SiC microspheres prior to testing their activity in the Fischer-Tropsch synthesis. A variety of liquids was attempted to re-disperse the Co_3O_4-nanocubes on to silicon carbide. Only dispersing the nanocubes into in a mixture of 10 % oleic acid in n-hexane together with β-SiC microspheres followed by ultra-sonication for 1 hour, drying at 393 K for 2 hours and calcination at 573 K for 3 hours in an oven utilizing a heating ramp of 3 K/min resulted in a reasonable dispersion of Co_3O_4-nanocubes on β-SiC (see *Figure 4.15*).

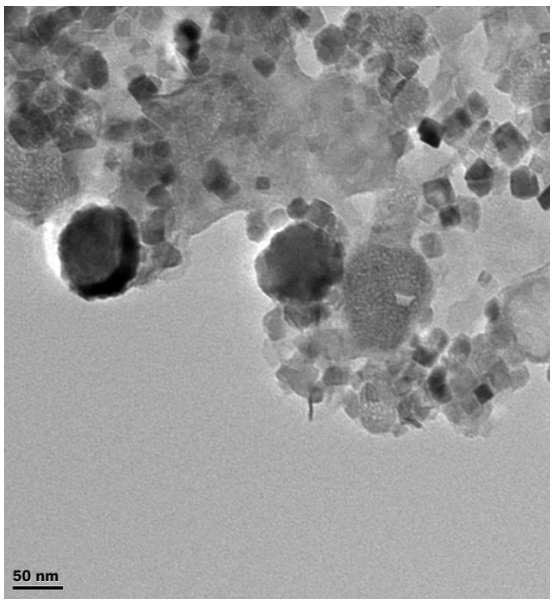

Figure 4.2: TEM images for Co_3O_4 –nanocubes (d_{Co3O4} = 25 nm) supported on b-SiC microspheres after re-suspending the nanocubes in a solution of 10% vol/vol (oleic acid in n- hexane).

4.4 Characterization of the model catalysts

4.4.1 Confirmation of presence of Co-O-Si bonds in model catalysts

The aim to this study is to understand the effect of strong metal support interactions via the ligand model on the physical characteristics, the reducibility and the performance of these materials in the Fischer-Tropsch synthesis. Hence, the formation of the bonds resembling the interface between the metal and the support should be confirmed. FTIR was used to confirm the presence of Co-O-Si bonds both prior to and after reduction. For *exsitu* studies, the sample was prepared by diluting 0.5 mg of the model catalyst with 0.2 g of KBr and then pressed into translucent pellets. The FTIR was recorded in the transmission mode. A total of 1200 scans were taken in the range between 400 and 4000 cm^{-1} at the resolution of 8 cm^{-1} with KBr as the background.

An *insitu* FTIR reduction study was also carried out to determine whether the Co-O-Si bond remains intact after H_2 reduction. The KBr diluted model Co_3O_4 catalyst (0.5 mg Co_3O_4 in 0.2 g KBr) were placed in the sample holder of the Praying Mantis high temperature chamber after a background scan of pure KBr was taken. An infrared spectrogram was immediately taken at room temperature with 500 scans at a resolution of 8 cm^{-1}. The temperature of the cell was then raised to 623 K at a ramp rate of 5 K/min in the presence of hydrogen (flow rate 40 mL/min (NTP)) to reduce the catalyst.

Confirmation of presence Co-O-Si bond prior to reduction

The presence of Co-O-Si and Si-O-Si upon treatment of Co_3O_4 surface with tetraethyl-orthosilicate was confirmed using Fourier transform infrared spectroscopy (FTIR). *Figure 4.16* shows the FTIR spectra of the pure Co_3O_4 as well as TEOS treated samples in the range of 500-700 cm^{-1}. This range was taken to confirm the presence of Co_3O_4 (Fouad *et al*., 2011). The band at 580 cm^{-1} is attributed to the vibrations of the Co-O stretch and the one at 668 cm^{-1} is due to the stretching vibrations of Co(III)-O bonds in Co_3O_4 lattice (Fouad *et al*., 2011). For the surface silylated samples, the peak at 668 cm^{-1} has a shoulder at 661 cm^{-1}. This shoulder is a band that is also reported by Fouad *et al*. (2011) as the peak attributed to the bending vibrations of Co-O-Si bond. It is evident that with increasing loading of TEOS, the intensity of this shoulder increases

resulting into a prominent peak at 661 cm^{-1}. It is difficult to identify this band as it overlaps with the band due to vibrations of Co(III)-O stretch in the Co_3O_4 lattice. The peak at 560 cm^{-1} is also due to the vibrations Si-O stretch (Kunarti and Moran, 2008). The Si-O band intensity increases with increasing loading of TEOS

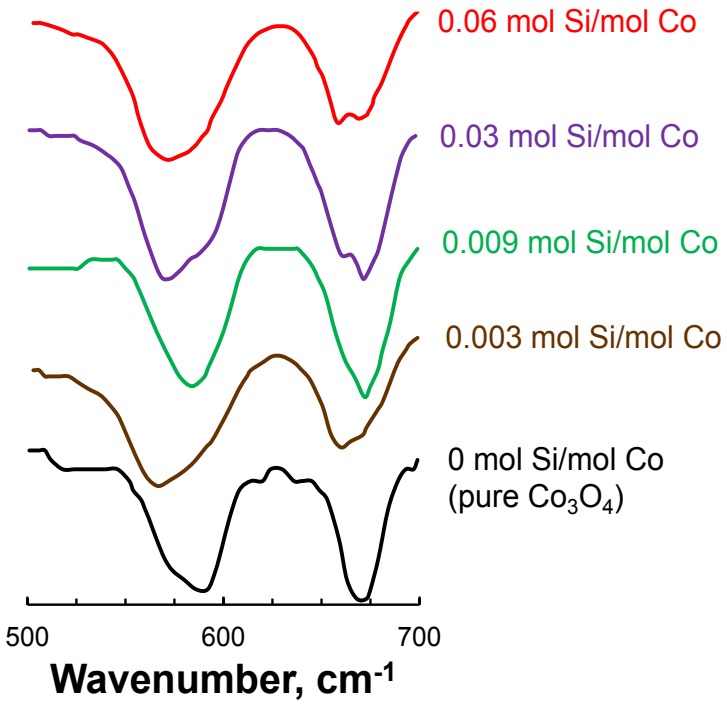

Figure 4.3: FTIR spectra of the calcined model catalyst in the range 500-700 cm^{-1}.

Figure 4.17 shows the FTIR spectra of samples in the range of 1200-700 cm^{-1}. The intensity of the bands at 1100 cm^{-1}, 1020 cm^{-1} and 800 cm^{-1} is minimal in the sample containing pure Co_3O_4. There are three bands, which are more pronounced in the samples which were contacted with a solution containing tetraethyl orthosilicate. The band at 1020 cm^{-1} is ascribed to the stretching vibrations of Co-O-Si bond (Kababji *et al*., 2009). The intensity of this adsorption band increases with increasing TEOS loading suggesting that the extent of Co-O-Si bond formation is dependent on TEOS loading as is the case with the peak at 661 cm^{-1} shown in *Figure 4.16.* The 1020 cm^{-1} peak is attributed to the formation of cobalt silicates by Puskas *et al*. (1992) in the silica supported cobalt system. However, the major bands due to cobalt orthosilicates at 900 cm^{-1} and 935 cm^{-1} as reported by Jong and Cheng (1995) are not observed. Thus it may be concluded that Co-O-Si bonds are present in these samples, but not as bulk Co_2SiO_4.

The bands at 1100 cm^{-1} and 800 cm^{-1} agree with the presence of SiO_2 (Feng *et al*., 2003; Huang and Chen, 2004; Yin *et al*., 2009). The band at 1100 cm^{-1} is attributed to the asymmetric stretching of the Si-O-Si of the amorphous SiO_4 tetrahedron (Huang and Chen, 2004) whilst that at 800 cm^{-1} is attributed to the bending vibrations of the Si-O-Si that resulted from the oxygen atom motion between the Si-O-Si plane and along Si-O-Si angle bisector (Yin *et al*., 2009; Shukla *et al*., 2011). It can thus be concluded that SiO_2 is present in the samples. With increasing content of the TEOS, the intensity of the absorption bands corresponding to Si-O-Si bonds increases (just like the adsorption band ascribed to the presence of Co-O-Si-bonds). The band assigned to Si-OH at 960 cm^{-1} by Fouad *et al*. (2011) is not observed in any of the samples. This implies that during the calcinations step all the $Si(OH)_4$ from TEOS was transformed to SiO_2.

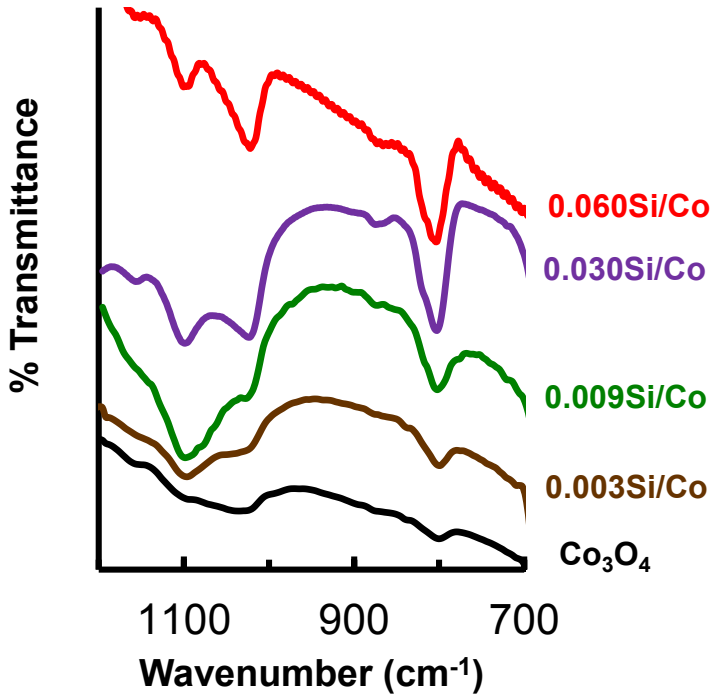

Figure 4.4: FTIR spectra for pure Co_3O_4 as well as TEOS modified Co_3O_4 in the range of 1200-700 cm^{-1}.

Presence of Co-O-Si bonds after reduction

Insitu FTIR studies were carried to determine the behaviour of the catalyst upon reduction as well as to confirm the presence of Co-O-Si after reduction. The KBr diluted 0.06 mol Si/mol Co catalyst sample was placed in the sample holder of the Praying Mantis high temperature chamber after a background scan of pure KBr was taken. An infrared spectrogram was immediately taken at room temperature with 500 scans at a resolution of 8 cm^{-1}. The temperature of the cell was then raised to 623 K at a ramp rate of 5 K/min in the presence of hydrogen (flow rate 40 mL(NTP)/min) to reduce the catalyst. The temperature was held at 623K for 16 hours. *Figure 4.18* shows the FTIR spectra of a 0.06 mol Si/mol Co prior and after the reduction in hydrogen at 623 K. The band at 580 cm^{-1} attributed to the vibrations of the Co-O stretch and the one at 668 cm^{-1} due to the vibrations of Co(III)-O bonds in Co_3O_4 reported by Fouad *et al*. (2011) disappear after the reduction process (albeit not completely). The reason for the disappearance of the peaks is due to the reduction of the Co_3O_4 species. However, the band at 1020 cm^{-1}, which is thought to be due to Co-O-Si vibrations as reported by Puskas and co-workers (1992) persists and remains intact after reduction. This implies that the interaction between Co-O-H and Si-OH (producing Co-O-Si) was strong enough to withstand high temperature reduction conditions in hydrogen.

The band at 1100 cm^{-1} attributed to the asymmetric stretching of the Si-O-Si of the amorphous SiO_4 tetrahedron (Huang and Chen, 2004) and that at 800 cm^{-1} attributed to the bending vibrations of the Si-O-Si that resulted from the oxygen atom motion between the Si-O-Si plane and along Si-O-Si angle bisector (Yin *et al*., 2009; Shukla *et al*., 2011) also remain intact after reduction.

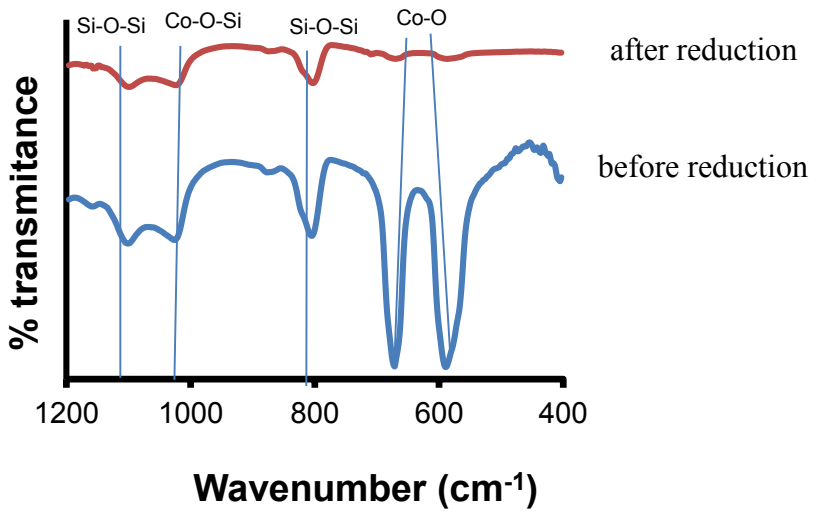

Figure 4.5: FTIR spectra of 0.06 mol Si/mol Co sample before and after reduction at 623K for 16 hours.

4.4.2 Effect of TEOS treatment on Co_3O_4 morphology

The samples modified with tetraethyl-orthosilicate were also characterized using TEM to determine the effect of surface modification on the Co_3O_4 nanocubes. Due to the low concentrations of silica on the surface of Co_3O_4, presence of the crystalline or amorphous silica on the surface of the nanocubes could not be confirmed using TEM. *Figure 4.19* shows the TEM micrographs of unmodified Co_3O_4 nanocubes with its crystal size distribution and *Figure 4.19* shows TEM micrograph of TEOS treated Co_3O_4 nanocubes at maximum loading of TEOS with is crystal size distribution. Both the shape and the size of the Co_3O_4 nanocubes were not affected by the TEOS surface modification of Co_3O_4. In order to determine if there was any amorphous silica present on the surface of the nanocubes, high resolution TEM should be used.

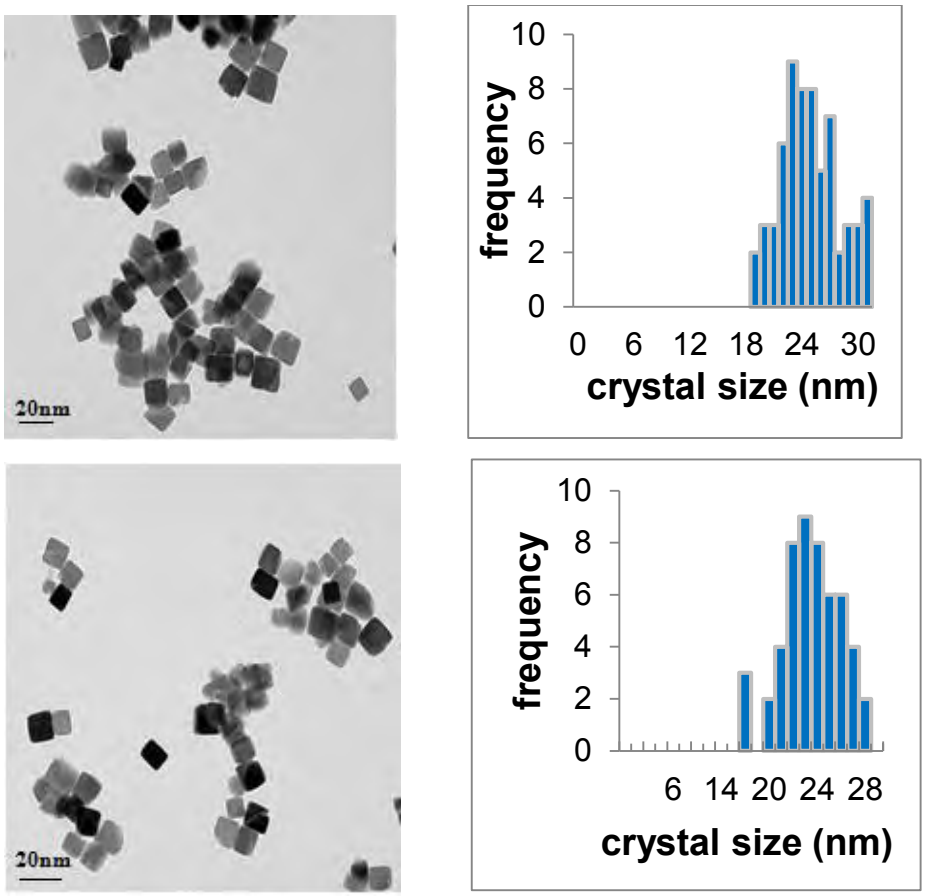

Figure 4.19: TEM micrographs of the synthesized unmodified (left top), 0.06 mol Si/mol Co sample (left bottom). The respective particle size distribution is shown on the right.

4.4.3 Reduction behaviour of the model catalysts

The reduction behaviour of the Co_3O_4 model catalysts was studied using temperature programmed reduction (TPR). 30 mg of each Co_3O_4 sample was loaded into a quartz reactor. Argon (50 mL/min (NTP)) was flown over the sample for 60 minutes at 393 K in order to degas the sample and to remove excess moisture and other contaminants from the sample. The temperature was reduced to 340 K and the gas was changed to 5% H_2/Ar (v/v) flowing at 50 mL/min (NTP). The temperature was increased from 340 K to 1100 K using a constant heating rate (5, 10 or 15 K/min).

The TPR profiles (*Figure 4.20)* of both TEOS treated Co_3O_4 and pure Co_3O_4 show two reduction peaks. For the Co_3O_4 sample, two peaks are observed at 610 K and at 675 K. These peaks, however, are not well separated and eventually occur as a single peak. This reduction peak occurs as the result of the reduction of Co_3O_4 to CoO (610 K) and the reduction of Co_3O_4 to CoO (675 K).

It is observed that the TEOS retards all the reduction steps. At a heating ramp of 10 K/min, these peaks shift to higher temperatures with silylation. With a 0.003 mol Si/mol Co samples, the reduction peaks shifted to 709 K. With further increase in silica loading to 0.06 mol Si/mol Co mol/mol (which corresponds to equilibrium coverage), the reduction temperature further increases to 753 K. This shift to higher reduction temperatures could be due to strong metal-support interactions.

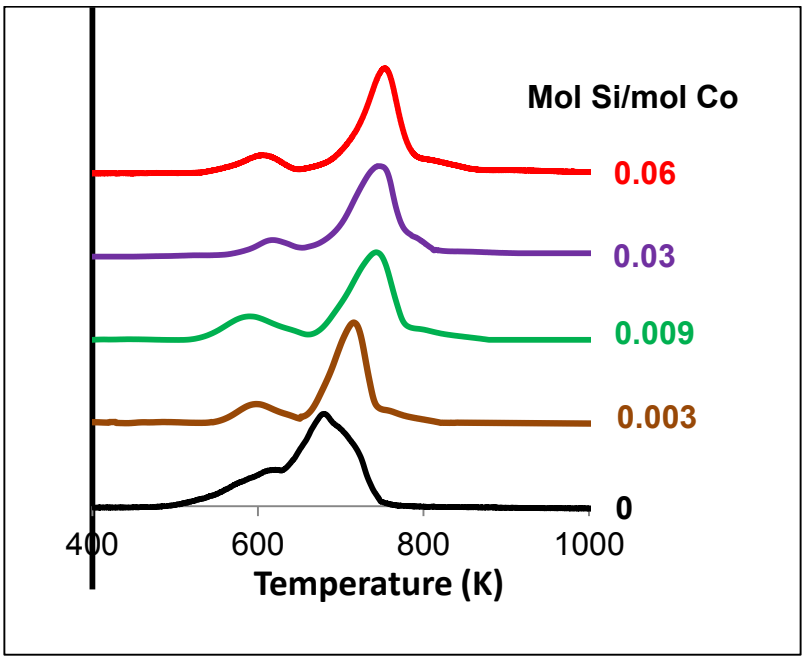

Figure 4.20: TPR profiles for Co_3O_4 and TEOS modified Co_3O_4 using a heating ramp of 10 K/min

A typical TPR profile of Co_3O_4 has two reduction peaks (Xie *et al*., 2011). The first reduction peak around 600 K occurs due to the reduction of Co_3O_4 to CoO while the second reduction peak around 690 K resemble the reduction of CoO to metallic cobalt as shown by *Equations 4.2 and 4.3* (Xie *et al*., 2011). It should be noted that the heating rate was 5 K/min.

$$Co_3O_4 + H_2 \longrightarrow 3CoO + H_2O \qquad \Delta H_r = -225.5\ kJ \qquad (4.2)$$

$$CoO + H_2 \longrightarrow Co + H_2O \qquad \Delta H_r = -47.6\ kJ \qquad (4.3)$$

Typically, the ratio of the hydrogen consumed in the first reduction step to that consumed in the second reduction step is the range of 1:3. The amount of hydrogen

consumed in the first reduction peak was 0.40 mmol H_2/mmol 0.003 mol Si/mol Co. That is only 40% of the expected amount, if the first step corresponds to the reduction of all Co_3O_4 to CoO. For all modified samples, the hydrogen consumption for the first reduction step also remains at 0.4 mol H_2/mol Co_3O_4. This could only be ascribed to the reduction of nitrates rather than the reduction of Co_3O_4. The amount of hydrogen consumed in the combined second and third reduction peak for the unmodified sample is 3.6 mmol H_2/mmol Co_3O_4. It can be suggested that the reduction of Co_3O_4 to CoO occurs concomitantly with the reduction of CoO to Co resulting into a single peak or rather a peak with a shoulder. However, for the modified samples, the hydrogen consumed in these combined reduction steps decreases with increasing silica loading. The comparison was done for the heating rate of 10 K/min after a reduction time of 45 minutes corresponding 800 K. A similar trend is observed for the same samples treated at different heating rates (5 K/min and 15 K/min). There is no particular trend, however, that is observed in terms of hydrogen consumption when comparing the hydrogen consumption of each sample at different heating rates.

The overall hydrogen consumption per sample has been calculated by integrating the area under each reduction peak. the hydrogen consumptions of the two reduction steps due to the reduction Co_3O_4 was determined by integrating the area after 45 minutes (corresponding to 800 K). At 800 K, any cobalt silicate present in the sample (if any), would still remain irreducible. The degree of reduction was determined from the total hydrogen consumption by integrating the area under the graph. For the pure sample of Co_3O_4 a 98% reduction is achieved. For the 0.003 mol Si/mol Co, Co, 0.009 mol Si/mol Co, 0.03 mol Si/mol Co and 0.06 mol Si/mol Co samples, the respective reduction degree achieved is 95, 94, 93, and 92%. This implies that the formation of Co-O-Si interface on the surface affects the degree of the second step of reduction. The incomplete reduction up to a temperature of 800 K might be due to the formation of a hard o reduce Co-O-Si bond. It can further be seen that the reduction peaks become broader with surface modification of samples with TEOS. This observation is explained by Xie *et al*. (2011) and Rosynek and Polansky (1991) as due to the difficulty reduce the Co_3O_4 due to the strong interaction between Co_3O_4 and surface silicate.

It is further observed that for all model catalyst samples, the total hydrogen consumed approaches 100% from 400 K to 1000 K in a time of 1 hour with a heating rate of 10 K/min. However, the hydrogen consumption varies with different heating rates. For the heating rate of 5 K/min the total hydrogen consumption for the unmodified sample is 100% while for the 15 K/min it is determined to be 98.1%. The TPR profile obtained for the model catalyst is not a normal two-stepped reduction. A quantitative analysis of the hydrogen consumed in the reduction of Co_3O_4 nanocubes shows that the amount of hydrogen consumed for the second reduction peak is ca. six to seven times larger than the amount of hydrogen consumed for the first reduction peak. It is observed from the TPR profile (see *Figure 4.21)* that the total hydrogen consumption in the first reduction step is lower than the theoretically expected consumption in all samples. From *Table 4.7,* the ratio of hydrogen consumed in the first reduction stage to that consumed in the second reduction step is 1:7.5 instead of 1:3 for the unmodified Co_3O_4 sample. This could not be due to incomplete reduction of Co_3O_4 to CoO in the first step the first reduction peak exists as an distinct peak rather than a shoulder, thus the first reduction could only be ascribed to the reduction of nitrate rather than the reduction of Co_3O_4. The Co_3O_4 reduction in this study seem to have both reduction steps (Co_3O_4 to CoO and CoO to Co) occurring concurrently.

Table 4.7: Hydrogen consumption analysis from TPR profiles taken for the reduction peaks due to the reduction of Co_3O_4 taken within 45 minutes.

Heating Rate	sample	T_2	n_{H2}	Degree of reduction
(°C/min)	Mol Si/mol Co	(K)	(mol H_2/mol Co_3O_4)	%
15	0.060	769	3.65	91
	0.030	766	3.65	91
	0.009	760	3.69	92
	0.003	756	3.80	95
	Co_3O_4	749	4.004	100
10	0.060	753	3.70	92
	0.030	742	3.72	93
	0.009	737	3.74	94
	0.003	728	3.81	95
	Co_3O_4	713	3.92	98
5	0.060	717	3.79	95
	0.030	710	3.82	95
	0.009	695	3.86	96
	0.003	694	3.88	97
	Co_3O_4	676	4.100	100

Reduction behavior of the model catalyst was determined upon varying heating ramp. With increasing heating ramp the maximum rate of hydrogen consumptions occurs at higher temperatures. The TPR profiles for the 0.003 mol Si/mol Co sample taken at different heating ramps are shown in *Figure 4.21.*

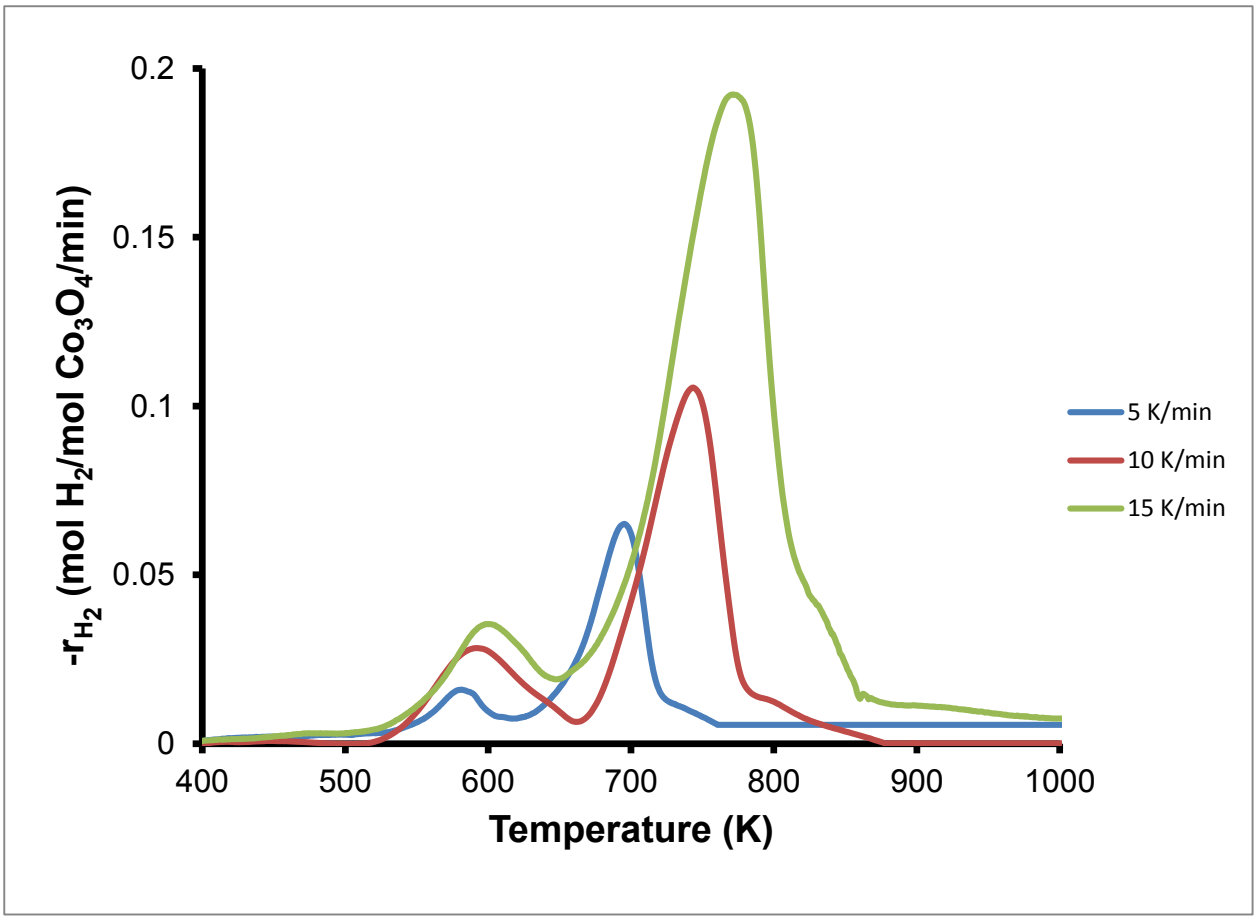

Figure 4.21: TPR profile of 0.003 mol Si/mol Co using different heating rates

From the different reduction temperatures, the activation energy of each sample could be determined from the Kissinger plot (Georgiev**,** 2008):

$$\ln\left(\frac{\beta}{T_{max}^2}\right) = -\ln\frac{Ea}{A\cdot R} - \frac{Ea}{R}\cdot\frac{1}{T_{max}} \qquad (4.5)$$

Where T_{max} is the reduction peak maximum temperature, β is the rate, Ea is the activation energy required for the reduction, R gas constant and A is the Arrhenius

parameter. The activation energy is determined from the slope in a plot of $\ln\left(\frac{\beta}{T_{max}^2}\right)$ versus $\frac{1}{T_{max}}$. The Kissinger plots for the determination of activation energy of the model catalysts for reduction of CoO to Co are shown in *Figure 4.22.*

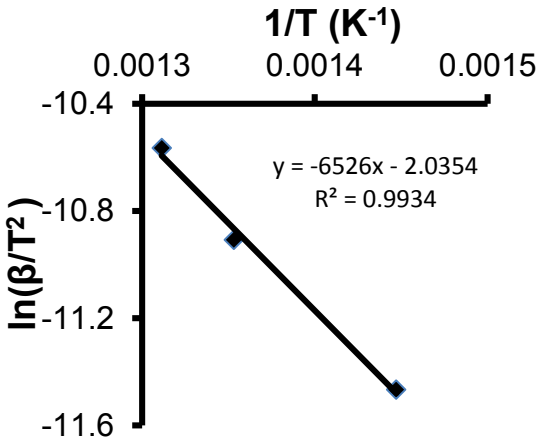

Figure 4.22: Kissinger plots for 0.003 mol Si/mol Co sample.

From the Kissinger plot, the slope of the graph is determined to be -6526 K and this is equivalent to the value of $\frac{-Ea}{R}$. Thus the activation energy can be obtained by multiplying the slope by R to get;

$$E_a = 58 \pm 4\ kJ/mol \qquad (4.6)$$

The activation energy for the 25 nm 0.003 mol Si/mol Co sample was determined to be 58 kJ/mol. This value is not very different from the value of 54 kJ/mol reported by Bustnes *et al*. (1995) for the reduction of CoO to metallic Co. The pre exponential factor A, is 129.67.

A similar approach was used to determine the activation energy of the silylated samples. In general, the presence of the Co-O-Si bonds on the surface of Co_3O_4 affects the activation energy for reduction. With increasing TEOS loading, the activation required for reduction increases. This therefore explains the shift towards higher reduction temperatures upon addition of TEOS to the Co_3O_4 nanocubes. This might be attributed to the strong metal support interaction. The activation energies of reduction for the model catalyst are shown in *Table 4.8.*

Table 4.8: Activation energies of reduction of the model catalyst

Sample	Activation energy ($kJmol^{-1}$)
	$CoO \longrightarrow Co$
Co_3O_4	57±5
0.003Si/Co	58±4
0.009Si/Co	67±2
0.03Si/Co	66±4
0.06Si/Co	73±6

4.5 Fischer-Tropsch synthesis

The Fischer-Tropsch synthesis was carried as a test reaction to test the activity of the model catalysts. This was carried out in a fixed bed reactor of length 28 cm. The β-SiC supported catalyst was loaded into the reactor and reduced with hydrogen at 623 K for 16 hours. After the reduction process, the temperature was reduced to 493 K and syngas with a ratio of CO to H_2 of 1:2, was flown over the catalyst at a space velocity of 20.5 mmol syngas/(min·g Co). The products were analyzed online using a TCD-micro GC and offline with FID-GC to determine the CO conversion and selectivity.

4.5.1 CO conversion over the model catalyst

The conversion of carbon monoxide was determined from the GC-TCD over a period of 44 hours by comparing the carbon monoxide in the products and that which goes into the feed (*see Figure in Appendix 9.5 for a sample TCD chromatogram*). *Figure 4.23* shows the graph of conversions against time on stream for different catalysts. For an unmodified sample of Co_3O_4 the maximum conversion over the 44 hours obtained was 0.02. Over a time frame of 44 hours, the silylated samples showed a relatively constant activity as the carbon monoxide conversion remain constants. The maximum conversion obtained for the 0.06 mol Si/mol Co sample was 0.27. This conversion is about 13 times larger than the conversion with unmodified Co_3O_4 sample.

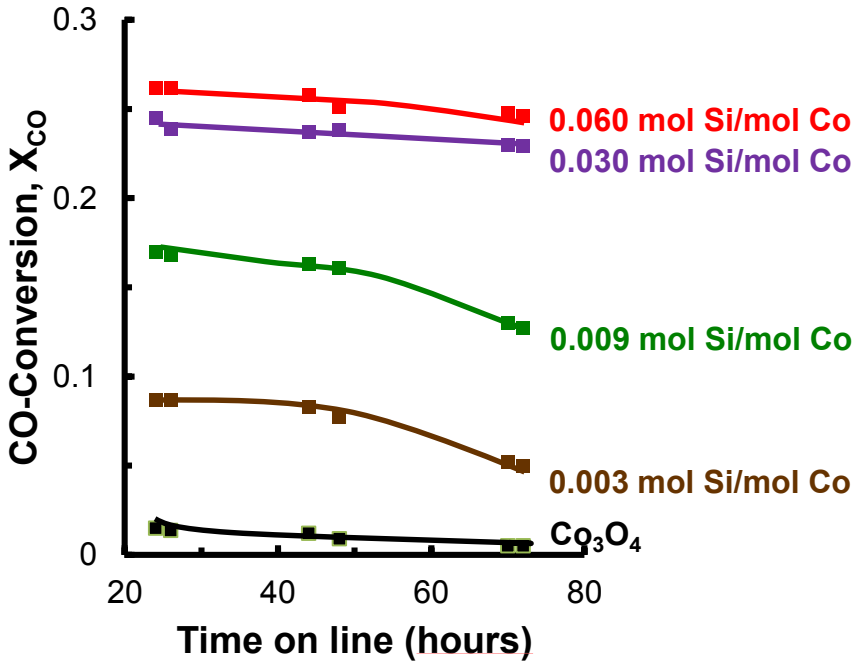

Figure 4.6: Effect of Si loading on CO conversion as a function of time on stream.

4.5.2 Catalyst activity

The activity of the catalyst is expressed as the integral rate of CO conversion per unit mass of the cobalt. The rate of CO conversion can be computed from the CO conversion over time on stream. The specific rate of conversion as function of Si loading shows a rapid increase upon modification (*see Figure 4.24)*. For the unmodified sample the rate of CO conversion is 0.13 mmol CO/min/g Co. The maximum rate was reached for the 0.06 mol Si/mol Co sample and was 1.7 mmol CO/min/g Co showing a 13 fold increase in the rate.

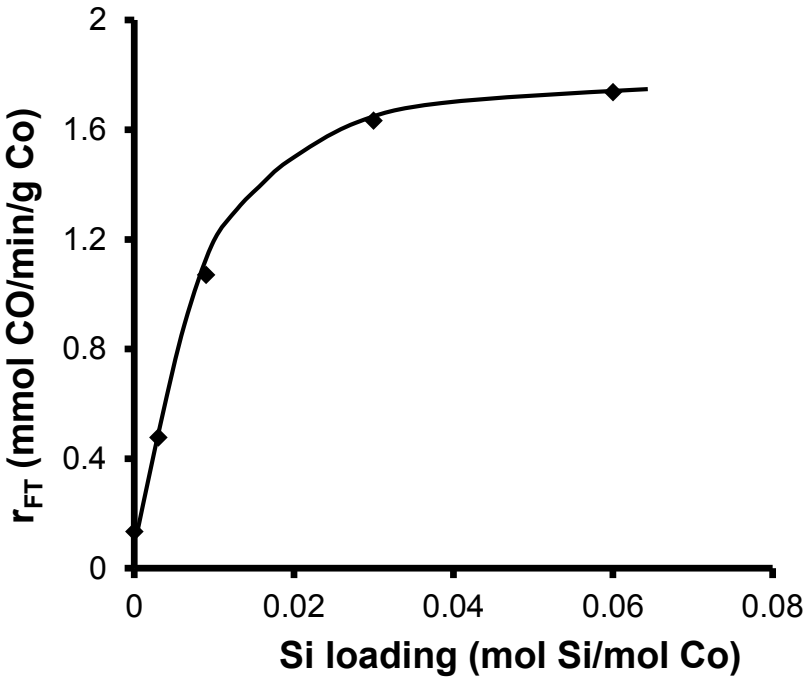

Figure 4.7: Rate of Fischer-Tropsch reaction per unit mass of cobalt found in the spent catalyst after 44 hours times on stream.

4.5.3 Methane selectivity

Methane is one of the products of Fischer-Tropsch synthesis. It can be formed via the associative desorption of a methyl surface species with a surface hydrogen. The formation of methane could be enhanced by high availability of hydrogen leading to rapid desorption of CH_4. The content of methane in the product stream was analyzed using TCD-GC (*see Figure in Appendix 9.5 for a sample TCD chromatogram. Figure 4.25* shows the methane selectivity of the model catalysts as a function of Si loading. It is observed that the methane selectivity decreases with increasing Si loading. The methane selectivity for unmodified samples is about 10%. This value does not vary from the methane selectivity reported by Stracey (2013) of 12%. In the study, the cobalt oxide was supported on carbon nanotubes (CNT).

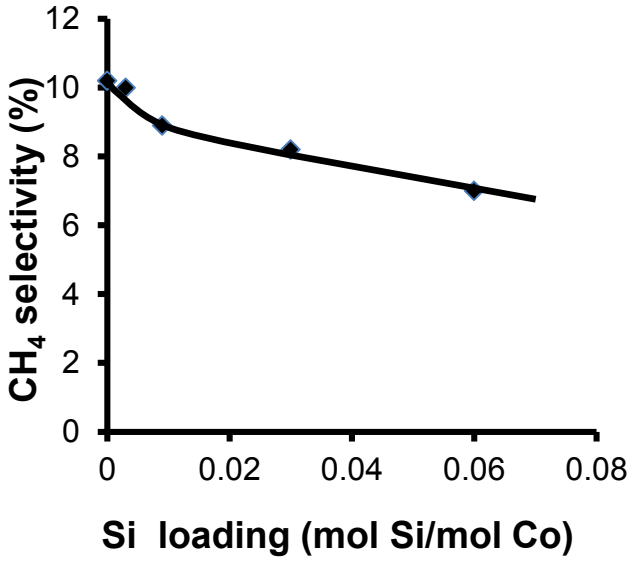

Figure 4.8: The effect of silicon loading on methane selectivity (TOS=44 hours).

4.5.4 Product Distribution and chain growth probability

The variation of selectivity of Fischer Tropsch synthesis products with chain growth probability alpha (α) is described by the Anderson Schulz Flory product distribution shown *in Figure 4.26*. At low values of α, shorter chain hydrocarbons are produced and at high values of α, mainly wax is produced (Dry, 1996). The petrol fraction (C_5-C_{11}) reaches a maximum at a chain growth probability of about 0.72 and the diesel fraction, C_{12}-C_{18}, reaches a maximum at an alpha value of approximately 0.83. The chain growth probability can be approximated from the corresponding product weight fraction.

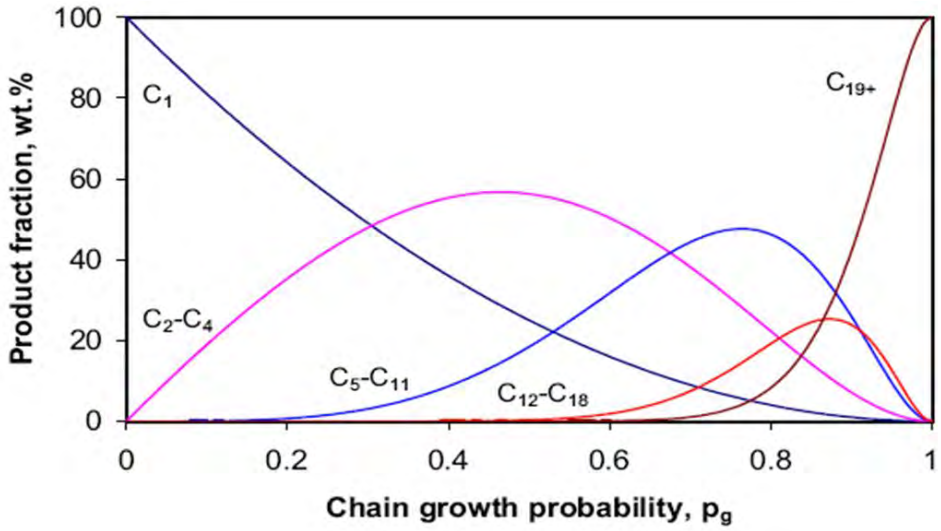

Figure 4.26: Anderson Schulz Flory product distribution (based on carbon number independent chain growth) redrawn after Dry (1996).

Chain growth probability is a tool used to indicate the inability of the product to desorb from the catalyst thus allowing for chain propagation. It is calculated using the Anderson-Schulz-Flory equation:

$$\log X_N = N \log \alpha + \log \frac{(1-\alpha)}{\alpha} \qquad (4.7)$$

where X_N is the mole fraction of products having N carbon atoms. The mole fraction of the various product compounds and product groups can be determined from the FID-GC chromatogram and α is the probability of chain growth. Here the probability of chain growth is assumed to be independent of chain length. A higher probability of chain growth implies an increase in the selectivity to longer chain compounds.

The calculated chain growth probabilities as are shown in *Table 4.9. Figure 4.27* shows the plot of chain growth probability as a function of Si loading. The chain growth probability increases with increasing Si loading. This was as expected as the methane selectivity was reduced upon loading of Si.

Table 4.9: The determined chain growth probabilities for the model catalyst.

Silicon loading (mol Si/mol Co)	Chain growth probability
0.000	0.68
0.003	0.71
0.009	0.73
0.030	0.76
0.060	0.77

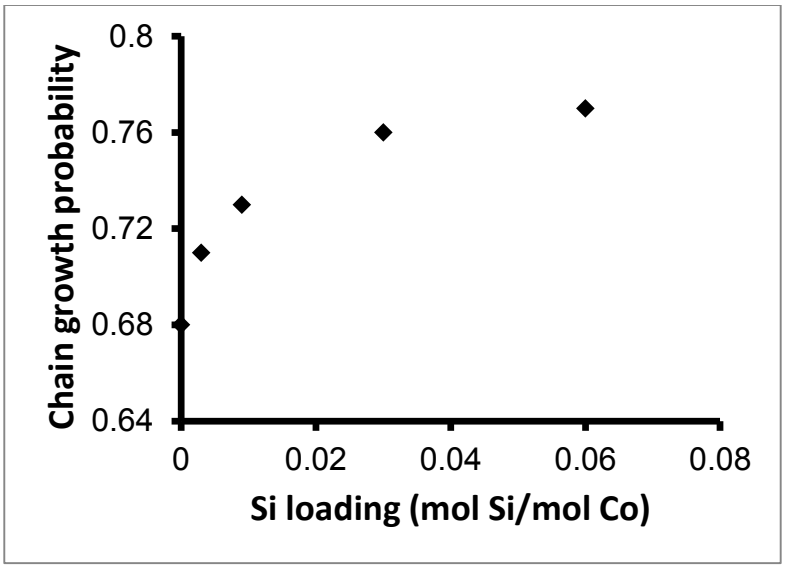

Figure 4.27: Chain grown probability as a function of the Si loading of the model catalyst.

4.5.5 Olefin content

Olefins are the primary products of the Fischer-Tropsch synthesis that constitutes 70-90% of the total products (Schulz, 1999). They may be formed through the dissociative desorption of surface alkyl species. However, formation of these species is prominent for low carbon number compounds over cobalt based catalysts (Anderson, 1984). C_{2-5} was used to investigate the effect of Si modification of cobalt on the olefin content. *Figure 4.28* shows the variation of linear 1-olefin/n-paraffin ratio for C_2 and C_5 olefin content over the model catalyst. For the model catalyst the linear 1-olefin content increases with time on stream only after 44 hours on stream. *Figure 4.29* depicts the variation of the linear 1-olefin/n-paraffin ratio with carbon number for the model catalysts. The maximum 1-olefin/n-paraffin ratio is obtained in the C_3 fraction. The olefin content decreases with chain growth for the modified catalysts. The linear 1-olefin/n-paraffin ratio becomes small with increasing silicon loading.

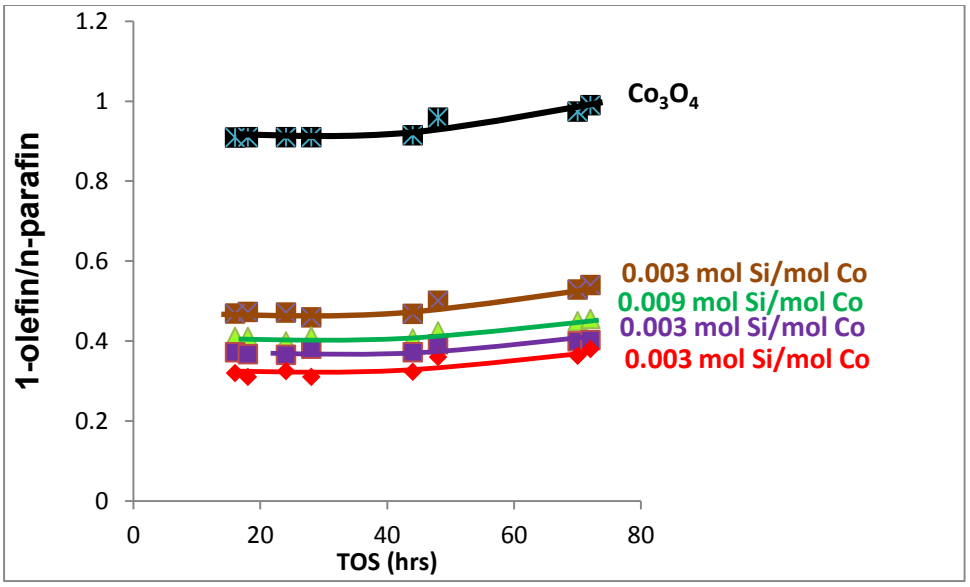

Figure 4.28: Variation of 1- olefin content in C_5 fraction with time on stream for the 0.06 mol Si/mol Co sample.

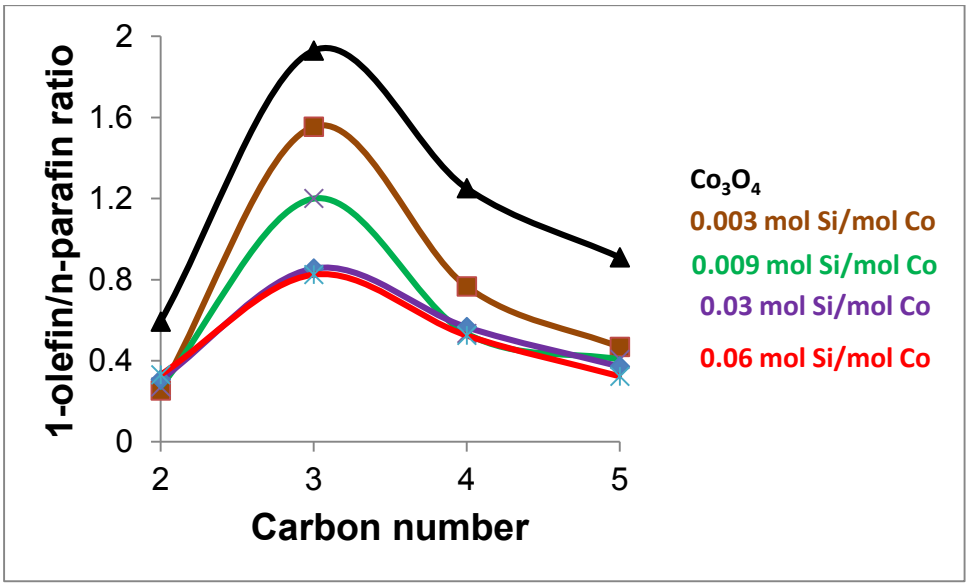

Figure 4.29*:* Variation of the 1-olefin/n-paraffin ratio with chain length from C_2 to C_5 for the different model catalyst determined after 44 hours on stream.

The variation of 1-pentene content in the C_5 fraction with silicon loading is shown in *Figure 4.30.* The selectivity of the model catalyst was obtained after 44 hours of time on stream. The olefin content in the fraction of linear C_5-hydrocarbons decreased from 48% for the unmodified catalyst to 24% for the 0.06 mol Si/mol Co sample.

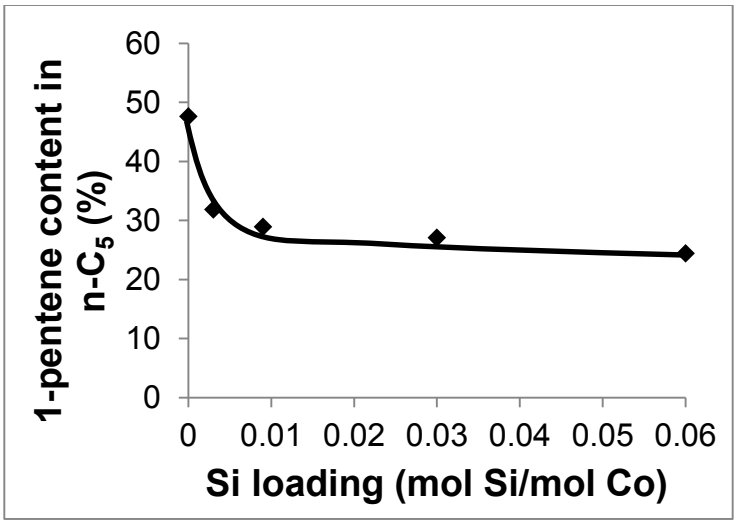

Figure 4.90: linear 1-pentene content in the C_5 fraction as a function of the silicon loading taken at 44 hours of time on stream.

4.5.6 Oxygenate content

Oxygen containing surface species can be formed via a CO insertion step accoding to Pichler and Schulz (1970). Johnston and Joyner (1993) postulated that the same species could be formed by addition of hydroxyl groups to an alkylidene species. Desorption of this species then leads to formation of alcohols or aldehydes respectively. The oxygenate fractions in this study were mainly alcohols. The total alcohol content as a function of carbon number for different catalysts is shown in *Figure 4.31.* For all model catalyst the content of oxygenates decreases with increasing chain length. C_1 fraction has the highest content of alcohol. The modification of Co_3O_4 with tetraethyl- orthosilicate affects selectivity to alcohols. With increasing silica loading the selectivity to alcohols decreases

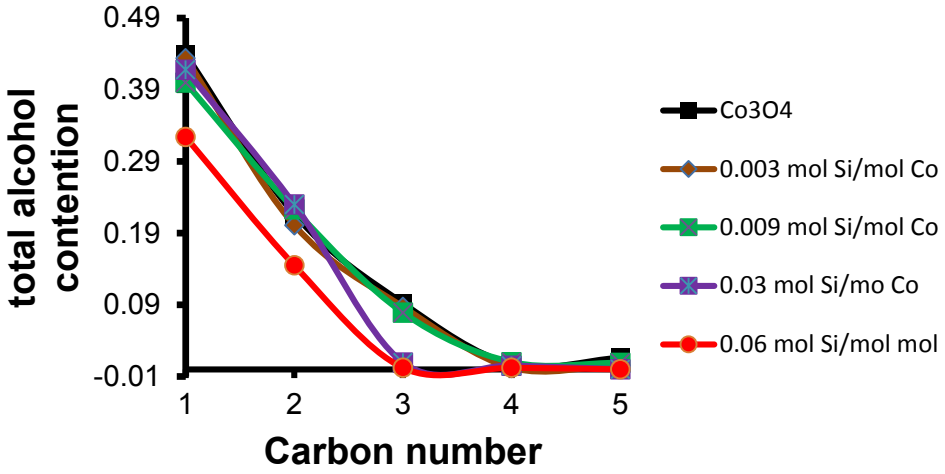

Figure 4.31: Alcohol content as a function of carbon number for different catalyst as determined after 44 hours on stream.

4.6 Analysis of the spent catalyst

The spent catalyst was passivated by flowing CO_2 over the catalyst bed at the flow rate of 20 mL/min (NTP) for 2 hours at room temperature. The catalyst was removed by first removing the 10.0 g of the SiC that was on top of the catalyst bed (added for the even heat distribution). The catalyst was then recovered by separating from the silicon carbide using a 150 µm sieve. The morphology of the spent catalyst was analysed with TEM. H_2-chemisorption was used to determine the effect of surface modification on the dispersion of the catalyst. Dispersion is determined as the number of active sites available per total amount of cobalt present. As such, the total amount of cobalt present in the recovered catalyst has to be determined using AAS.

4.6.1 Actual cobalt loading in SiC-supported spent samples as determined using AAS

The actual cobalt loading on the spent silicon carbide support was determined using atomic absorption spectroscopy. The sample was prepared by dissolving the sample in 3 M HF. *Table 4.10* shows cobalt loading of the model catalyst as determined using AAS. The variance in the measurement was carried by repeating the measurement 3 times. Cobalt loading of ca. 6 wt.-% was achieved.

Table 4.10: Cobalt loading in the spent catalyst as determined using AAS

Sample ID	Cobalt loading % w/w
Co_3O_4	5.8±0.3
0.003 mol Si/mol Co	6.0±0.1
0.009 mol Si/mol Co	6.2±0.1
0.03 mol Si/mol Co	5.9±0.2
0.06 mol Si/mol Co	6.0±0.2

4.6.2 Metal dispersion of the spent catalyst

The dispersion of the spent catalyst was determined using isothermal hydrogen chemisorption. This technique gives a precise measure of the dispersion of the metal since each surface atom chemisorbs (in most cases) a single hydrogen atom at temperatures higher than 90 K (Khodakov *et al*., 2007). However, the limitation of using H_2-chemisorption is that H_2-chemisorption cannot be used to determine metal dispersion in SMSI catalysts in the catalysts where hydrogen does not chemisorb due to SMSI (Tauster, 1981). From the graph of Normalised adsorbed H_2 against pressure (see *Figure 4.32*), it could be noted that the normalised H_2 chemisorption followed a classical Langmuir isotherm. The dispersion of the cobalt is affected by surface silylation as the hydrogen uptake at a given pressure increases with increasing Si loading. The increase in the H_2-uptake indicates that there were new active sites available for hydrogen chemisorption. The normalised adsorbed H_2 was computed by determining the volume of H_2 adsorbed per mass of cobalt as determined from the AAS.

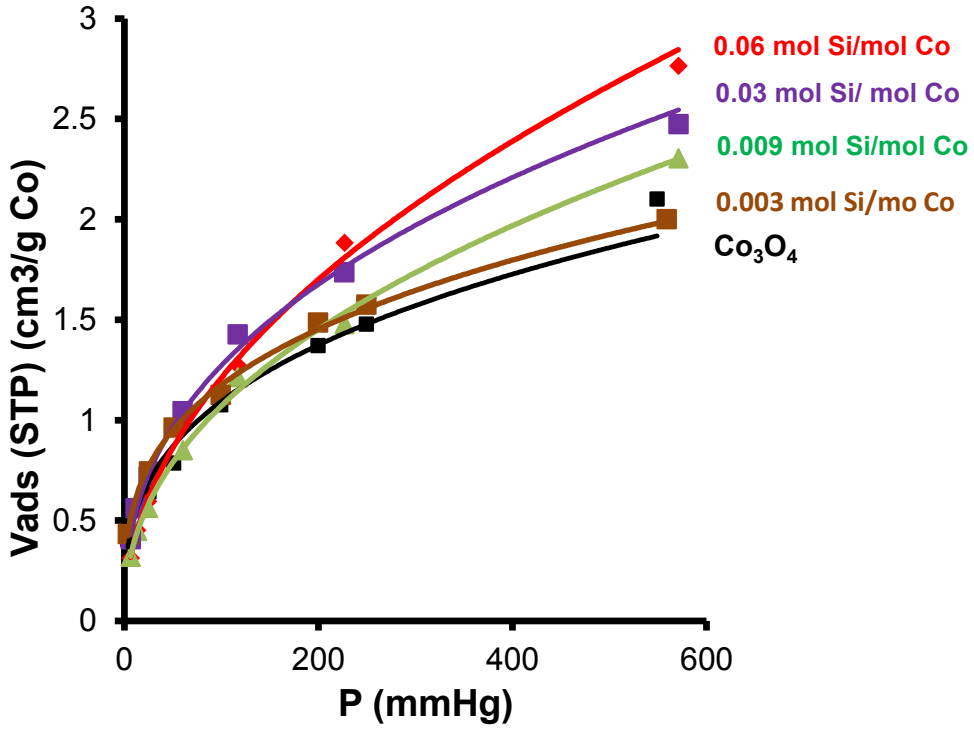

Figure 4.32: Normalized hydrogen chemisorption isotherms of model catalyst samples. The mass of the cobalt was determined from AAS.

The monolayer capacity for the uptake of the hydrogen on the surface of the model spent catalyst was then determined from the linearized form of the Langmuir equation for dissociative adsorption by plotting the inverse of volume adsorbed $\frac{1}{V_{ad}}$ against the inverse of the square of the root partial pressure of H_2 at which adsorption took place$\frac{1}{(\sqrt{P_{H_2}})}$. This plot should give a straight line given by:

$$\frac{1}{V_{ad}} = \left(\frac{1}{V_m}\right)\frac{1}{\sqrt{P_{H_2}}\sqrt{K}} + \frac{1}{V_m} \qquad (4.8)$$

Where V_{ad} is the amount of solute adsorbed per unit quantity of, V_m is monolayer capacity, P_{H_2} is the equilibrium partial pressure of hydrogen and K is a constant associated with energy of adsorption and can be calculated from the slope $\left(\frac{1}{V_m\sqrt{K}}\right)$. The constants in *equation 4.8* have a strong theoretical basis. V_m correlates the surface concentration of monolayer coverage and denotes the maximum value of adsorbed hydrogen that can be obtained as the equilibrium partial pressure of hydrogen is increased. The other Langmuir equation constant, ***K***, represents the energy associated with adsorption and increases as the strength of the adsorption bond increases. From the plot in *Figure 4.33* (0.06 mol Si/mol Co sample), the slope of the

graph is 3.98 $mmHg^{0.5}/g_{Co}$ and the value of $\frac{1}{V_m}$ is 0.22 cm^{-3} (STP)/g_{Co}, thus the resulting value of K is 3.1 x 10^{-3} $mmHg^{-0.5}$ and V_m is 4.5 cm^3 (STP)/g of cobalt respectively. Dispersion was calculated as shown in *Appendix 9.6.*

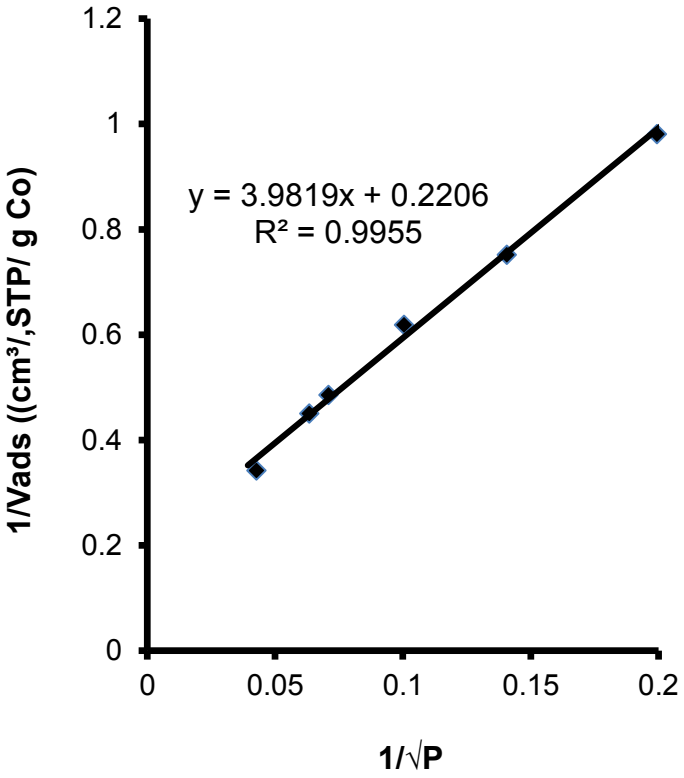

Figure 4.33: Linearized H_2-Chemisorption isotherms of 0.06 mol Si/mol Co sample.

The dispersion determined using this model gives large particle sizes which do not correspond to those determined from XRD and TEM as shown in *Table 4.11.* This may be attributed to the formation of agglomerates (partially fused crystallites) during reduction.

Table 4.11: Calculated V_m, K, dispersion, crystallite size values determined from the hydrogen chemisorption analysis of the spent catalysts and metal surface area.

Si loading (mol Si/mol Co)	Dispersion, %	V_m, cm^3(STP)/g·Co	K, X 10^{-3} $(mmHg)^{-0.5}$	Crystallite size of the spent catalyst (nm)	Metal Surface area ($m^2 \cdot g^{-1}$)
0.000	1.5	2.8	2.2	66	0.16
0.003	1.6	3.0	2.6	60	0.17
0.009	1.7	3.3	3.0	56	0.18
0.030	1.9	3.7	2.8	50	0.21
0.060	2.3	4.5	3.1	41	0.25

From the TEM micrographs shown in *Figure 4.34,* it is difficult to determine particle size as there is cluster formation during Fischer-Tropsch synthesis. However, average particle size obtained from the hydrogen chemisorption experiment show that particle size varies from 66 nm for the unmodified sample to 41 nm in the case of 0.06 mol Si/mol Co sample suggesting that for the modified samples, sintering is observed to decrease with silicon loading. This suggests that the Si surface species prohibits sintering of the particles upon reduction.

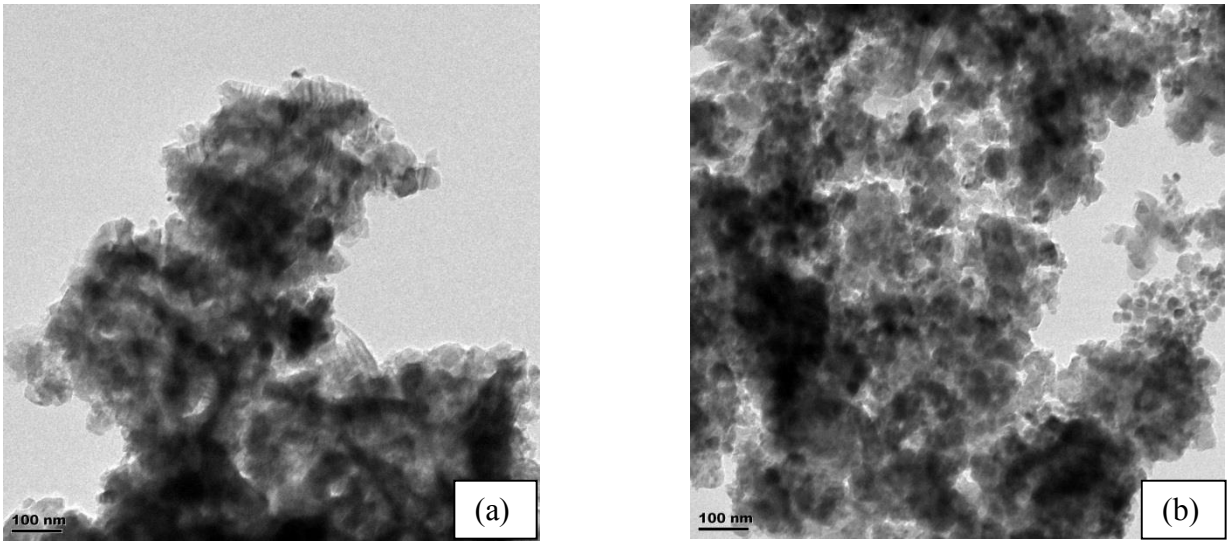

Figure 4.34: TEM micrograph of (a) the unmodified Co spent catalyst sample supported on SiC), (b) for 0.06 mol Si/mol Co sample after the Fischer-Tropsch synthesis.

The relationship between silicon loading and the calculated specific surface area of the spent catalyst is shown in *Figure 4.35.* With increasing Si loading, the specific surface area increases indicating that the modification process reduces sintering.

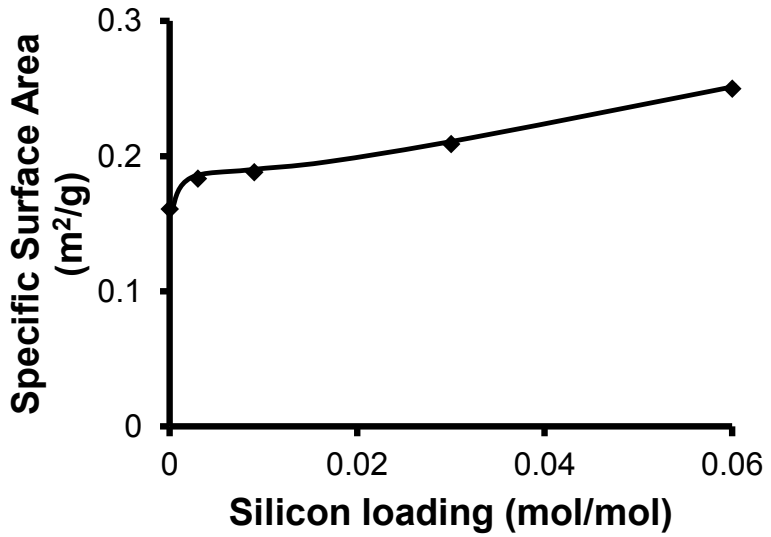

Figure 4.10: Effect of Si loading on the specific surface area of the spent catalyst for the determination of sintering upon Si loading.

5

5.0 Discussion

5.1 Characterization

The catalysts were prepared in two steps: The synthesis and characterization of the cobalt oxide nanocubes via the sodium dodecylsulphate assisted hydrothermal oxidative precipitation and the surface modification of the nanocubes with tetraethyl orthosilicate. The morphology of the Co_3O_4 nanocubes is affected by the temperature at which the reagents are mixed, the rate at which they are mixed as well as the time of reaction. The crystallite size of the nanocubes synthesized was in the range of 16 nm-50 nm.

The surface of the Co_3O_4 nanocubes was modified with tetraethyl orthosilicate. The proposed reaction path for the surface modification of Co_3O_4 with tetraethyl orthosilicate is shown in *Figure 5.1.* The four oxygen atoms that are bonded to silicon are more electronegative than silicon and thus pull electrons towards themselves thereby leaving the silicon atom partially positive. An oxygen forming hydroxyl on the surface of Co_3O_4 then transfers a lone pair of electrons to the partially positive silicon atom (Jiang *et al*., 2008). As the Si-O-Co bond is formed, the alkoxide bond is broken yielding the corresponding alcohol as a by-product.

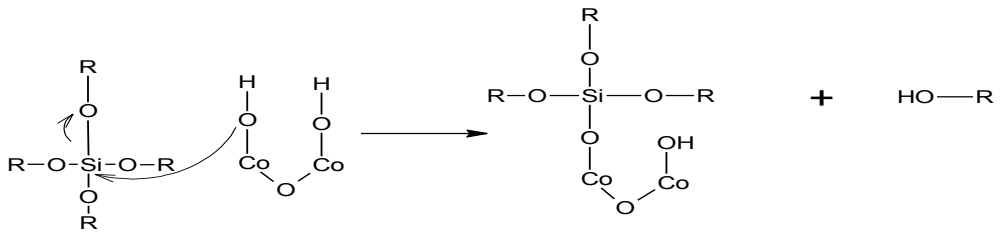

Figure 5.1: Proposed reaction path for the surface modification of Co_3O_4

The tetraethyl orthosilicate uptake on the surface of Co_3O_4 follows the classical Langmuir isotherm achieving equilibrium coverage at the Si:Co mol ratio of 0.067. Different Si loadings were achieved by using different initial tetraethyl-orthosilicate concentrations over a period of 5 hours.

The formation of Co-O-Si and Si-O-Si surface species was confirmed with Fourier transform infrared spectrometry. The reduction behaviour of the Co_3O_4 is affected by the presence of SiO_2. With increasing SiO_2 loading, the reduction temperature increases. This occurs as a result of increased activation energy for the reduction of the model catalysts upon modifying with SiO_2. The activation energy increases due to strong interaction between cobalt and silica. The reducibility of the model catalyst decreases with increasing silica loading due to the formation of strong cobalt silica interaction. The XRD data shows that the crystallite size is not affected by the modification.

The CO-hydrogenation requires a further pre-treatment of the catalyst, i.e. reduction. The temperature programmed reduction (TPR) profiles of these materials showed the development of a high temperature shoulder implying the presence of cobalt which is more difficult to reduce due to the surface modification. The presence of Co-O-Si bonds could be confirmed in the surface modified samples. These bonds remained intact after reduction.

5.2 Fischer-Tropsch Synthesis

The activity of the catalyst is enhanced by surface silylation. The increase in activity could be attributed to an improved metallic dispersion upon silylation. It is also postulated that the improved activity may be due to improved CO dissociation facilitated by the modification with silica through the mechanism in Figure *5.2.* It was proposed that hydroxyl groups on the silica substrate interaction with the adsorbed CO and hence facilitates its dissociation. A similar postulate was made by Stracey (2013) for the modification of Co_3O_4 with Ti substrates.

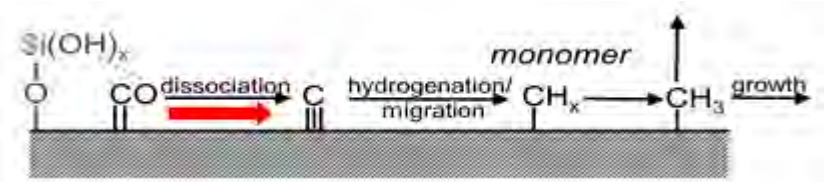

Figure 5.2: Proposed Fischer-Tropsch mechanism as a result of interaction of surface hydroxyl groups on Ti ligand with CO

The evidence supporting this mechanism was the slight deactivation seen in the modified samples with time on stream due to hydrolysis of the $Si(OH)_x$ upon reaction with adsorbed surface species thereby detaching the Si from the surface of the cobalt hence further interaction is introverted and the catalyst activity starts to decrease with time.

The methane selectivity of each model catalyst remained constant until the TOS = 44 hours. After 44 hours the catalyst showed some deactivation that resulted in an increase in methane selectivity. The methane selectivity decreases with increasing silica loading. This could be attributed to the increased dispersion of cobalt. With increasing dispersion, the number of CO molecules adsorbed increase resulting in an increase in the concentration of monomer available on the surface of the catalyst thereby increasing the chances of chain propagation as such reduction in methane selectivity. In the Co/TiO_2 system, where the surface of Co_3O_4 was decorated with titania, de la Pena O'Shea *et al*. (2011), attributes the increased activity to the suppression of hydrogenation of the CO. This could therefore suggest that the hydrogen chemisorption properties of the model catalyst were affected by the formation of Co-O-Ti. This explanation does not best describe the reduction in methane selectivity seen in this current study where the Co_3O_4 surface was modified with silica as the hydrogen adsorbed on each sample increases with Si loading. This could be attributed to the strength change in the CO adsorption strength upon modification with Si. The other possible explanation could be that the Co-O-Si surface hence increases the amount of CH_2 monomers on the surface of the catalyst.

The increased chain growth probability with increasing silicon loading could be due to the increase in conversion. Since a greater concentration of monomer is available on the surface of the catalyst there is an increased probability of chain growth. This is reflected in the decrease in the methane selectivity with increasing Si loading. These observations further regards the explanation of an increase in the strength of adsorption of CO as this would have resulted in an increase in chain growth probability and a decrease in methane selectivity with increasing loading observed.

Surface modification of Co_3O_4 with SiO_2 prohibits sintering as the SiO_2 particles act as spacers between the cobalt particles. The particle sizes of the modified samples did not change during the Fischer-Tropsch synthesis whereas the unmodified samples sintered. However, further Si loading may introduce the interaction of Si with Si rather than forming Co-O-Si bridges. It is thus expected that with further loading the rate of CO conversion will decrease rapidly as the Si loaded will form a layer around the Co thus denying CO the access to the active metal. The specific rate of CO conversion, over the catalysts, increase with increasing Si loading. The specific rate of CO conversion over the 0.06 mol Si/mol Co is 1.74 mol/min/g of Co which is about 13 times more than the specific rate of CO conversion over the unmodified sample which is 0.09 mol/min/g of Co.

The linear C_5 1-olefin content remains constant for the model catalyst within 44 hours on stream. This implies that the ratio of the rate of olefin desorption to that of paraffin desorption is approximately constant for the active catalyst. However, the 1-olefin selectivity for the C_5 fraction increase as the catalyst deactivates. The 1-olefin selectivity for the C_2, C_3, C_4 and C_5 cut decreases with increasing loading of silica. This could be due to the fact that the modification with silica provides new active sites for the re-adsorption of the C_{2-5} 1-olefins. In a comparable study by Stracey (2013), where cobalt oxide was modified with Ti, the olefin selectivity did not vary with increasing Ti loading. However, olefin content is known to decrease with increasing conversion (Anderson, 1984). A possible reason why olefin content varies in the case of Si modified sample but not in Ti modified sample is that olefin could re-adsorb in the case of Si modified sample as the active sites remain intact for a longer period compared to the Ti modified samples where the Co-O-Ti bond is broken within a short period of time.

It was initially thought that the formation of alcohols is through the formation of acyl groups via the CO-insertion mechanism (Mogorosi, 2012). The formation of primary alcohols decreases with increasing silicon loading. This may be due to the decreased ability of the catalyst to allow formation of surface acyl groups due to surface modification.

6

6. Conclusion

The objective of the study is to understand the interaction between the silica and Co_3O_4 nanocube crystallites, its effect on the reducibility of Co_3O_4, activity and selectivity in Fischer-Tropsch synthesis through the surface modification of Co_3O_4 with tetraethyl orthosilicate mimicking strong metal support interactions. This type of model induced the "ligand effect" type of strong metal support interactions which was confirmed by the formation of Co-O-Si surface species with FTIR in the region of 1020 cm^{-1} and 661 cm^{-1}. The Si-O-Si bands at 1080 cm^{-1} and at 800 cm^{-1} confirmed the presence of the Si-O- species on the surface of Co_3O_4. The presence of Co_2SiO_4 could not be confirmed with TPR but rather the formation of Co-O-Si bond. The Co-O-Si surface species were found to remain intact after 16 hours of hydrogen reduction at 623 K.

The formation of this surface species increased the temperature of reduction due to the increase in activation energy required to initiate the reduction. The activation energies increased from 57 ± 5 kJ/mol to 73 ± 6 kJ/mol. The degree of reduction of the model catalysts is affected by the modification. The degree of reduction up to 800 K of the unmodified sample was 100% and reduced to 91% for the 0.06 mol Si/mol Co sample.

Both the rate of reaction and the activity of the catalyst were increased by a factor of 13. The unmodified sample showed 2% CO conversion, with 0.06 mol Si/mol Co samples a showing a CO conversion of 27.3%. The other intermediate catalysts showed an increasing activity with increasing loading of SiO_2. This increase in conversion may be due to the increased metal surface area upon modification. The surface modification of Co_3O_4 with tetraethyl orthosilicate affected the methane selectivity. With increasing SiO_2 loading the methane selectivity dropped from 11% to 7%, with the olefin selectivity decreasing upon Si loading. The chain growth probability increases with increasing silica loading.

7. Recommendations

Although the 13 fold increase in activity and CO conversion was attributed to strong metal support interactions of Co and SiO_2, Fischer-Tropsch synthesis could be further performed on physical mixtures of Co and SiO_2 to conclusively evince that the change in activity is due to a metal-support interaction rather than the physical presence of SiO_2 species.

In order to confirm the nature of the surface species after modification, XPS studies could be done on the model catalyst. XPS analysis of a cobalt silicate compounds could be performed to further substantiate the claim made that the surface species formed experiences an environment more similar to silica than silicates. The use of high resolution TEM to distinguish between the amorphous silica and the crystalline Co_3O_4 is recommended.

In order to test if the Co-O-Si offers new active sites for the adsorption of CO, CO chemisorption studies should be performed. Temperature programmed desorption studies could also be performed in order to determine if there is a change in the strength of CO adsorption upon modification with Si.

8. References

Aghazadeha M., Abbas-Ali H., Barmia M. “Uniform β-$Co(OH)_2$ disc-like nanostructures prepared by low-temperature electrochemical route as an electrode material for supercapacitors”, *Applied Surface Science* **273** (2013) 237.

Ali S., Mohd-Zabidi N.A.M., Subbarao D. “Correlation between Fischer-Tropsch catalytic activity and composition of catalysts”, *Chemistry Central Journal* **5** (2011) 68.

Anderson R.B. “The Fischer-Tropsch synthesis”, *Academic Press, New York* (1984).

Bell A.T. “The impact of nanoscience on heterogeneous catalysis”, *Science* **299** (2003) 1688.

Bianchi L.C., Martino F., Moggi P. “Co/SiO_2 sol–gel catalysts for Fischer–Tropsch synthesis“, *Catalysis Letters* **76** (2001) 65.

Brinker C.J., Scherer G.W. “Sol-gel science: the physics and chemistry of sol-gel processing”, *Academic Press, New York* (1990).

Bustnes J.A., Du Sichen, Seetharaman S. “Kinetic studies of reduction of CoO and $CoWO_4$ by hydrogen”, *Metallurgical and Materials Transactions B* **26** (1995) 547.

Cargnello M., Fornasiero P., Gorte R.J. “Opportunities for tailoring catalytic properties through metal-support interactions”, *Catalysis Letters* **142** (2012) 1043.

Cheshechnikova I.T., Vorotyntsev V.M., Gette A.V., Golodets G.I. “Effects of rutile/anatase ratio on catalytic properties of Co-TiO_2 catalysts for Fischer-Tropsch synthesis”, *Reactor Kinetics and Catalysis Letters* **40** (1989) 47.

Coville N.J., Liu J. “Effect of boron source on the catalyst reducibility and Fischer–Tropsch synthesis activity of Co/TiO_2 catalysts”, *Catalysis Today* **71** (2002) 403.

de la Pena O’Shea V.A., Galvan M.C.A., Prats A.E.P., Campos-Martin J.M., Fierro J.L.G. “Direct evidence of the SMSI decoration effect: the case of TiO_2 catalyst”, *Chemical Communications* **47** (2011) 7131.

de la Osa A.R., de Lucas A., Diaz-Maroto J., Romeo A., Valverde J.L., Sanchez P. “FTS fuels production over different Co/SiC catalyst”, *Catalysis Today* **18** (2012) 173.

de Smit E., Cinquini F., Beale A.M., Safonova O.V., van Beek W., Sautet P., Weckhuysen B.M. “Stability and reaction of *ε-χ-θ* iron carbide catalyst phases in Fischer-Tropsch synthesis: controlling μ_c”, *Journal of American Chemical Society* **132** (2010) 14928.

de Souza M.F., Batista P.S., Regiani I., Liborio J.B.L, de Souza P.D.F. “Rice hull-derived silica: applications in portland cement and mullite whiskers”, *Materials Research* **3** (2000) 25.

Diehl F., Khodakov, A.Y. “Promotion of Cobalt Fischer-Tropsch Catalysts with Noble Metals: a Review*”, Oil & Gas Science and Technology – Rev. IF.* **64** (2009) 11.

Dry M.E. “Practical and theoretical aspects of the catalytic Fischer-Tropsch process”, *Applied Catalysis A* **13** (1996) 319.

Dry M.E. *“*High quality diesel via the Fischer-Tropsch process-a review”, *Journal of Chemical Technology and Biotechnology* **77** (2001) 43.

Dry M.E. “The Fischer–Tropsch process: 1950–2000”, *Catalysis Today* **71** (2002) 227.

Dry M.E. “Chemical concepts used for engineering purposes“, *Studies in Surface Science and Catalysis* **152** (2004) 196.

Dry M.E., Steynberg, A.P. “Commercial FT process applications“, *Studies in Surface Science and Catalysis* **152** (2004) 406.

Feng J., Zeng H.C. “Size-controlled growth of Co_3O_4 nanocubes”, *Chemistry of Materials* **15** (2003) 2829.

Feng Y.S., Zhou S.M., Li Y., Li C.C., Zhang, L.D. “Synthesis and characterization of tin oxide nanoparticles dispersed in monolithic mesoporous silica*”, Solid State Science* **5** (2003) 729.

Fischer N., Minneman M., Baeumer M., van Steen E., Claeys M. “Metal support interactions in Co_3O_4/Al_2O_3 catalysts prepared from w/o micro-emulsions”, *Catalysis Letters* **142** (2012), 830-837.

Fischer N., van Steen E., Claeys M. “Structure sensitivity of the Fischer-Tropsch activity and selectivity on alumina supported catalysts”, *Journal of Catalysis* **299** (2013) 67.

Fouad O.A. , Makhlouf A.A., Ali G.A.M., El-Sayed A.Y. “Cobalt/silica nanocomposite via thermal calcination-reduction of gel precursors”, *Materials Chemistry and Physics* **128** (2011) 70.

Fu Q., Wagner T., Olliges S., Carstanjen H.D. “Metal-oxide interfacial reactions: encapsulation of Pd on TiO_2 (110)”, *Journal of Physical Chemistry* **109** (2005) 944.

Gardezi, S. A., Landrigan, L., Joseph, B., John T. Wolan, T. J. “Synthesis of tailored eggshell cobalt catalysts for Fischer–Tropsch synthesis using wet chemistry techniques”, *Industrial Engineering Chemistry Research.* **51** (2012) 1703.

Gandia L., Montes M. “Effect of the reduction temperature on the selectivity of the high temperature reaction of acetone and hydrogen over alumina and titania supported nickel and cobalt catalysts“, *Journal of Molecular Catalysis* **94** (1994) 347.

Gao Y., Liang Y., Chembers S.A. “Thermal stability and the role of oxygen vacancy defects in strong metal support interaction — Pt on Nb-doped TiO_2 (100*)”, Surface Science* **365** (1996) 638.

Georgiev J., Bendereva E., Selecká M., Ďurišin J., Gyurov S., Valov R. “Reduction kinetics of TiO_2 powder coated with hydrocarbons”, *Powder Metallurgy Progress* **8** (2008) 320.

Gu1n’ko V.M., Vedamuthu M.S., Henderson G.L., Blitzy J.P. “Mechanism and kinetics of hexamethyldisilazane reaction with a fumed silica surface”, *Journal of Colloid and Interface Science* **228** (2000) 157.

Gracia J.M., Prinsloo F.F, Niemantsverdriet J.M. “Mars-van Krevelen-like mechanism of CO hydrogenation on an iron carbide surface”, *Catalysis Letters* **133** (2009) 257.

Hayashi H., Chen L.Z., Tago T., Kishida M., Wakabayashi K. “Catalytic properties of Fe/SiO_2 catalysts prepared using microemulsion for CO hydrogenation”, *Applied Catalysis A: General* **231** (2002) 81.

Hench L.L., West J.K. “The sol-gel process”, *Chemical Reviews* **90** (1990) 33.

Herranz T., Deng X., Cabot A., Guo J., Salmeron M. “Influence of the cobalt particle size in the CO hydrogenation reaction studied by *insitu* X-ray absorption spectroscopy”, *Journal of Physical Chemistry B* **113** (2009) 10721.

Hou X,D., Wang Y.Z., Zhao Y.X. “Effect of CeO_2 doping on structure and catalytic performance of Co_3O_4 catalyst for low-lemperature CO oxidation”, *Catalysis Letters* **23** (2008) 321.

Huang H., Chen Z. “Preparation of $CoFe_2O_4/SiO_2$ nanocomposites by sol–gel method”, *Journal of Crystal Growth* **271** (2004) 287.

Huber G.W., Butala S.J.M., Lee M.L, Bartholomew C.H. “Gadolinium promotion of Co/SiO_2 Fischer-Tropsch synthesis catalysts”, *Catalysis Letters* **74** (2001) 45.

Huffmann G.P., Shah N., Zhao J., Huggins, E.F., Hoost, R.E. Halvorsen S., Goodwin J.G. Jr. “In situ XAFS Investigation of K-promoted Co catalysts”, *Journal of Catalysis* **151** (1995) 17.

Iglesia, E. *“*Design, synthesis, and use of cobalt-based Fischer-Tropsch synthesis catalysts”, *Applied. Cataysis A: General* **161** (1997) 59.

Iglesia E., Reyes S.C., Madon R.J., Soled S.L. “Selectivity control and catalyst design in the Fischer-Tropsch synthesis: sites, pellets, and reactors*”, Advances in Catalysis* **39** (1993) 221.

Iler, R. K. *The Chemistry of Silica: Solubility, Polymerization, Colloid and Surface Properties, and Biochemistry*; Wiley-Interscience: New York, (1979).

Jacobs G., Das T,K., Zhang Y., Li J., Racoillet G., Davis B.H. *“*Fischer–Tropsch synthesis: support, loading, and promoter effects on the reducibility of cobalt catalysts”. *Applied Catalysis A: General* **233** (2002) 263.

Jacobs G., Ji Y., Davis B.H., Cronauer D., Kropf A.J., Marshall C.L. “Fischer–Tropsch synthesis: temperature programmed EXAFS/XANES investigation of the influence of support type, cobalt loading, and noble metal promoter addition to the reduction behavior of cobalt oxide particles”. *Applied Catalysis A: General* **333** (2007) 177.

Jal P.K., Dutta R.K., Sudarshan M., Saha A., Bhattacharyya S.N., Chintalapudi S.N., Mishra B.K. *“*Extraction of metal ions using chemically modified silica gel: a PIXE analysis”, *Talanta* **55** (2001) 233.

Jal P.K., Patel S., Mishra B.K. “Chemical modification of silica surface by immobilization of functional groups for extractive concentration of metal ions*”, Talanta* **62** (2004) 1005.

Jiang M., Song X., Ye G., Xu J. “Preparation of PVA/paraffin thermal regulating fiber by *in situ* microencapsulation”, *Composites Science and Technology* **68** (2008) 2231.

Jiang X.Z., Hayden F.T., Dumesic J.A. “Evidence for slow uptake of hydrogen by titania-supported metal samples: Consequences for estimating metallic surface areas”, *Journal of Catalysis* **83** (1983) 168.

Jong S., Cheng S. “Reduction behavior and catalytic properties of cobalt containing ZSM-5 zeolites*”, Applied Catalysis A: General* **126** (1995) 51.

Jongsomjit B., Panpranot J., Goodwin J.G. jr. “Co-support compound formation in alumina-supported cobalt catalysts”, *Journal of Catalysis* **204** (2001) 98.

Johnston, O., Joyner, R. “Structure function relationships in heterogeneous catalysis: the embedded surface molecule approach and its application”, In: L. Guczi, F. Solymosi, and P. Tetenyi (eds.): Proceedings of the “10th Int. Congr. on catalysis”, Budapest .*Studies in Surfaces Science and Cataysis*. **75A** (1992) 165, Elsevier, Amsterdam.

Jun H., Wu B.S., An X., Li T.Z., Tao C.C., Xiang H.W., Li Y.W. “Effect of Al_2O_3 binder on the precipitated iron-based catalysts for Fischer-Tropsch synthesis”, *Journal of Natural Gas Chemistry* **16** (2007) 130.

Kababji A.H., Joseph B., Wolan J.T. “Silica-supported cobalt catalysts for Fischer–Tropsch synthesis: effects of calcination temperature and support surface area on cobalt silicate formation”, *Catalysis Letters* **130** (2009) 72.

Kaiser R. “Chromatographie in der Gasphase”, *Bibliographisches Institut, Mannheim, Band iii*, 2nd edition (1969).

Khan, R.A. “Life cycle assessment of Fischer-Tropsch fuels”, *Civil and Environmental Engineering Postgraduate conference”,* (2009). http://people.eng.unimelb.edu.au/lua/Khan_Rezwan_Proc.pdf (accessed 11 April 2014).

Khodakov A.Y., Chu W., Fongarland P. "Review: advances in the development of novel cobalt Fischer−Tropsch catalysts for synthesis of long-chain hydrocarbons and clean fuels", *Chemical Reviews* **107** (2007) 1692.

Kim D.J., Dunn B.C., Cole P., Turpin G., Ernst R.D., Pugmire R.J., Kang M., Kim J.M., Eyring E.M. "Enhancement in the reducibility of cobalt oxides on a mesoporous silica supported cobalt catalyst", *Chemical Communications* **11** (2005) 1462.

Kogelbauer A., Weber J.C., Goodwin J.G. "The formation of cobalt silicates on Co/SiO_2 under hydrothermal conditions", *Catalysis Letters* **34** (1995) 259.

Koo H.M., Lee B.S., Park M.J., Roh H.S., Bae J.W. "Fischer-Tropsch synthesis on cobalt/Al_2O_3-modified SiC catalysts: effect of cobalt-alumina interactions", *Catalysis Science and Technology* **4** (2014) 343.

Kuboa M., Kubota T., Junga C., Ando M., Sakahara S., Yajima K., Seki K., Belosludov R., Endou A., Takami S., Miyamoto A. "Design of new catalysts for ecological high-quality transportation fuels by combinatorial computational chemistry and tight-binding quantum chemical molecular dynamics approaches", *Catalysis Today* **89** (2004) 479.

Kunarti S.S. Moran G.M. "Entrapment of avidin in sol-gel derived silica glasses", *Journal of Physical Science* **19** (2008) 31.

Ling C.K., Mohd-Zabidi N.A.., Mohan C. "Synthesis and characterization of silica-supported cobalt nanocatalysts using strong electrostatic adsorption", *Journal of Applied Science* **11** (2011a) 1436.

Ling C.K., Mohd-Zabidi N.A., Mohan C. "Synthesis of cobalt nanoparticles on silica support using the strong electrostatic adsorption (SEA) method", *Defect and Diffusion Forum* **312** (2011b) 370.

Liu X., Qiu G., Li X. "Shape-controlled synthesis and properties of uniform spinel cobalt oxide nanocubes", *Nanotechnology* **16** (2005) 3035.

Lutz B. “New age gas-to-gasoline processing”, *Hydrocarbon Engineering* **6** (2001) 23.

Mirzaei A., Vahid D., Feyzi M. “Fischer-Tropsch synthesis over iron manganese catalysts: effect of preparation and operation conditions on catalyst performance”, *Advances in Physical Chemistry* **2009** (2009).

Mogorosi R.P. “Metal-support interaction on Fe-based Fischer-Tropsch catalysts”, *Ph.D. Thesis, University of Cape Town* (2012).

Morales F., Weckhuysen B.M. “Promotion effects in Co-based Fischer–Tropsch catalysis”, *Catalysis* **19** (2006) 1.

Muhler M., Schütze J., Wesemann M., Rayment T., Dent A., Schlögl R., Ertl G. “The nature of the iron oxide-based catalyst for dehydrogenation of ethylbenzene to styrene: solid-state chemistry and bulk characterization”, *Journal of Catalysis* **126** (1990) 339.

Niemela M. “Reactions of synthesis gas on silica supported transition metals catalysts”, *DTech thesis, Helsinki University of Technology*, (1997).

O’Brien, R.J., Xu, L., Spicer, R.L. and Davis, B.H. “Activation Study of Precipitated Iron Fischer-Tropsch Catalysts”, *Energy and Fuels* **10** (2006) 921.

Oh J.H., Ba J.W., Park S.J., Khanna P.K.., Jun K.W. “Slurry-phase Fischer–Tropsch synthesis using Co/γ-Al_2O_3, Co/SiO_2 and Co/TiO_2: effect of support on catalyst aggregation”, *Catalysis Letters* **130** (2009) 403.

Ojeda, M., Pérez-Alonso, F.J., Terreros, P., Rojas S., Herranz T., Granados M.L., Fierro J.L.G. *“*Silylation of a Co/SiO_2 Catalyst. Characterization and exploitation of the CO hydrogenation reaction”, *Langmuir* **22** (2006) 3131.

Okamoto Y., Polansky C.A. “Effects of starting cobalt salt upon the cobalt-alumina interactions and hydrodesulfurization activity of CoO/Al_2O_3”, *Applied Catalysis* **73** (1991).

Ortega-Zarzosa G., Araujo-Andrade C., Compean-Jasso M.E., Martinez J.R. *“*Cobalt oxide/silica xerogels powders: X-ray diffraction, infrared and visible absorption studies”, *Journal of Sol-Gel Science and Technology* **24** (2002) 23.

Park J.Y., Lee, J.Y., Karandikar R.P., Jun K.W, Ha K.S., Park H.G. “Fischer–Tropsch catalysts deposited with size-controlled Co_3O_4 nanocrystals: Effect of Co particle size on catalytic activity and stability”, *Applied Catalysis A: General* **411-412** (2012) 15.

Parks G.A., de Bruyn P.L. “The point of zero charge of oxides”, *Journal of Physical Chemistry* **66** (1962) 972.

Petersen A.M., van der Berg J-.A., van Rensburg W.J. “Role of step sites and surface vacancies in the adsorption and activation of CO on the χ-Fe_5C_2 surfaces”, *Journal of Physical Chemistry: C* **144** (2010) 7863.

Pichler, H., Schulz H. ‘Neuere Erkenntnnisse auf dem Gebiet der Synthese von Kohlenwasserstoffen aus CO und H_2”, *Chemie Ingenieur Technik* ***42*** (1970) 1162.

Prins M.J., Ptasinski K.J., Janssen F.J.J.G. “Exergetic optimisation of a production process of Fischer–Tropsch fuels from biomass*”, Fuel Processing Technology* **86** (2004) 375.

Puskas I., Fleisch T.H., Hall J.B., Meyers B.L., Roginski R. “Metal-support interactions in precipitated, magnesium-promoted cobalt-silica catalysts”, *Journal of Catalysis* **134** (1992) 615.

Qing M., Yang Y., Wu B., Xu J., Zhang C., Gao P., Li Y. “Modification of Fe-SiO_2 interactions with zirconia for iron-based Fischer-Tropsch catalysts”, *Journal of Catalysis* **279** (2011) 111.

Rayner M.K. “Pretreatment of TiO_2-supported Fe, Co and Ru catalysts: An in situ powder diffraction study”, *PhD. thesis, University of Witwatersrand* (2011).

Reinikainen M., Niemela M.K., Kakuta N., Suhonen S. *“*Characterisation and activity evaluation of silica supported cobalt and ruthenium catalysts”, *Applied catalysis A: General* **174** (1998) 61.

Resasco D.E., Haller G.L. “A model of metal-oxide support interaction for Rh on TiO_2”, .*Journal of Catalysis* **82** (1983) 279.

Rodriguez J.A., Hrbek J. “Inverse oxide/metal catalyst: a versatile approach for activity and mechanistic studies”, *Surface Science* **604** (2010) 241.

Romanowski, W. “Equilibrium forms of very small metallic crystals”, *Surface Science* **18** (1969) 373.

Rosynek M.P., Polansky C.A. “Effect of cobalt source on the reduction properties of silica-supported cobalt catalysts“, *Applied Catalysis* **73** (1991) 97.

Saib A.M., Borgna A., van de Loosdrecht J., van Berge P.J., Geus J.W. Niemantsverdriet J.W. “Preparation and characterisation of spherical Co/SiO_2 model catalysts with well-defined nano-sized cobalt crystallites and a comparison of their stability against oxidation with water“, *Journal of Catalysis **239*** (2006) 326.

Schulz H. *“*Kinetics of Fischer-Tropsch selectivity”, *Molecular Chemistry* **1** (1985) 231.

Schulz H. “Short history and present trends of Fischer–Tropsch synthesis”, *Applied Catalysis A* **186** (1999) 3.

Schwab G.M., Koller K. “Combined action of metal and semiconductor catalyst”, *Journal of the American Chemical Society* **90** (1968) 3078.

Shag D. “Coal as a low-carbon fuel?”, *Nature Geoscience* **2** (2009) 818.

Shah Y.T., Perrotta J.A. “Catalysts for Fischer-Tropsch and isosynthesis”, *Industrial Engineering Chemistry Product Research and development* **15** (1976) 12310.

Shi L., Chen J., Fang K., Sun Y. “CH_3-modified Co/Ru/SiO_2 catalysts and the performances for Fischer–Tropsch synthesis”, *Fuel* **87** (2008) 521.

Shukla P., Sun H., Wang S., Ang H.M., Tade M.O. “Nanosized Co_3O_4/SiO_2 for heterogeneous oxidation of phenolic contaminants in waste water”, *Separation and Purification Technology* **77** (2011) 230.

Soled S.L., Iglesia E., Fiato R.A. Baumgartner J.E., Vroman H., Miseo S. “Control of metal dispersion and structure by changes in the solid-state chemistry of supported cobalt Fischer–Tropsch catalysts”, *Topics in Catalysis* **26** (2003) 101.

Storsæter S., Borg Ø., Blekkan E.A., Holmen A. “Study of the effect of water on Fischer–Tropsch synthesis over supported cobalt catalysts”, *Journal of Catalysis* **231** (2005) 405.

Stracey R. “Metal-support interactions in Co/TiO_2 Fischer-Tropsch catalysts”, *MSc Dissertation, University of Cape Town* (2013).

Suriye K., Praserthdam P., Jongsomjit B. “Impact of Ti^{3+} present in titania on characteristics and catalytic properties of the Co/TiO_2 catalyst”, *Industrial and Engineering Chemistry Research* **44** (2005) 6599.

Swart J.C., Van Helden P., van Steen, E. “Surface Energy Estimation of Catalytically Relevant fcc Transition Metals Using DFT Calculations on Nanorods*”, Journal of Physical Chemistry,* **111** (2007) 4998.

Takeuchi K., Matsuzaki T. Arakawa H., Sugi Y. “Synthesis of ethanol from syngas over Co-Re-Sr/Si0_2 Catalysts”, *Applied Catalysis* **18** (1985) 325.

Tauster S.J. “Strong metal-support interactions”, *Accounts of Chemical Research* **20** (1987) 11.

Tauster S.J., Fung S.C., Garten R.L. “Strong metal-support interations: Group 8 noble metals supported on TiO_2”, *Journal of the American Chemical Society* **100** (1978) 170.

Tauster S.J., Fung S.C., Baker R.T.K., Horsley J.A. “Strong interactions in metal-support catalysts”, *Science* **211** (1981) 1121.

Tavasoli A., Sadagiani K., Khorashe F., Seifkordi A.A., Rohani A.A., Nakhaeipour, A. “Cobalt supported on carbon nanotubes — a promising novel Fischer–Tropsch synthesis catalyst”, *Fuel Processing Technology* **89** (2008) 491.

Tijmensen M.J.A., Faaij A.P.C., Hamelinck C.N., van Hardeveld M.R.M. “Exploration of the possibilities for production of Fischer-Tropsch liquids and power via biomass gasification”, *Biomass and Bioenergy* **23** (2002) 129.

Titmuss S., Wander A., King D. A. “Reconstruction of Clean and Adsorbate-Covered Metal Surfaces”, *Chemical Review* **96** (1996) 1291.

Unruh D., Pabst K., Schaub G. “Fischer-Tropsch synfuels from biomass: maximizing carbon efficiency and hydrocarbon yield”, *Energy and Fuels **24*** (2010) 2634.

US Environmental Protection Agency. “Clean alternative fuels: Fischer Tropsch”, *http://www.afdc.energy.gov/pdfs/epa_fischer.pdf, EPA 420-F-00-036 (March 2002).*

van Berge P.J., Everson R.C. “Cobalt as an alternative Fischer-Tropsch catalyst to iron for the production of middle distillates”, *Studies in Surface Science and Catalysis* **107** (1997) 207.

Vannice M.A., Hasselbring L.C., Sen, B**. “**Metal-support effects on H_2 and CO heats of adsorption on TiO_2-supported platinum”, *Journal of Physical Chemistry* **89** (1985) 2972.

Vannice M.A., Sudhakar C. “A model for the metal-support effect enhancing CO hydrogenation rate over Pt-TiO_2 catalysts”, *Journal of Physical Chemistry* **88** (1984) 2429.

van Steen E., Claeys M. “Fischer-Tropsch catalysts for the biomass-to-liquid process”, *Chemical Engineering and Technology* ***31*** (2008) 655.

van Steen E., Claeys M., Dry M.E. “Stability of nanocrystals: thermodynamic analysis of oxidation and re-reduction of cobalt in water/hydrogen mixtures”, *Journal of Physical Chemistry B* **109** (2005) 3575.

White C., Gray D. “Production of zero sulfur diesel fuel from domestic coal: configurational options to reduce environmental impact”, *US-Department of Energy/National Energy Technology Laboratory, DOE/NETL-2012/1542 http://www.netl.doe.gov/File%20Library/Research/Energy%20Analysis/Publications/DOE-NETL-2012-1542-CBTL052012.pdf* (2011).

Xie R., Li D., Hou B., Wang J., Jia L., Sun Y. “Silylated Co_3O_4-m-SiO_2 catalysts for Fischer–Tropsch synthesis”, *Catalysis Communications* **12** (2011) 589.

Xiong H., Zhang Y., Wang S., Li J. “Fischer–Tropsch synthesis: the effect of Al_2O_3 porosity on the performance of Co/Al_2O_3 catalyst”, *Chemical Communications* **6** (2005) 512.

Yang, Y., Jia L., Meng Y., Hou B., Li D., Sun Y. “Fischer–Tropsch Synthesis over Ordered Mesoporous Carbon Supported Cobalt Catalysts: The Role of Amount of Carbon Precursor in Catalytic Performance”, *Catalysis Letters* **142** (2012) 195.

Yin X.J., Penga K., Hu A.P., Zhou, L.P., Chen J.H., Du Y.W. “Preparation and characterization of core–shell structured Co/SiO_2 nanosphere”, *Journal of Alloys and Compounds* **479** (2009) 372.

Yu L., Liu X., Fang Y., Wang C., Sun Y. “Highly active Co/SiC catalysts with controllable dispersion and reducibility for Fischer–Tropsch synthesis”, *Fuel* **112** (2013) 483.

9. APPENDIX

9.1 Calibration graph for AAS

The calibration was performed by determining the absobance of three standard solutions of cobalt (i.e 5mg/L, 25 mg/L and 50 mg/L). A calibration graph (*Figure 9.1*) of absorbance against concentration was plotted and it resulted into a straight line with the regression of 0.9998.

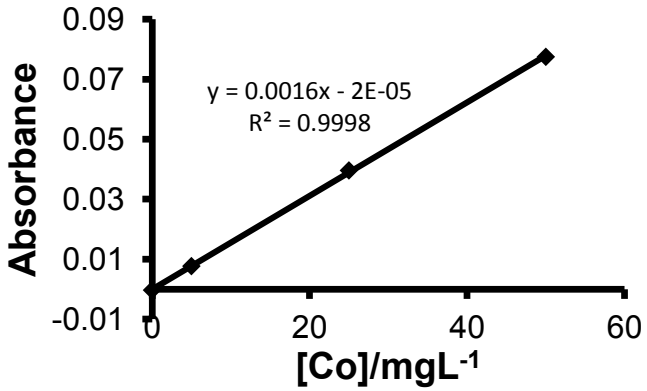

Figure 9.1: An AAS calibration graph for the determination of Cobalt loading on the spent catalyst.

9.2 Sample calculation for an acceptable leak rate in a fixed bed reactor

The leak rate can be determined as a ratio of the flow rate of the gas that leaked out of the system to the flow rate of the gas going into the system. The number of moles in the isolated system at 20 bar can be estimated from the ideal gas law. The volume of the isolated system was calculated from the diameters and lengths of the tubes used and was determined to be 25mL:

$$PV = NRT$$

$$N = PV/RT$$

$$N = 20\ bar * 25\ mL/(8.314 jmol^{-1}K^{-1} * 298k)$$

$$N = 0.2\ mmol$$

The number of moles that remains in the system after 24 hours (only if you allow a pressure drop of 1 bar)is given by:

$$PV = NRT$$

$$N = PV/24RT$$

$$N = 19\ bar * 25mL / (8.314 jmol^{-1}K^{-1} * 298K)$$

$$N = .0.19\ mmol$$

Number of moles lost

$$0.2-0.19 = 0.01mmol$$

$$0.01mmol/24hours = 4.2*10^{-4}\ mmol/hour$$

$$7*10^{-6}\ mmol/min$$

$$0.17mL/min$$

For syngas flowing at 30 mL/min a loss of 0.17mL/min constitute 0.5% loss. A loss which is 3 times more would correspond to 2% loss which is not acceptable.

9.3 TCD-GC calibration

The TCD was calibrated using calibration gas mixtures with known composition. The peak areas obtained from the TCD analysis were then used to calculate the relative calibration factors normalized for nitrogen, f_{TCD}, for each species. The calibration factors used in this study are shown in *Table 9.1.* Relative standard deviation (repeatability of this analysis technique) are typically ± 3.0 % for TCD as determined from the repeated calibration data obtained at different calibration times *(Table 9.1).*

Table 9.1: Calibration factor for the TCD-reading of the various gases relative to nitrogen gas

Gas	Calibration factor
Hydrogen	13.49 ± 0.10
Nitrogen	1.00 ± 0.05
Carbon monoxide	0.76 ± 0.02
Methane	0.67 ± 0.03
Argon	0.87 ± 0.05

Table 9.2. Determination of calibration factor fot the TCD-GC

	Ar	N2	CH4	CO	H2
	461.3	304.6	489.5	805.5	32580
	475.9	317.6	521.3	825.6	32567
	475	316.7	520.7	824.3	32516
	476.7	317.9	522.8	827.6	32578
	477.8	318.5	523.6	828.7	32509
Average	**473.34**	**315.06**	**515.58**	**822.34**	**32550.00**
STDEV	**6.090189**	**5.262167**	**13.08089**	**8.55771**	**31.016125**
% DEV	**1.320223**	**1.727566**	**2.672296**	**1.06241**	**0.0951999**
Ai/AN2	**1.50238**	**1**	**1.63645**	**2.610106**	**103.31365**
fi	**1.205634**	**1**	**0.590013**	**0.688237**	**13.486758**

9.4 Sample EDX pattern

Figure 9.2 shows a sample EDX pattern of 0.004 mol Si/mol Co synthesized with an initial concentration of tetraethyl orthosilicate of 0.24 mM.

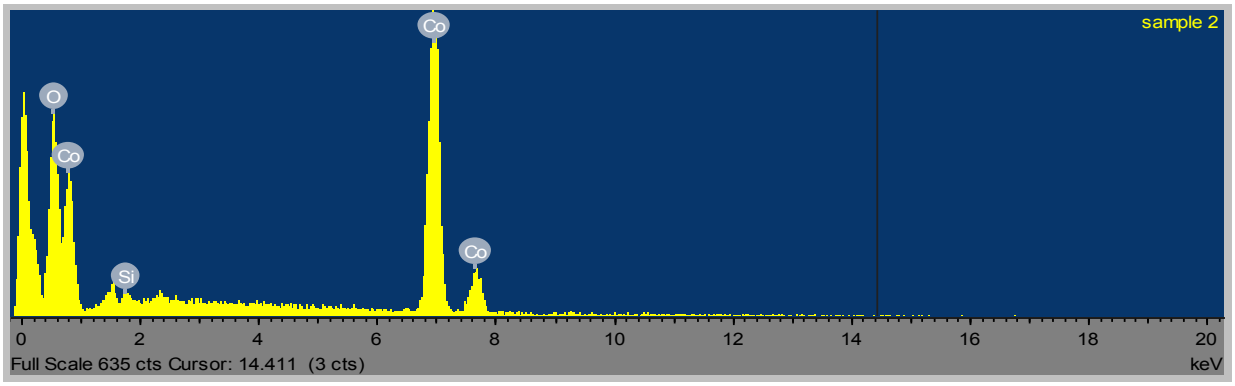

Figure 9.2: EDX patterns of 0.003 mol Si/mol Co synthesized with an initial concentration of tetraethyl orthosilicate of 0.24 mM

9.5 TCD-GC sample chromatogram

Sample TCD-GC chromatogram taken online using unmodified Co_3O_4 catalyst is shown in *Figure 9.3*. The chromatogram shows the argon peak eluting at 0.79 minutes, nitrogen peak at 0.97 minutes and the CO peak at 1.67 minutes. The methane peak could not be identified by the TCD-GC and hence methane was analysed with FID-GC with the rest of the organic compounds

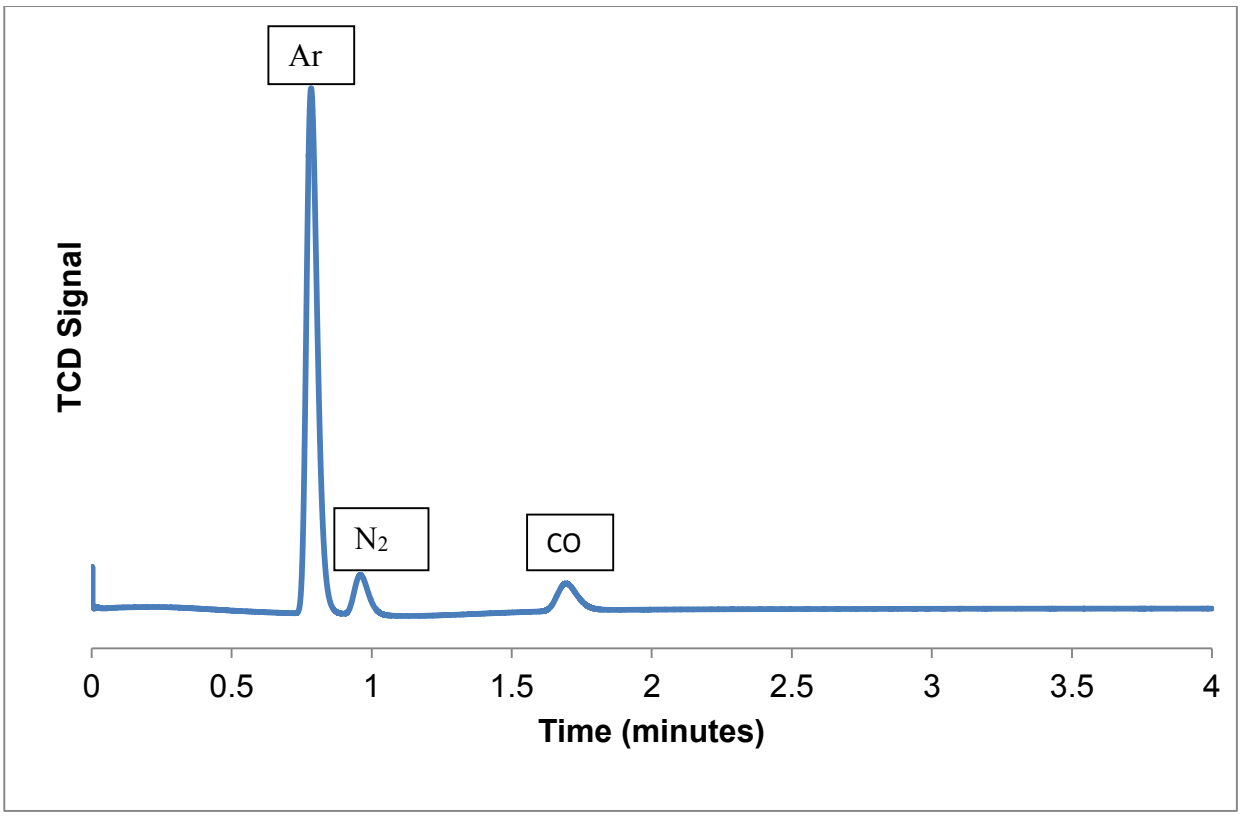

Figure 9.3: Sample TCD-GC chromatogram taken online using unmodified Co_3O_4 catalyst.

9.6 FID-GC sample chromatogram

FID-GC was used to analyse the presence of organic materials in the products of the Fischer-Tropsch synthesis. It was used to determine the selectivity of the catalyst. *Figure 9.4* shows a typical FID-GC chromatogram of the products of Fischer-Tropsch synthesis.

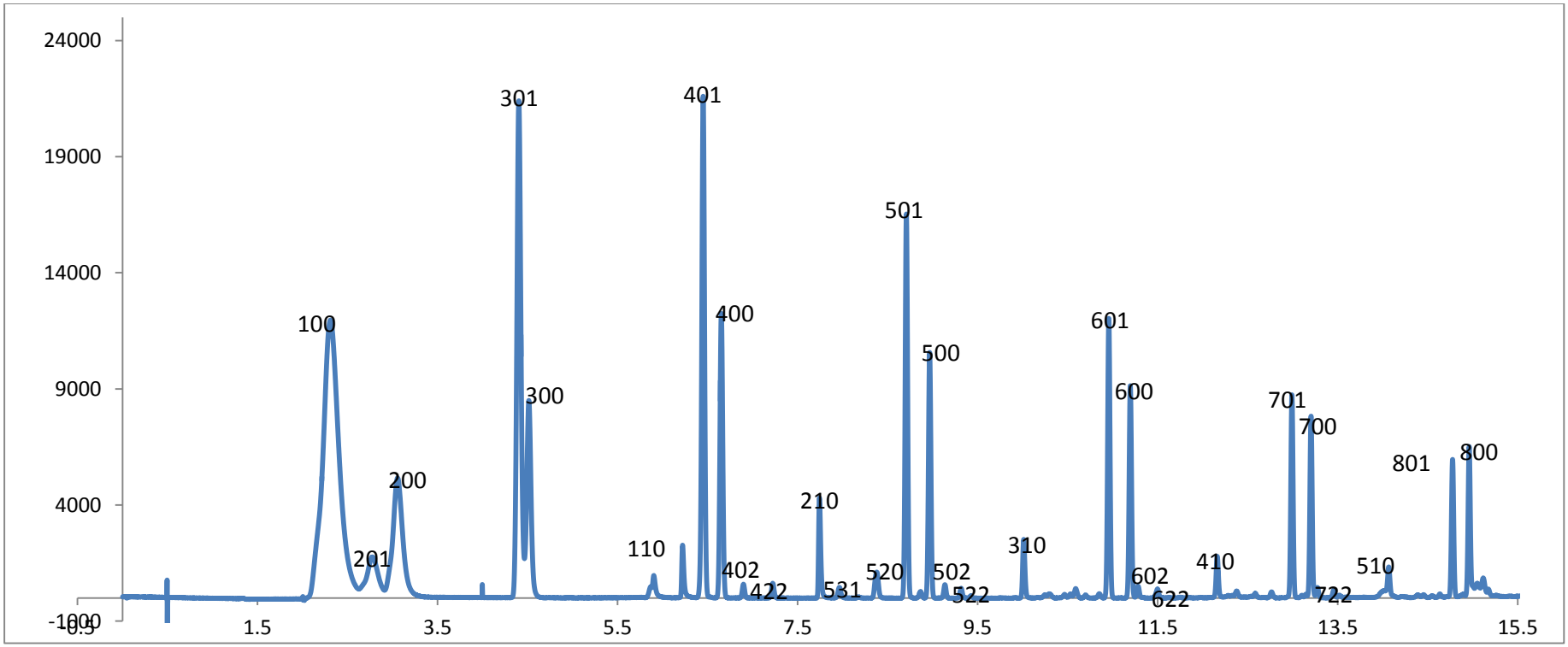

Figure 9.4 A typical chromatogram obtained from a GC-FID analysis (compounds labeled according to their compound codes; see *Table 9.3*)

Table 9.3: FID peak assignment

Code	Compound
100	Methane
110	Methanol
200	ethane
201	ethene
210	ethanol
300	propane
301	propene
310	propanol
400	butane
401	butene
402	cis-butene-2
422	trans-butene-2
410	butanol
500	pentane
501	pentene
502	cis-pentene-2
522	trans-penene-2
520	1-methyl-butane
531	3-methyl-butene-1
510	pentanol
600	hexane
601	hexene
602	cis-hexene-2
622	trans-hexene-2
700	heptane
701	heptene
702	cis-heptene-2
722	trans-heptene-2
720	2-methyl-hexane
800	octane
801	octene
802	cis-octene-2
822	trans-octene-2

9.7 Calculating the dispersion using hydrogen chemisorption

The hydrogen volume required for monolayer coverage on the sample was determined from the linearized Langmuir isotherms. The dispersion D, of the Co was calculated from the equation 9.1:

$$D = \frac{S * Ar * V_m}{M * L} \qquad (9.1)$$

Where S = 2 is the stoichiometric factor between hydrogen and cobalt, Ar is the atomic weight of cobalt, V_m is the monolayer volume of the hydrogen adsorbed (usually reported as cm^3/g of total catalyst) M is the total mass of the catalyst and L is the weight percentage of Co in the catalyst determined from atomic absorption spectrometry.

9.8 Calculating the final concentration of TEOS

Amount of cobalt used = 0.5 g

Amount of cobalt withdrawn per sampling = 0.1 g

Taking the 0.006 mol Si/ mol Co sample

Number of moles of Co in 0.1g Co_3O_4 = 0.1 g / 241 g /mol * 3

=1.2 mmol

The ratio of Si:Co = 0.06

The amount of TEOS adsorbed can therefore be determined from the ration as;

n_{ad} = 0.06*1.2mmol
n_{ad} = 0,072 mmol of TEOS

The initial amount of TEOS in the solution can be calculated from the initial concentration and volume of TEOS.

i.e n_i = 6mM * 0.350 L
= 2.1mmo

The final amount of TEOS in solution thus become;

$N_f = n_{i} - n_{ad}$

= 2.1mmol-0.072mmol

= 2.028 mmol

The final concentration thus become

C_f = 2.028mmol / 0.350 L

= 6.00 mM